AN ABSTRACT OF THE DISSERTATION OF

Kevin R. Caple for the degree of Doctor of Philosophy in Chemical Engineering presented on January 24, 2014.

Title: Detailed Analysis of the Hydrogen Sulfide Production Step in a Sulfur-Sulfur Thermochemical Water Splitting Cycle

Abstract approved: _____

Alexandre F.T. Yokochi

The production of hydrogen has been one of the most heavily studied, energy related fields over the past half century, yet few methods are commercially or economically viable and none are currently sustainable. Of those aiming at the sustainable production of hydrogen using renewable resources, perhaps the most widely studied are those attempting to thermochemically split water via various chemical intermediates. These provide an attractive conceptual alternative to other methods due to lower energy input requirements and to the production of the targeted hydrogen and oxygen in separate reaction steps.

One of the most widely studied thermochemical cycles is the Sulfur-Iodine cycle, the development of which has recently slowed due to the difficulty in the separation of hydrogen iodine from a hydrogen iodide-iodine-water azeotrope, material compatibility issues, and the perceived need use large amounts of iodine in the process. A modification of the Sulfur-Iodine thermochemical cycle that attempts to avoid those issues along with mitigating the need to process large amounts of water in the cycle was

developed, in a cycle we describe as the Sulfur-Sulfur cycle. This new thermochemical cycle can be summarized by the reaction sequence shown below.

$$4I_{2_{(IL)}} + 4SO_{2_{(IL)}} + 8H_2O_{(IL)} \rightarrow 4H_2SO_{4_{(IL)}} + 8HI_{(IL)}$$

$$8HI_{(IL)} + H_2SO_{4_{(IL)}} \rightarrow H_2S_{(IL)} + 4H_2O_{(IL)} + 4I_{2_{(IL)}}$$

$$3H_2SO_{4_{(IL)}} \rightarrow 3H_2O_{(g)} + 3SO_{2_{(g)}} + 1.5\ O_{2_{(g)}}$$

$$H_2S_{(g)} + 2H_2O_{(g)} \rightarrow SO_{2_{((g))}} + 3H_{2_{(g)}}$$

Previous work in our group demonstrated the viability of implementing the cycle's low temperature reactions (the first reaction pair, which we call the Bunsen reaction and the Hydrogen Sulfide Production (HSP) reactions) in ionic liquids, which removes the need to process large amounts of water and iodine in the reaction sequence, and minimizes the material compatibility issues, and also demonstrated the feasibility of stream reforming hydrogen sulfide. The present work focuses on an exergetic analysis of the Sulfur-Sulfur cycle, the careful determination of reaction kinetics for the HSP reaction, and developing a model of the kinetics of the low temperature reactions.

The exergetic analysis was carried out based on the published therrmochemical parameters for the species involved. The analysis showed that the maximum theoretical exergetic efficiency of the Sulfur-Sulfur cycle is nearly 70% with a strong dependence on the reaction temperature of the low temperature reactions.

The kinetics of the Bunsen and HSP were investigated through iodine colorimetery and the effect of water was determined. This kinetic data was used for the development of a predictive kinetic model that could accurately monitor the progression of iodine through the reaction system. The work showed that the Bunsen reaction is very fast with an activation energy (E_{a_B}) of 92.83 kJ/mol and a pre-

exponential factor (k_0) of 7.65E+14 min^{-1}, while for the HSP reaction, they were determined to be 117.09 kJ/mole and 7.73E+16 min^{-1}. Integration of these two reactions into a single differential model based on iodine concentration fit the experimental profile extremely well

The effect of including a Lewis base other than water in the reaction mixture yielded promising results that warrant future development. Specifically, the rates of both the Bunsen and HSP reactions increased with an increase in the pK_b of the added Lewis base.

A local protocol to recycle the ionic liquid, enabling it to be reused in new experiments, was successfully developed. When the recycled ionic liquid is employed, effects similar to those found through the inclusion of the Lewis base were observed, suggesting that a decomposition product remains in the recycled ionic liquid. This effect could be minimized by acid washing the recycled ionic liquid prior to use.

Detailed Analysis of the Hydrogen Sulfide Production Step in a Sulfur-Sulfur Thermochemical Water Splitting Cycle

Kevin R. Caple

A DISSERTATION

Submitted to

Oregon State University

in partial fulfillment of
the requirements for the
degree of

Doctor of Philosophy

Presented January 24, 2014

Commencement June 2014

Doctor of Philosophy dissertation of Kevin R Caple presented on January 24, 2014

APPROVED:

_____

Major Professor, representing Chemical Engineering

_____

Head of the School of Chemical, Biological, and Environment Engineering

_____

Dean of the Graduate School

I understand that my dissertation will become part of the permanent collection of Oregon State University libraries. My signature below authorizes release of my dissertation to any reader upon request.

_____

Kevin R. Caple, Author

ACKNOWLEDGEMENTS

I would first like to acknowledge and thank the National Science Foundation who supplied financial support for this project. This material is based upon work supported by the National Science Foundation under Grant No. 0748280

I would like to thank my advisor, Dr. Alex Yokochi, who took me on as a fresh faced graduate student with no engineering background. Through his patience, teaching, time, and effort, he has allowed me to grow as an engineer, a researcher, and a person. I seek to emulate his enthusiasm and optimism towards his professional career as I begin my own and I will be forever thankful for allowing my pursuit of interests outside of the academic setting and focusing on living a balanced and full life.

My graduate committee has been extremely helpful during my time here at Oregon State. I have had close interaction with Dr. Goran Jovanovic both in class and my research activities, from my Master's degree to this PhD. I have taken classes from Drs. Chih-Hung Change and Greg Herman, as well as my Graduate Council Representative, Dr. John Conley. I would like to make special mention of the influence of Dr. Greg Rorrer during my time here at Oregon State. Through the undergraduate and graduate classes I took from him, to working closely with him as a teaching assistant, and him offering me a teaching position over the summer of 2013, he has shown the highest level of professionalism and work ethic that I would strive to model myself after.

I would like to acknowledge my labmates in the Yokochi lab: Alex Bistrika, Malachi Bunn, Peter Kreider, Omar Muhammed, Yu Miao, Travis Campbell, Justin Pommerenck, Matt Delaney, and Nathan Coussens. I would like to especially thank Nick Auyeung for his initial work on this project and taking the time to bring me up to speed on that work before he graduated. I'd also like to thank Jeremy Campbell as a sounding board, compatriot, and friend throughout our time in the corner of the graduate offices in Gleeson. Thanks also go to Andy Brickman and Manfred Dittrich for their assistance with the development of any task that I needed, whether it be machining a new part, or finding the right tool for the job.

I would like to thank my parents and older brother Ryan for their unquestioned support during my time as a graduate student here at OSU. My parents instilled in me the principles of hard work, discipline, and not taking anything too seriously while always supporting the professional decisions that I have made.

Most importantly, I would like to thank my wife, Ratih Lusianti. As we navigated the difficult world of our PhD's together, she provided me with support, a professional opinion that I could always ask advice of, a person that I was happy to go home with every day, and a loving home. I would not have been able to complete my PhD without her. A final thanks to Layla, whose happy face and wagging tail always lifted my spirits when it was needed

TABLE OF CONTENTS

TABLE OF CONTENTS (continued)

Page

TABLE OF CONTENTS (continued)

Page

LIST OF FIGURES

LIST OF FIGURES (continued)

LIST OF FIGURES (continued)

LIST OF TABLES

LIST OF TABLES (continued)

1. Introduction

1.1 Background

Due to rising concerns over the effect of fossil fuel emissions on global warming, dwindling non-renewable fuel supplies, and political instability in regions with large oil reserves, the need for a cheap, renewable, and efficient fuel source is more pressing than ever. Of the many alternative fuels being researched, hydrogen may be the most theoretically attractive, as it possesses the highest specific energy content of all conventional fuels and is the most abundant element in the universe.[1] Despite its natural abundance, hydrogen cannot be "mined" directly but rather must be manufactured through the input of energy into a feedstock, ideally something renewable and abundant such as water or biomass. Through combined use with fuel cells, which have greater overall efficiencies when compared to more traditional methods of electricity generation, the use of hydrogen as a theoretical energy carrier shows nothing but promise.[2]

However, there are many obstacles preventing the theoretical application of hydrogen to the world economy as a fuel source. Fuel cell development, storage, and global hydrogen infrastructure will all require significant advancements in order to make hydrogen an economically viable energy solution, but the overwhelming limiting factor is a reliable, efficient, and cost effective method of hydrogen production. The ideal method for producing hydrogen would include a non-fossil fuel based feedstock, would not generate hazardous waste as a by-product, and, most importantly, would have a favorable cost and energetic efficiency.

The current global market for hydrogen production is already greater than $40 billion per year, a majority of which is utilized in established industries. Upwards of 50% of hydrogen produced annually is used in the Haber-Bosch process for the production of ammonia, while 35% is used for the refining of petroleum and the remainder is spread

out through other various applications.[3,4] One of the benefits of utilizing hydrogen is that it can be produced from a wide array of starting materials. However, over 96% of the hydrogen currently produced worldwide utilizes fossil fuels as the hydrogen source, with 48% from natural gas, 30% from oil, and 18% from coal. A mere 4% is produced using an alternative starting material, through electrolysis of water, but this still requires the application of electricity which is more than likely produced through fossil fuels.[5] The use of these fossil fuels as a hydrogen source produces both carbon monoxide and carbon dioxide as co-products in the hydrogen production steps, two of the main species responsible for the greenhouse effect thought to be responsible for climate change. In order for hydrogen to be fully utilized as a sustainable fuel, production methods using a renewable fuel source that do not produce environmentally hazardous byproducts must be developed.

In light of the various shortcomings of other methods for sustainable hydrogen production, a thermochemical cycle, utilizing the chemical potential of various reactants, has the potential to be an efficient and realistic method of carbon-free hydrogen production.[6] In thermochemical cycles, heat from a non-fossil fuel based energy source is used to drive endothermic reactions to essentially create a roundabout pathway for the cracking of water into hydrogen and oxygen. In contrast to the intensive heat requirements for the direct thermal decomposition of water which requires temperatures north of 2700 K, thermochemical cycles can be carried out at temperatures easily achievable through nuclear reactors (~1000 K) or solar concentrators (~2000 K).[7]

While theoretically attractive and desirable, there are several limiting factors that prevent the application of thermochemical cycles to the worldwide marketplace, the largest of which is the cycle itself. Several iterations of various cycles have been researched, but, among the various proposed cycle, the sulfur-iodine cycle appears to be the most heavily explored. The S-I cycle utilizes molecular iodine and sulfur dioxide,

as well as various sulfur and iodine based intermediates, in conjunction with heat and water to produce the requisite hydrogen and oxygen while regenerating its initial reactants. The simplistic reaction pathway for the S-I cycle is shown below

$$I_{2_{(aq)}} + SO_{2_{(aq)}} + 2H_2O \rightarrow 2HI_{(aq)} + H_2SO_{4_{(aq)}} \quad \text{Eq. 1.1}$$

$$2HI_{(l)} \rightarrow H_{2_{(g)}} + I_{2_{(l)}} \quad \text{Eq. 1.2}$$

$$H_2SO_{4_{(aq)}} \rightarrow SO_{2_{(g)}} + H_2O_{(g)} + \frac{1}{2}O_{2_{(g)}} \quad \text{Eq. 1.3}$$

However, despite the fairly simplistic reaction pathway and decades of research, the current iteration of the sulfur-iodine cycle is plagued by various limitations, including high heat loads, refining of the acid products to produce hydrogen and oxygen efficiently, material limitations and compatibility and undesirable side reactions. A potential solution to some of these limitations may be the use of an alternative reaction medium other than water, such as an ionic liquid. These solvents, relatively new to the industrial world, are typically composed of an organic cation and inorganic anion, and possess desirable physical characteristics including high boiling points, negligible vapor pressure, and the capability to be "tailor made" for a specific application with upwards of 10^{18} identified organic salts.[8]

Previous work by Auyeung has explored the application of the Sulfur-Iodine thermochemical cycle in an ionic liquid.[9] Through his initial exploration of the reaction viability, he found that, rather than separate into two aqueous layers as is the norm for the cycle, the reaction mixture remained homogenous in the ionic liquid. This lead to the subsequent activation of a previously undesired side reaction that produced hydrogen sulfide, which was confirmed through the detection of hydrogen sulfide in the gas phase.

$$8HI_{(IL)} + H_2SO_{4_{(IL)}} \rightarrow H_2S_{(IL)} + 4H_2O_{(IL)} + 4I_{2_{(IL)}} \quad \text{Eq. 1.4}$$

Further work by Auyeung explored the full development of a novel Sulfur-Sulfur thermochemical cycle, which eliminated the need for the refining of hydroiodic acid and replacing it with the steam reformation of the hydrogen sulfide produced in Eq. 1.4.[10]

$$H_2S_{(g)} + 2H_2O_{(g)} \rightarrow SO_{2_{((g))}} + 3H_{2_{(g)}} \qquad \text{Eq. 1.5}$$

1.1.1 Objectives

The following document will further explore the conceptualization of the new Sulfur-Sulfur thermochemical cycle through expanding upon the use of ionic liquids as a medium for the production of hydrogen sulfide. The energetic efficiency explored in the work by Auyeung will be expanded through visiting the exergetic efficiency and processing questions such as the complete recovery of iodine and the regeneration of the ionic liquid will be answered. The main focus of the work will be examining the effect of water on the in situ kinetics of Eq. 1.1 and Eq. 1.4 and the development of a predictive model to accurate track the progress of the in situ reaction pair. Further kinetic studies will be displayed including studying an equilibration period of the reaction pair, as well as exploring the use of homogenous catalysts. Early studies on the evolution of hydrogen sulfide and the behavior of sulfur dioxide in the liquid phase will be shown. To summarize, the conceptualized all fluid thermochemical cycle has been shown to be feasible based off various thermodynamic calculations as well as previous and current experimental exploration, laying the base for future development.

1.2 Literature Review

This literature review encompasses the major facets of this work, with focuses on competing thermochemical cycles, ionic liquids, and exergetic efficiency.

1.2.1 Thermochemical Cycles

1.2.1.1 Initial Development

The simplest form of utilizing thermochemical energy to produce hydrogen is the direct thermolysis of water. This well established reaction pathway is known to occur at approximately 2500°C with an efficiency of close to 50%.[11] Unfortunately, materials that are stable at these temperatures, as well as a sustainable and reliable heat sources are of limited availability.[12] However, at the International Round Table on Direct Production of Hydrogen with Nuclear Heat in Ispra, Italy in 1969, several alternative reagents have been proposed to lower the temperature and perhaps increase the overall efficiency. Several proposed cycles were judged based on ten criteria: thermal efficiency, conversion of reactions, side reaction, toxicity, cost and availability of chemicals, separations, corrosion, materials handling, temperature, and heat transfer.[13]

Three phases of the research program at Ispra were undertaken: examination of the Mark 1 cycle, the iron chloride cycle, and various closures for the decomposition of sulfuric acid.[11] Ultimately, 24 cycles were initially explored at Ispra, with temperature ranges from 920-1120 K, 3-6 reaction steps, and a variety of species involved, though most of the proposed cycles involved metal halides or some kind of sulfur. A second screening of viable thermochemical cycles was performed by General Atomics in 2000, which accounted for the number of elements, steps, phases of matter, and chemical compatibility. The five highest rated cycles from this work were found to be the Hybrid Sulfur, Mark 13, UT-3, sulfur-iodine, and iron sulfates.[14] A great deal of the current research is through the examination of various metal/metal oxide pairings in conjunction with solar heat.[15]

1.2.1.2 Metal/Metal Oxide Thermochemical Cycles

The metal/metal oxide based thermochemical cycles utilize what is ideally a two-step reduction-oxidation cycle in which a metal is reduced and generates oxygen through high temperature solar irradiation and then is oxidized back to its original state through the addition of water and lower temperatures, while producing hydrogen. One of the more significant benefits of this type of thermochemical cycle is the production of

oxygen and hydrogen is separate steps, eliminating the need for difficult and costly gas phase separation of the desired products. The original proposal for the metal oxide redox pairing was proposed by Nakamura, utilizing the Fe_3O_4/FeO pairing.[16]

$$Fe_3O_{4(s)} \rightarrow 3FeO_{(s)} + \frac{1}{2}O_{2(g)} \qquad \text{Eq. 1.6}$$

$$H_2O_{(g)} + 3FeO_{(s)} \rightarrow Fe_3O_{4(s)} + H_{2(g)} \qquad \text{Eq. 1.7}$$

Eq. 1.6 is a highly endothermic process and thusly requires temperatures upwards of 2500 K in order to achieve spontaneity ($\Delta G < 0$).[17] Tofighi et al. explored the decomposition of magnetite (Fe_3O_4) and found that, due to the excessive temperatures needed, the magnetite decomposition occurs with a great deal of vaporization and, due to oxidation of vaporized wustite (FeO), irreversibility was introduced to the process.[18] Sibieude et al. continued with this work to study the redox pairings of Mn_3O_4/MnO and Co_3O_4/CoO, and found that the required temperature for the reduction reaction ($M_3O_{4(s)} \rightarrow MO_{(s)} + \frac{1}{2}O_{2(g)}$) was significantly lowered by both the Mn and Co redox pairs by approximately 500 K each.[19] However, Sibieude et al. also found that, of the three redox pairs studied, only the Co pairing was able to produce hydrogen in significant amounts on a theoretical basis. Another redox pair that has received a substantial amount of attention has been the ZnO/Zn pairing. The Paul Scherrer Institute (PSI) in Switzerland has explored this pairing since the late 1990's and early 2000's and has found similar limiting issues with gaseous products and vaporization limiting the amount of Zn that is able to be re-oxidized in the hydrogen producing step.[20-24]

To balance a decrease in the necessary reaction temperature and a high hydrogen yield, solid solutions between the Fe_3O_4/FeO and M_3O_4/MO pairings (where M can be Mn, Co, or Mg) have been extensively explored.[25] This is performed through the partial substitution of iron in magnetite by Mn, Co, or Mg to form what is commonly referred to as a mixed metal oxide, typically denoted as $(Fe_{1-x}M_x)_3O_4$. These mixed metal oxides have been found to decrease the temperature needed for the hydrogen production step, although this came at a cost of a decrease in the overall kinetics of the reaction.[26,27]

Despite the abundance of research into the metal/metal oxide based thermochemical cycles, there have been no reports demonstrating good repeatability of the cyclic two step reactions to satisfy practical use of these processes. The inability to completely regenerate the initial metal oxide is by far the most significant limiting factor in the implementation of these cycles, mainly due to the sintering of the metal due to the high temperatures needed to initialize the reactions.[17]

1.2.1.3 Metal Halide Thermochemical Cycles

Of the 24 Ispra thermochemical cycles, more than half can be qualified as utilizing metal halides as their chemical species. Table 1.1 highlights the major species involved with these various cycles, while Table 1.2 demonstrate the representative reaction pathways for two of the more common species pairings from this list: the Mark 1 (mercury halide) and the Mark 15 (iron chloride), respectively.

Mark	Elements	Mark	Elements
Mark 1	Hg, Ca, Br	Mark 6C	Cr, Cl, Fe (V), Cu
Mark 1B	Hg, Ca, Br	Mark 7	Fe, Cl
Mark 1C	Cu, Ca, Br	Mark 7A	Fe, Cl
Mark 1S	Hg, Sr, Br	Mark 7B	Fe, Cl
Mark 3	V, Cl, O	Mark 8	Mn, Cl
Mark 4	Fe, Cl, S	Mark 9	Fe, Cl
Mark 5	Hg, Ca, Br, C	Mark 14	Fe, Cl
Mark 6	Cr, Cl, Fe (V)	Mark 15	Fe, Cl

Table 1.1: Summary of the Ispra thermochemical cycles that utilize metal halides

Mark 1	Mark 15
$CaBr_2 + 2H_2O \rightarrow Ca(OH)_2 + 2HBr$	$3FeCl_2 + 2H_2O \rightarrow Fe_3O_4 + 6HCl + H_2$
$2HBr + Hg \rightarrow HgBr_2 + H_2$	$Fe_3O_4 + 8HCl \rightarrow FeCl_2 + 2FeCl_3 + 4H_2O$
$HgBr_2 + Ca(OH)_2 \rightarrow CaBr_2 + HgO + H_2O$	$2FeCl_3 \rightarrow 2FeCl_2 + Cl_2$
$HgO \rightarrow Hg + .5O_2$	$Cl_2 + H_2O \rightarrow 2HCl + .5O_2$

Table 1.2: Mark 1 and Mark 15 Thermochemical Cycles

Despite the age and abundant research on the Mark 1 and Mark 15 cycles, they are no closer to industrial implementation. The Mark 1 suffers from utilizing mercury, nearly eliminating it from feasibility on a large scale due to the industrial difficulties of handling and chemical reactions with mercury, while the Mark 15, though much more industrially viable, suffered from limiting factors in the hydrolysis of $FeCl_2$ (the first reaction in the Mark 15) and the thermal decomposition of $FeCl_3$ (reaction 3 in the Mark 15).[11]

While the Ispra metal halide cycles have proven difficult to make chemically or economically feasible, two other cycles have undergone a great deal of research as well: the UT-3 cycle, discovered by Kameyama et al., and the copper-chloride cycle. Both are shown below in Table 1.3.[28,29]

UT-3	Cu-Cl
$CaBr_2 + H_2O \rightarrow CaO + 2HBr$	$2Cu + 2HCl \rightarrow 2CuCl + H_2$
$CaO + Br_2 \rightarrow CaBr_2 + .5\ O_2$	$CuCl_2 + H_2O \rightarrow Cu_2OCl_2 + 2HCl$
$Fe_3O_4 + 8HBr \rightarrow 3FeBr_2 + 4H_2O + Br_2$	$2Cu_2OCl_2 \rightarrow 4CuCl + O_2$
$3FeBr_2 + 4H_2O \rightarrow Fe_3O_4 + 6HBr + H_2$	$2CuCl \rightarrow CuCl_2 + Cu$

Table 1.3: UT-3 and Cu-Cl thermochemical cycles

Maximum sustainable reaction temperatures for the UT-3 reaction series have been found to be 1033, 845, 493, and 833K, respectively, while the Cu-Cl cycle temperatures have been found to be 700, 675, 775K, and ambient temperature respectively.[30,31] These reaction temperatures are significantly less than those associated with the metal/metal oxide cycles, eliminating some of the issues associated with the required temperature. The copper chloride cycle also institutes the use of electrolysis in the fourth reaction, a unique wrinkle that is utilized in other thermochemical cycles.[31]

The UT-3 cycle has been studied extensively over the years, including reaction and kinetic measurements, bench scale tests, and engineering evaluations for scaling to industrial size facilities.[32-39] Tadokoro et al. has found that the UT-3 process in conjunction with an electric power generating system can reach 45-48% efficiency, depending upon the membrane recovery rate.[39] Efficiencies on the Cu-Cl cycle have been found to be upwards of 43%, excluding the additional gains of utilizing waste heat from the cycle itself.[40]

Despite their promise, the UT-3 and Cu-Cl cycles, as with all thermochemical cycles, possess limitations that prevent them from industrial application. Both involve the presence of large amounts of halides, difficult and reactive chemicals to handle in an industrial setting, as well as the increased presence of solid state chemistry, a difficult reaction progression to control and regenerate the initial reactants.[31] An ideal cycle

would utilize an all fluid system in which a continuous stream of reactions would take place and there would be no need halting of production for solid regeneration.

1.2.1.4 Hybrid Sulfur and Mark 13 Thermochemical Cycles

The Hybrid Sulfur, also known as the Westinghouse and the Mark 13cycles are thermochemical cycles that utilize the reduction of sulfuric acid to sulfur dioxide as an initial reactant. The reaction pathways for both cycles are shown below

Hybrid Sulfur	**Mark 13**
$2H_2SO_4 \rightarrow 2SO_2 + 2H_2O + O_2$ Thermochemical, 850°C	$2H_2SO_4 \rightarrow 2SO_2 + 2H_2O + O_2$ Thermochemical, 850°C
$SO_2 + 2H_2O \rightarrow 2H_2SO_4 + H_2$ Electrochemical, 77°C	$2HBr \rightarrow Br_2 + H_2$ Electrochemical, 77°C
	$Br_2 + SO_2 + 2H_2O \rightarrow 2HBr + H_2SO_4$ Thermochemical, 77°C

Table 1.4: Reaction pathways, method of reaction, and reaction temperature for the Hybrid Sulfur and Mark 13 thermochemical cycles

The Westinghouse cycle is a simple, all fluid process for the decomposition of water into hydrogen and oxygen, rated the most viable in a screening by Brown et al.[14] One of the most direct benefits of utilizing the Hybrid sulfur cycle is in the comparison between the potential required for the electrochemical step (0.17 V) and the potential required for the direct electrolysis of water (1.23 V).[41] The thermal efficiency for the Hybrid Sulfur cycle was found to be between 35% and 41%, depending on the heating value used, operating under the assumption of the available electrical power operated at an efficiency of 45% and using a high temperature gas cooled reactor (HTGR).[42]

A benefit of utilizing the Hybrid Sulfur cycle is the utilization of solar photovoltaic electricity as a power source for the electrochemical reaction. Due to the lower potential needed to drive the electrochemistry, fewer solar cells or percentage of power produced is required to run the reaction, producing lower overall costs. Hinkley et al. predicted that a hybrid sulfur plant operating with a grid powered electrolyser and a solar thermal acid decomposition reactor would have a lower hydrogen price ($5.16 vs. $5.47/kg hydrogen) than a conventional system.[43]

The Mark 13 cycle is analogous to the sulfur-iodine cycle that will be discussed shortly, with the hydrobromic acid and molecular bromide replacing the hydroiodic acid and molecular iodine.

1.2.1.5 The Sulfur-Iodine Thermochemical Cycle

The sulfur-iodine thermochemical cycle (Ispra Mark 16) is perhaps the most widely studied thermochemical water splitting cycle. The scheme for the reaction series is as follows

$$I_{2_{(aq)}} + SO_{2_{(aq)}} + 2H_2O \rightarrow 2HI_{(aq)} + H_2SO_{4_{(aq)}} \qquad \text{Eq. 1.8}$$

$$2HI_{(l)} \rightarrow H_{2_{(g)}} + I_{2_{(l)}} \qquad \text{Eq. 1.9}$$

$$H_2SO_{4_{(aq)}} \rightarrow SO_{3_{(g)}} + H_2O_{(g)} \qquad \text{Eq. 1.10}$$

$$SO_{3_{(g)}} \rightarrow SO_{2_{(g)}} + \frac{1}{2}O_{2_{(g)}} \qquad \text{Eq. 1.11}$$

In the literature, there exists varying opinions on whether the reduction of sulfuric acid to sulfur trioxide and then onto sulfur dioxide constitutes two reactions or a single reaction (illustrated in Eq. 1.10 and 1.11).[14] This work will operate under the assumption that this is a two- step reaction. Equation 1.8 is typically referred to as the Bunsen reaction and is typically carried out in an excess of water to make the reaction spontaneous.[44]

The products of the Bunsen reaction produce two aqueous acid phases consisting of hydroiodic and sulfuric acids that are partitioned gravimetrically. The acids are then separated, purified, and, through use of catalysis, thermally decomposed to their initial reactants and producing the desire hydrogen and oxygen products.

While theoretically simple, the implementation of the sulfur-iodine cycle has several limiting factors. Despite the relatively simple stoichiometry proposed in Eq. 1.8-1.11, the initial proposal for the actual stoichiometry, proposed by General Atomics, is significantly more complicated.[45]

$$9I_{2_{(L)}} + SO_{2_{(g)}} + 16H_2O_{(L)} \rightarrow (2HI + 10H_2O + 8I_2)_{(L-2)} + (H_2SO_4 + 4H_2O)_{(L-1)}$$

Eq. 1.12

$$(2HI + 10H_2O + 8I_2)_{(L-2)} \rightarrow 2HI_{(g)} + (8I_2 + 10H_2O)_{(L)}$$ Eq. 1.13

$$2HI_{(g)} \rightarrow H_{2_{(g)}} + I_{2_{(L)}}$$ Eq. 1.14

$$(H_2SO_4 + 4H_2O)_{(L-1)} \rightarrow (H_2SO_4)_{(L)} + 4\,(H_2O)_{(L)}$$ Eq. 1.15

$$(H_2SO_4)_{(L)} \rightarrow (H_2SO_4)_{(g)}$$ Eq. 1.16

$$(H_2SO_4)_{(g)} \rightarrow (SO_3)_{(g)} + (H_2O)_{(g)}$$ Eq. 1.17

$$(SO_3)_{(g)} \rightarrow (SO_2)_{(g)} + 0.5O_{2_{(g)}}$$ Eq. 1.18

The excess of iodine and water displayed in Eq. 1.12 allows for the formation of the previously stated aqueous states: a lighter, sulfuric acid layer (L-1) and a heavier, iodine/iodide-water phase (L-2). This binary aqueous phase allows for simple phase separation. The separation and reformation steps of this process are extremely energy and therefore, cost, intensive. Part of this is due to the low HI azeotrope in water. Due to the low azeotrope present in what is commonly referred to as the HIx mixture ($HI - H_2O - I_2$), a conventional distillation under atmospheric pressure consumes enormous sums of excess heat to vaporize the water with HI. Several attempts have been made to

develop an energy efficient process to concentrate HI from the HIx mixture for further processing, with three methods standing out: extraction distillation, reactive distillation, and electrodialysis (membrane separation).

Besenbruch et al., in conjunction with General Atomics, proposed extractive distillation in 1982 through the addition of phosphoric acid. The presence of phosphoric acid induces the separation of iodine from the HIx mixture, and then allows for a more straightforward direct distillation of HI. HI can then be decomposed in gaseous through Eq. 1.14 above.[46] Reactive distillation was proposed in the 1980's by Roth et al. in which HIx distillation and HI decomposition occur in the same reactor at elevated temperatures. A gas liquid equilibrium is achieved in the reactor, allowing for the separation of soluble iodine in the lower liquid phase and the removal of hydrogen and water in the higher gas phase.[47]

Stewart et al., suggested the use of membrane separation, utilizing the Nafion-117® membrane to physically remove the HI from the HIx stream, ultimately concentration HI from water by a separation factor range of 200-700. However, due to the extremely corrosive nature of the HIx stream, the membrane lifetime and long term viability of this process is of significant concern.[48] The development of an electro-electrodialysis (EED) process for concentrating HI was developed by Onuki et al, and the process viability explored in subsequent work, focusing on the effects of iodine content, operating temperature, membrane type, electrode properties, and the durability of membranes in the system.[49-54]

While perhaps not as energy intensive or specifically tied to the sulfur-iodine cycle, the processing of sulfuric acid possesses the largest energy demand and shows the largest kinetic barrier.[55] A wide variety of catalysts are utilized to lower the energy demands. Dokiya et al. tested $SiO_2, Al_2O_3, ZnO, CuO, NiO, CoO, Fe_2O_3, MnO, Cr_2O_3, V_2O_5$, and TiO_2 for the reduction of sulfuric acid to sulfur dioxide in the temperature range of 1073 to 1143 K at atmospheric pressures.[56] Sintered iron (III) oxide presented with the highest activity,

while the remainder of the species studied showed decreased activity due to the formation of highly stable sulfates. Norman et al. investigated noble metals and further metal oxides and their capabilities, finding that Pt supported on SiO_2, ZrO_2, TiO_2 and $BaSO_4$ all performed the necessary reduction with varying degrees of success at high temperatures.[57] Several more authors explored the use of various catalysts, generally some kind of metal oxide, for this reaction, with a mix of results.[58-67] Ultimately, however, this reaction still requires a great deal of study for the sulfur-iodine process to be economically viable.

Due to the difficulties associated with the handling of the two acid products, a great deal of research has gone into performing the Bunsen reaction in such a manner to produce acids that require minimal processing. One of the most significant problems with the Bunsen reaction and the subsequent acid processing is the poisoning of both acid phases. It has been determined that a non-negligible amount of sulfur containing species are dissolved in the HIx phase, requiring purification downstream.[6,68,69] A majority of the works focusing on the Bunsen section of the sulfur-iodine cycle have focused on the liquid-liquid equilibrium phase separation performance. Byung et al. compiled some of the previous work performed on the Bunsen reaction and identified an ideal operating window: represented by a 4 to 6 mole excess of iodine and an 11 to 13 mole excess of water in the stoichiometry at a temperature range of about 50°C-80°C.[70] These and other works highlight the need for extreme purity in the acid phases due to the presence of two dominant side reactions, both of which would occur in either of the poisoned acid phases.

$$H_2SO_{4_{(aq)}} + 6HI_{(aq)} \rightarrow S_{(s)} + 3I_{2_{(aq)}} + 4H_2O_{(l)} \qquad \text{Eq. 1.19}$$

$$H_2SO_{4_{(aq)}} + 8HI_{(aq)} \rightarrow H_2S_{(aq)} + 4I_{2_{(aq)}} + 4H_2O_{(l)} \qquad \text{Eq. 1.20}$$

Sakurai et al. reported that the production of sulfur dominates the production of hydrogen sulfide and that they typically occur as the Bunsen reaction nears completion with an increase in the acid content and decrease in iodine. Sakurai also observed that raising the temperature may also lead to the reverse of the Bunsen reaction.[71] Despite all

of the difficulties listed with this process, Kubo et al. managed to run the sulfur iodine cycle continuously at a hydrogen production rate of 32 liters per hour for 20 hours.[72]

Several of these side reactions have led to the development of alternative reaction cycles based around the framework of the sulfur-iodine cycle, including the basis for this work explored by Auyeung.[9,10] Mason and Bowman sought to utilize magnesium oxide to minimize the amount of water required:

$$MgO_{(s)} + SO_{2(g)} \rightarrow MgSO_{3(s)} \quad \text{Eq. 1.21}$$

$$MgO_{(s)} + MgSO_{3(s)} + I_2 \rightarrow MgSO_{4(s)} + MgI_{2(s)} \quad \text{Eq. 1.22}$$

$$MgI_{2(s)} + H_2O_{(l)} \rightarrow MgO_{(s)} + 2HI_{(g)} \quad \text{Eq. 1.23}$$

$$2HI_{(g)} \rightarrow H_{2(g)} + I_{2(g)} \quad \text{Eq. 1.24}$$

$$MgSO_{4(s)} \rightarrow MgO_{(s)} + SO_{2(g)} + 0.5O_{2(g)} \quad \text{Eq. 1.25}$$

Mason and Bowman also suggested the use of tantalum and lanthanum as alternative to magnesium in this reaction pathway, as their respective sulfates decompose at lower temperatures than $MgSO_4$. This approach, while negating the need for the processing of sulfuric acid, has been largely discounted due to the solid-solid interactions and limiting regeneration capability of some of the solid products.[73] Giaconia et al. explored a similar strategy using lead sulfates in the Bunsen reaction and treating the resulting lead iodide with phosphoric acid.[74]

$$PbSO_{4(s)} + 2HI_{(aq)} \rightarrow PbI_{2(s)} + H_2SO_{4(aq)} \quad \text{Eq. 1.26}$$

$$PbI_{2(s)} + 2H_3PO_4 \rightarrow 2HI_{(g)} + Pb(PO_4)_2 \quad \text{Eq. 1.27}$$

$$Pb(PO_4)_2 + 3H_2SO_{4(aq)} \rightarrow 3PbSO_{4(s)} + 2H_3PO_{4(aq)} \quad \text{Eq. 1.28}$$

Eq. 1.26-1.28 can be carried out simultaneously with the Bunsen reaction with continuous feeding of gaseous sulfur dioxide and lead sulfate and production of lead

iodide and liquid sulfuric acid. The benefit of this reaction pathway is the limitation of side reactions through the removal of iodide via the Bunsen reaction and eliminating both the need for large excesses of iodide and for separate HIx separation and purification before processing. However, this process still suffers from the production of solid materials and requires further energetic and cost analysis.

Similar to the work laid out in this document, several modification to the sulfur-iodine cycle have been focused on various sulfur species. Moniri et al. explored 5 alternative pathways, all of which utilize the Bunsen reaction but vary in the method to produce sulfur dioxide.[75] The following equations highlight the method to produce sulfur dioxide, as well as the net chemical equation for the entire cycle, which is the final equation for each Route.

Route 1

$$H_2S_{(g)} + H_2SO_{4(l)} \rightarrow SO_{2(g)} + S_{(s)} + 2H_2O_{(l)} \qquad \text{Eq. 1.29}$$

$$H_2S_{(g)} \rightarrow H_{2(g)} + S_{(s)}$$

Route 2

$$0.5\ H_2S_{(s)} + .5\ H_2SO_{4(l)} \rightarrow .5\ SO_{2(g)} + .5\ S_{(s)} + H_2O_{(l)} \qquad \text{Eq. 1.30}$$

$$.5\ S_{(s)} + .5\ O_{2(g)} \rightarrow .5\ SO_{2(g)}$$

$$.5\ H_2S_{(g)} + H_2O_{(l)} + .5\ O_{2(g)} \rightarrow H_{2(g)} + .5\ H_2SO_{4(l)}$$

Route 3

$$H_2S_{(g)} + 1.5\ O_{2(g)} \rightarrow SO_{2(g)} + H_2O_{(g)} \qquad \text{Eq. 1.31}$$

$$H_2S_{(g)} + H_2O_{(l)} + 1.5\ O_{2(g)} \rightarrow H_{2(g)} + H_2SO_{4(l)}$$

Route 4

$$S_{(s)} + O_{2(g)} \rightarrow SO_{2(g)} \qquad \text{Eq. 1.32}$$

$$S_{(s)} + 2H_2O_{(l)} + O_{2(g)} \rightarrow H_{2(g)} + H_2SO_{4(l)}$$

Route 5

$$SO_{2(g)} + 2H_2O_{(l)} \rightarrow H_{2(g)} + H_2SO_{4(l)} \qquad \text{Eq. 1.33}$$

Again, all five Routes use the sulfur dioxide produced (or capture in Route 5) in the Bunsen reaction, producing sulfuric acid and hydrogen iodide with the HI being subsequently treated to reform the initial iodine and the desired hydrogen. Note that Routes 1 and 2 are essentially the same stoichiometrically, with the exception of adding an additional step to oxides elemental sulfur into sulfur dioxide. While Moniri et al. found that all five of these routes could be potentially viable through exergetic analyses, Routes 1, 2, and 4 all require processing of solid sulfur, Route 3 requires the direct, energy intensive cracking of hydrogen sulfide, and Route 5 requires purification of stack gas in order to accumulate the necessary sulfur dioxide. These difficulties in the production of sulfur dioxide and the need to treat either sulfuric acid or elemental sulfur make these reaction pathways analogous to the original cycle.

1.2.2 Exergetic Efficiency

Exergy is defined as the maximum theoretical work during a process in which a system passes from a give state to what is commonly referred to as a "dead state." The dead state means that the process system is in thermal and mechanical equilibrium with its environment in which the value of the exergy is exactly zero.[76] Through the conversion of the system pressure and temperature to those of the environment, thermomechanical exergy is calculated, amounting to the maximum possible work in the system. However, due to the nature of the components making up both the system and the environment, a system way still be out of equilibrium with the environment when the thermomechanical exergy is equal to zero. These differences can be attributed to the chemical exergy.[77] Analysis of the thermomechanical and chemical exergies (the sum of

which is called the total exergy) is performed to determine the steps of a specific process that require energetic improvements to enhance the overall efficiency of the process.[78]

Unlike energetic balance, exergy accounts for the irreversibility of a process due to the increase in entropy. It is therefore common to see exergetic efficiency to be defined as a 2nd law efficiency whereas purely energetic efficiencies are defined as 1st law efficiencies, accounting for the Law of Thermodynamics that each follow. The losses associated with energy and exergy vary as well. Energy losses are typically associated with waste emissions (mainly with cooling water) whereas exergetic losses are from internal consumptions such as combustion and heat transfer across large temperature differences.[79] One of the benefits of performing an exergetic balance on a system is that it allows for a comparison between the actual system and a thermodynamically perfect one operating under the same conditions.

A wide array of exergetic analyses have been performed on hydrogen producing processes, often times paired with economic or cost analysis. Steinfeld et al. performed an exergetic and cost analysis on the Zn/ZnO thermochemical cycle utilizing solar energy, reaching a maximum exergetic efficiency of 29% and a hydrogen cost range of 0.11-0.17 $/kWh, making it competitive on an industrial scale for the solar electrolysis of water.[80,81] Abanades et al. highlighted that, for processes requiring solar energy, there is a temperature in which a further increase would result in a lower reactor exergetic efficiency, which was found to be highly dependent on the solar flux concentration obtained through the solar collection facility.[82] Tied to this finding, Hammache et al. highlighted the need for higher exergetic efficiencies for solar based thermochemical cycles, find that an increase in the efficiency would lower the solar heliostat field area needed for a given amount of hydrogen produced.[83]

Rosen and Scott highlighted the differences in the energetic and exergetic efficiencies in a wide range of hydrogen producing processes with various energy inputs including a hypothetical heat source, a high temperature heat, and a combination of

electricity and high temperature heat. A summary of their findings is seen below in Table 1.5.[79]

Heat Source	**Hypothetical**		**High Temperature**		**High Temp /Electricity**	
Hydrogen production process	Energy η	Exergy η	Energy η	Exergy η	Energy η	Exergy η
Steam Reformation of Methane (SMR)	86	78	89	78	86	78
Coal Gasification	59	49	59	49	59	49
Current H2O electrolysis	30	26	30	46	77	67
Advanced H2O electrolysis	49	41	49	73	92	83
Thermochemical	21	19	21	25	21	16
SMR/Current H2O electrolysis	55	48	55	64	85	76
SMR/Advanced H2O electrolysis	70	62	70	78	89	81
SMR/ Thermochemical	45	40	45	47	45	49

Table 1.5: Summary of energetic and exergetic efficiencies for a wide range of hydrogen producing methods (originated and altered from Ref. 79)

Several key factors can be extracted from this work. The efficiencies of hydrogen production methods that require fossil fuel feedstock vary little with a change in heat

source with the only significant change occurring with the combination of steam reformation of methane and electrolysis utilizing a high temperature and electricity as external energy inputs. The use of SMR with an alternative method of hydrogen production such as current/advanced water electrolysis or thermochemical water decomposition tends to increase the overall efficiencies of the alternative processes, especially when tied with thermochemical water decomposition. The combination of thermochemical water decomposition or electrolysis with steam reformation of methane could provide a stable bridge between the development of alternative processes and the use of current technology with built in infrastructure.

Orhan et al. performed a complete exergetic analysis of the Cu-Cl thermochemical cycle which was used as a basis for this work.[84-89] For this analysis, Orhan utilized five reactions for the chemical process, differing from the four reactions explored by Rosen et al. (2006), each of which was defined by a reaction temperature, inlet species and outlet species. The reaction pathway defined by Orhan is as follows:

$$2CuCl_{2(s)} + H_2O_{(g)} \rightarrow CuO * CuCl_{2(s)} + 2HCl_{(g)} \quad \text{Eq. 1.34}$$

$$CuO * CuCl_{2(s)} + Q \rightarrow 2CuCl_{(l)} + \frac{1}{2}O_{2(g)} \quad \text{Eq. 1.35}$$

$$CuCl_{(s)} + H_2O_{(l)} \rightarrow 2CuCl_{2(s)} + 2Cu_{(s)} + H_2O_{(l)} \quad \text{Eq. 1.36}$$

$$2CuCl_{2(aq)} \rightarrow 2CuCl_{2(s)} \quad \text{Eq. 1.37}$$

$$2HCl_{(g)} + 2Cu_{(s)} \rightarrow 2CuCl_{(l)} + H_{2(g)} \quad \text{Eq. 1.38}$$

The total exergetic efficiency found for the fluidized bed, oxygen production, copper production, evaporator, and hydrogen production steps (Eq. 1.34-1.38, respectively) are 76%, 96%, 99%, 67%, and 99%, respectively. Combining these five efficiencies, a total exergetic efficiency of 47.9% is found. It is important to note that this efficiency does not take into account the necessary work typically associated with operating these systems in an industrial setting, such as pump work and the generation of

electricity from renewable resources. The application of industrial work to the exergetic efficiency of the chemical reactions listed above would make the total efficiency much more in line with the values listed by Rosen and Scott. A more in depth explanation of the process in with Orhan et al. determined these efficiencies will take place later in this work.

1.2.3 Ionic Liquids and Alternative Reaction Media

1.2.3.1 Ionic Liquids

Over the last decade, ionic liquids have emerged as an ideal solvent for green chemistry. They are generally non-volatile, non-flammable, thermally stable, and are liquids with negligible vapor pressure at room temperature.[90,91] The high boiling points are speculated by Rebelo et al. to be due to the Coloumbic interactions of the ionic species preventing the formation of a gas phase.[92] Lee et al. was able to determine that the [BMIM][BF4] and [BMIM][PF6] ionic liquids displayed thermal stability at temperatures ranging from ambient to 673K.[93] They are available commercially and can be synthesized onsite from two initial regents: one bearing the organic cation and one bearing the inorganic anion. Due to the versatile nature of the liquid salt formation, ionic liquids can be "tailor-made" by altering the specific anion or cation used.[94] Unfortunately, with ionic liquids being generally new to the industrial and academic research world, many of the traditional physical and chemical properties remain unavailable.[95]

One of the significant advantages of ionic liquids, especially in regards to this work, is the high solubility that they possess. Jiang et al. reported on the solubility of sulfur dioxide in two imidazolium based ionic liquids, 1-butyl-3-methylimidazolium tetrafluoroborate ([BMIM][BF4]) and 1-butyl-3-methylimidazolium bis(trifluoromethylsulfonyl)imide ([BMIM][TF2N]), finding saturation mole fractions of 0.57 and 0.552, respectively.[96] Lee et al. and Huang et al. both concluded that the cation has a minimal effect on the absorption capacity of various ionic liquids.[93,97] Shokouhi et

al. explored the solubility of hydrogen sulfide in various tetrafluouroborate[BF4] anion ionic liquids and found that it was more soluble than carbon dioxide, implying the possible use in oil and gas refining.[98] All of these interactions give ample reasoning for the use of ionic liquids as a solvent for the novel sulfur-sulfur thermochemical cycle discussed in this work. However, progressing forward must be undertaken with caution. Pomelli et al. found that hydrogen sulfide interacts significantly with the [Cl], [BF4], [TF2N], [OTf], and [PF6] anions.[99] The findings of Anderson et al. and Rahmati-Rostami et al. were used for theoretical calculations for the solubility of sulfur dioxide and hydrogen sulfide in [BMIM][TF2N], operating under the assumption made by Lee et al. and Huang et al. that the cation has little effect on gaseous solubility.[93,97,100,101]

1.2.3.2 Alternative Reaction Media

One of the key components of this work is the application of the previously discussed ionic liquid as an alternative reaction medium for the novel sulfur-sulfur thermochemical cycle. There have been several previous instances in which alternative media have been used to mitigate some of the issues associated with the sulfur iodine cycle, with a primary focus on the separation of the two acids produced in the Bunsen reaction.

De Beni et al. sought to utilize tri-n-butyl phosphate as a solvent for the Bunsen reaction, due to its high boiling point.[102] The theoretical goal of applying TBP would be to evaporate pure HI from the reaction mixture. De Beni et al. found that TBP forms a complex with HI, preventing some of the side reactions previously discussed from occurring and allowing the reaction to progress to completion. Following the separation of the sulfuric acid phase, it was discovered that the concentration of the products in the organic TBP phase were found to be above the normal azeotrope of HI in water. However, it was found that the sulfuric acid phase was significantly more dilute. Unfortunately, efforts to recover the HI from the TBP phase by thermal means have failed as the TBP was found to degrade at elevated temperatures.[74,102]

Barbarossa et al. proposed using polystyrene-divinyl-benzene (PVDVB) for use in the Bunsen reaction, seeking to use the PVDVB to immobilize the sulfuric acid to form an insoluble sulfonated solvent phase, allowing for simpler HI separation. The recovery of the sulfuric acid from the sulfonated PVDVB phase was found to be approximately 56%, much too low to be feasible, though work is ongoing.[103] Toluene has also been applied, though to a hydrogen sulfide based water splitting cycle rather than the sulfur-iodine, though the cycle still utilizes the Bunsen reaciton.[104] Zhu et al. found that both acids were present in the same aqueous phase and that only iodine remained in the toluene phase.

Ionic liquids are just beginning to be investigated for use in the Bunsen reaction and the sulfur-iodine cycle in general. Taylor et al. sought to examine the capabilities of eleven various ionic liquids for use in the Bunsen reaction, specifically seeking for one that could behave similarly to TBP, as discussed in the work of De Beni et al.[105] Utilizing various imidazolium, morphonium, phosphonium, and pyrollidinium based cations with either tri(pentafluoroethyl)trifluorophosphate [FAP], bis(trifluoromethylsulfonyl)imide [TF2N], or trimethylpenthylphosphine [TMPP], Taylor sough to determine the best extraction agent for HI. The ionic liquids studied were all hydrophobic to increase the purity of the extracted HI, though this does have the side effect of diluting the sulfuric acid aqueous phase. Taylor et al. ultimately determined that none of the listed anions were suitable for the Bunsen reaction, due to the extreme hydrophobicity of the [FAP] ionic liquids preventing extraction of HI from the ionic liquid phase, the [TMPP] ionic liquids appearing to be susceptible to hydrolysis, and low yields from the [TF2N] ionic liquids. While perhaps not entirely suitable for the process that Taylor et al. designed, it was found that the [TF2N] anion ionic liquids were able to remove upwards of 25% of HI into the organic phase, up from 16% using TBP. However, organic cations from the ionic liquid were found in the aqueous Bunsen phase, suggesting poor solvent stability.

1.2.4 Summary of Previous Work on Sulfur-Sulfur Thermochemical Cycle

Initial exploration of the new Sulfur-Sulfur thermochemical cycle has been undertaken by Auyeung.[9] The initial drive of the previously proposed work was to employ a new solvent to the Bunsen reaction, e.g. ionic liquids, with the ultimate goal of successfully facilitating the Bunsen reaction and eventually releasing the desired HI as a vapor for treatment without the use of expensive distillation or membrane techniques.

Several ionic liquids were explored as potential solvents for the new HI extraction hypothesis and are shown in Table 1.6.

Ionic Liquid	**Abbrev.**	**Anion (A^-)**	**Hydrophilic/ Hydrophobic**
1-Butyl-3-methylimidazolium tetrafluoroborate	BMIM.BF_4	BF_4^-	Hydrophilic
1-Butyl-3-methylimidazolium Hexafluorophosphate	BMIM.PF_6	PF_6^-	Hydrophobic
1-Hexyl-3-methylimidazolium bis(triflluoromethylsulfonyl)imide	HMIM.Tf_2N	$N(CF_3SO_3)^-$	Hydrophobic
1-Ethyl-3-methylimidazolium hydrogensulfate	EMIM.HSO_4	HSO_4^-	Hydrophilic
1-Butyl-3-methylimidazolium trifluoromethanesulfonate	BMIM.OTf	$CF_3SO_3^-$	Hydrophilic
1-Butyl-1-methylpyrrolidinium tris(pentafluoroethyl)trifluorophosphate	BMPL.FAP	$(C_2F_5)_3PF_3^-$	Hydrophobic
Tetrabutylammonium trifluoromethanesulfonate	TBA.OTf	$CF_3SO_3^-$	Hydrophilic

Table 1.6: Ionic liquids studied in initial Bunsen Reaction tests

While successfully in driving the Bunsen Reaction, none of the seven ionic liquids studied were found to be a suitable solvent for releasing HI from the liquid system.

However, hydrogen sulfide was found to elute rapidly from the liquid phase in several of these ionic liquids, which would ultimately lead to the development of the Sulfur-Sulfur Cycle.

With the failure to elute HI from the ionic liquid phase, the kinetics of the Bunsen reaction was explored. The hydrophobic ionic liquid BMIM OTF was chosen to act as the liquid media. Dilute solutions of iodine in the ionic liquid (.012M) were made in small glass vials and varying amounts of sulfur dioxide and water were added to initiate the Bunsen Reaction in order to determine the Arrhenius parameters of the Bunsen reaction. The Arrhenius pre-exponential term and activation energy derived from the experimental data were found to be 61,500 ± 4900 s^{-1} and 32.9 ± 3.0 kJ/mol, respectively.

With at least a basic understanding of the progress of the Bunsen reaction and the knowledge gained from the previous experiments that hydrogen sulfide, typically thought of as an undesirable side reaction, the previous researcher focused on the percent of sulfur dioxide that was converted into hydrogen sulfide. This was done by taking headspace samples of the equilibrated reaction system and monitoring the concentration of hydrogen sulfide via use of an SRI 8610 GC equipped with an FPD and a 2 meter Restek Rt-XLSulfur micropacked column. Table 1.7 shows the “high” and “low” values for the parameterization of these experiments while Figure 1.1 shows the results of the experiments.

Parameter	Low Value	High Value
Temperature	75˚C	100˚C
Water	1.85 M	3.70 M
Iodine	19.6 mM	39.3 mM
Sulfur Dioxide	0.1 M	0.2 M

Table 1.7: "High" and "Low" vales for parameters studied for hydrogen sulfide evolution

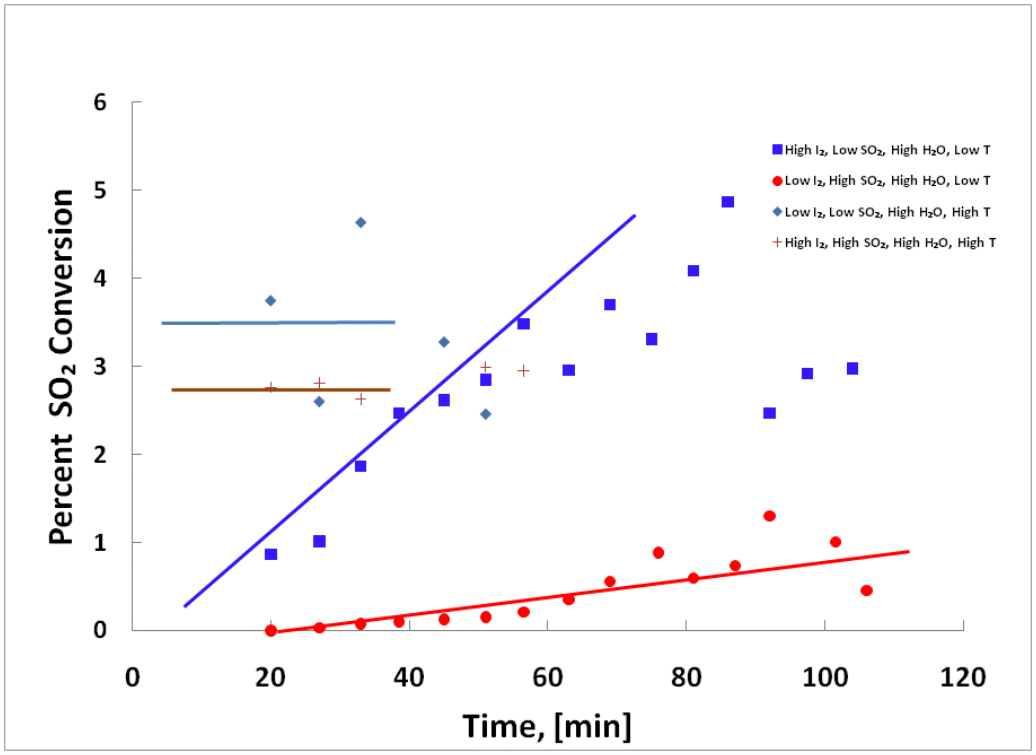

Figure 1.1: Experimental results for parameterization of iodine and sulfur dioxide concentration, as well as temperature.

From the experimental results in Figure 1.1, several conclusions can be drawn. An increase in iodine concentration and temperature results in faster evolution of hydrogen sulfide and that a large excess of water is needed to drive the reaction. From

these experimental results, namely the failure to liberate HI vapor from the ionic liquid phase and ready evolution of hydrogen sulfide from the reaction suggest the development of a new thermochemical cycle for hydrogen production that would utilize the "undesirable" side reaction that produces hydrogen sulfide in conjunction with the Bunsen reaction, shown in Equations 1.39-1.42.

$$4I_{2_{(IL)}} + 4SO_{2_{(IL)}} + 8H_2O_{(IL)} \rightarrow 4H_2SO_{4_{(IL)}} + 8HI_{(IL)} \quad \text{Eq. 1.39}$$

$$8HI_{(IL)} + H_2SO_{4_{(IL)}} \rightarrow H_2S_{(IL)} + 4H_2O_{(IL)} + 4I_{2_{(IL)}} \quad \text{Eq. 1.40}$$

$$3H_2SO_{4_{(IL)}} \rightarrow 3H_2O_{(g)} + 3SO_{2_{(g)}} + 1.5\ O_{2_{(g)}} \quad \text{Eq. 1.41}$$

$$H_2S_{(g)} + 2H_2O_{(g)} \rightarrow SO_{2_{((g))}} + 3H_{2_{(g)}} \quad \text{Eq. 1.42}$$

To determine the viability of this new process, the steam reformation of hydrogen sulfide (Eq. 1.42) was explored. Dilute hydrogen sulfide was run through a tubular quartz reactor at various temperatures, residence times, initial concentrations of water and catalysts, including bare quartz, nichrome, and molybdenum. Of these, experiments run at 900°C, a 200:1 excess of water to hydrogen sulfide and in the presence of molybdenum catalysts yielded roughly half of the stoichiometric amounts of hydrogen (1.5 moles) and sulfur dioxide (.5 moles) expected. Figure 1.2 shows the amount of sulfur dioxide produced at various temperatures and under the presence of various catalysts per initial amount of hydrogen sulfide.

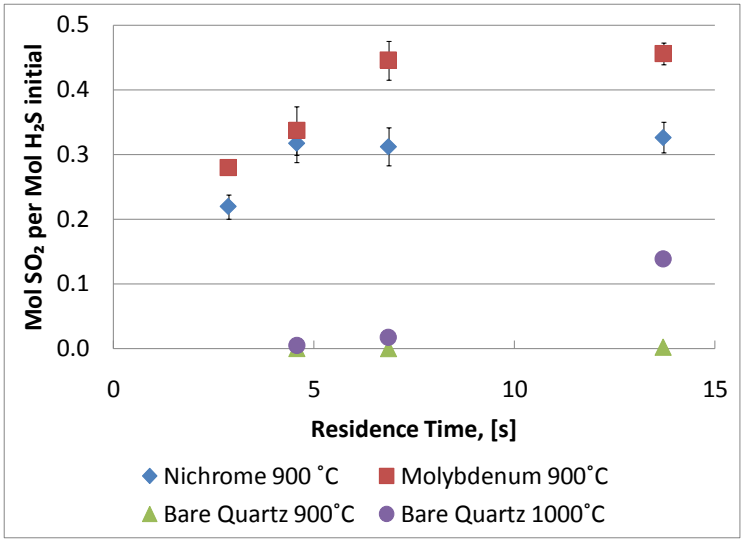

Figure 1.2: Moles of sulfur dioxide per mole of initial hydrogen sulfide produced via steam reformation under various conditions

To complete the summary of the previous work, two studies were undertaken. The first was a kinetic study performed on the steam reformation of hydrogen sulfide, which concluded that the Arrhenius parameters extracted from the experimental results matched up well with previously published data. The second was a theoretical estimation of the overall thermal efficiency of this new cycle. The calculations show, using a modest water to hydrogen sulfide ratio of 20:1, an upper bound thermal efficiency of approximately 37% using the higher heating value of hydrogen. This is a significant improvement over any currently existing renewable hydrogen production method. The overall upper-bound efficiency is estimated to be 59%, utilizing higher temperatures and higher water to hydrogen sulfide ratios, making the Sulfur-Sulfur cycle a viable candidate for future consideration as a thermochemical water splitting cycle.

2. Exergetic Efficiency

The conceptual layout of the Sulfur-Iodine Thermochemical Water Splitting Cycle is well known and it will be used as a general guide for the development of the new Sulfur-Sulfur Thermochemical Water Splitting Cycle. This new cycle consists of four major reactions: the Low Temperature Reaction, the Gasification of Sulfuric Acid, the Treatment of Sulfur Trioxide, and the Hydrogen Producing Reaction. The Low Temperature Reaction, for theoretical purposes, is the combination of two reactions in series, the previously coined Bunsen reaction from the Sulfur-Iodine Cycle, and what was previously thought of as an undesirable side reaction in the Sulfur-Iodine Cycle that produces hydrogen sulfide. These two reactions (Eq. 2.1 and 2.2) are shown below followed by the four major reactions that will be studied in this work (Eq. 2.3-2.6).

$$4I_{2_{(IL)}} + 4SO_{2_{(IL)}} + 8H_2O_{(IL)} \rightarrow 4H_2SO_{4_{(IL)}} + 8HI_{(IL)} \quad \text{Eq. 2.1}$$

$$8HI_{(IL)} + H_2SO_{4_{(IL)}} \rightarrow H_2S_{(IL)} + 4H_2O_{(IL)} + 4I_{2_{(IL)}} \quad \text{Eq. 2.2}$$

$$4SO_{2_{(IL)}} + 4H_2O_{(IL)} \rightarrow H_2S_{(IL)} + 3H_2SO_{4_{(IL)}} \quad \text{Eq. 2.3}$$

$$3H_2SO_{4_{(IL)}} \rightarrow 3SO_{3_{(g)}} + 3H_2O_{(g)} \quad \text{Eq. 2.4}$$

$$3SO_{3_{(g)}} \rightarrow 3SO_{2_{(g)}} + 1.5O_{2_{(g)}} \quad \text{Eq. 2.5}$$

$$H_2S_{(g)} + 2H_2O_{(g)} \rightarrow SO_{2_{((g))}} + 3H_{2_{(g)}} \quad \text{Eq. 2.6}$$

Eq. 2.3-2.6 form a closed loop in which 3 kmol of water enter the reaction system and 3 kmol of hydrogen and 1.5 kmol of oxygen exit the reaction system. This, along with all other thermochemical cycles, is an ideal solution to the generation of renewable energy without the emission of greenhouse gases. For the upcoming theoretical analysis, the four reaction steps are further described in Table 2.1.

Step	Reaction	Temp. (°C)	P kPa	Feed	Output
1	$4SO_{2(IL)} + 4H_2O_{(IL)} \rightarrow H_2S_{(IL)} + 3H_2SO_{4(IL)}$	100	101	$SO_{2(IL)}$ $H_2O_{(IL)}$	$H_2S_{(IL)}$ $H_2SO_{4(IL)}$
2	$3H_2SO_{4(IL)} \rightarrow 3SO_{3(g)} + 3H_2O_{(g)}$	160	101	$H_2SO_{4(IL)}$	$SO_{3(g)}$ $H_2O_{(g)}$
3	$3SO_{3(g)} \rightarrow 3SO_{2(g)} + 1.5O_{2(g)}$	850	101	$SO_{3(g)}$	$SO_{2(g)}$ $O_{2(g)}$
4	$H_2S_{(g)} + 2H_2O_{(g)} \rightarrow SO_{2_{((g))}} + 3H_{2(g)}$	827	101	$H_2S_{(g)}$ $H_2O_{(g)}$	$SO_{2(g)}$ $H_{2(g)}$

Table 2.1 – Main Steps in the S-S cycle with their reactions, T, P, and the physical inlets and outlets

2.1 Analysis

Efficient application and use of energy is one of the critical steps in any sustainable plan for meeting growing energy needs. In order to accurately compare a novel hydrogen producing process to those that have been previously studied, it is necessary to compare the two processes using either energetic or exergetic efficiencies. For this work, the four major reactions listed in Eq. 2.3-2.6 will have an exergetic analysis performed upon them to determine the useable work that is recovered via their chemical reactions compared to the work that is put into the system as heat. The theoretical analysis was based upon the work of Orhan et al. and their similar work on the Copper-Chloride thermochemical water splitting cycle.[89]

The basis for any efficiency analysis is through first principle mass and energy balances. Eq. 2.7 shows the energy balance for a steady state chemical process with no work interaction.

$$Q = \Sigma\left[n\left(\bar{h}_f^0 + \bar{h} - \bar{h}^0\right)\right]_P - \Sigma\left[n\left(\bar{h}_f^0 + \bar{h} - \bar{h}^0\right)\right]_R \quad \text{Eq. 2.7}$$

To find the heat transfer for each of the four major reactions, the enthalpy of formations and temperature dependent enthalpy change with respect to reference temperature are needed for each of the species in the feed and exit streams.

The exergy balance for an individual chemical reaction can be written as

$$\Sigma Ex_{in} - \Sigma Ex_{out} - Ex_{destruction} = \Delta Ex_{system} \quad \text{Eq. 2.8}$$

Where in this steady state case, $\Delta Ex_{system} = 0$. To assist in determining the exergy balance, the specific exergy of a species can be found through Eq. 2.9.

$$\overline{ex} = \left(\bar{h} - \bar{h}^0\right) - T_0(\bar{s} - \bar{s}_0) + \frac{V^2}{2} + gz + \overline{ex}^{ch} \quad \text{Eq. 2.9}$$

The final term in Eq. 2.9 is chemical exergy, which is a tabulated value that can be found in the literature, while the terms before it can be called the thermomechanical exergy.[106] For all of the chemical reactions in the S-S cycle, it is reasonable to assume that the specific kinetic ($\frac{V^2}{2}$) and potential (gz) exergies are negligible. Combining Eq. 2.8 and 2.9 yields a more complete exergy balance for any given process.

$$\overline{ex}_{dest.} = \Sigma n\left[\left(\bar{h} - \bar{h}^0\right) - T_0(\bar{s} - \bar{s}_0) + \overline{ex}^{ch}\right]_i - \Sigma n\left[\left(\bar{h} - \bar{h}^0\right) - T_0(\bar{s} - \bar{s}_0) + \overline{ex}^{ch}\right]_o + \left(1 - \frac{T_0}{T_{rxn}}\right)Q \quad \text{Eq. 2.10}$$

In Eq. 2.10 Q is the heat flow into or out of a system, dependent upon whether the reaction is endothermic or exothermic, respectively. As an example, Eq. 2.10 is applied to the Hydrogen Producing Reaction.

$$\overline{ex}_{dest} = n_{H_2S}\left[\left(\bar{h} - \bar{h}^0\right) - T_0(\bar{s} - \bar{s}_0) + \overline{ex}^{ch}\right]_{H_2S} + n_{H_20}\left[\left(\bar{h} - \bar{h}^0\right) - T_0(\bar{s} - \bar{s}_0) + \overline{ex}^{ch}\right]_{H_2O} - n_{H_2}\left[\left(\bar{h} - \bar{h}^0\right) - T_0(\bar{s} - \bar{s}_0) + \overline{ex}^{ch}\right]_{H_2} - n_{SO_2}\left[\left(\bar{h} - \bar{h}^0\right) - T_0(\bar{s} - \bar{s}_0) + \overline{ex}^{ch}\right]_{SO_2} + (1 - \frac{T_0}{T_{rxn}})Q \quad \text{Eq. 2.11}$$

After the completion of the energy and exergy balances, the necessary entropy and enthalpy values are determined from the Shomate equations:

$$\bar{h} - \bar{h}^0 = AT + B\frac{T^2}{2} + C\frac{T^3}{3} + D\frac{T^4}{4} - E\frac{1}{T} + F - H \quad \text{Eq. 2.12}$$

$$\bar{s} = Aln(T) + BT + C\frac{T^2}{2} + D\frac{T^3}{3} - E\frac{1}{2T^2} + G \quad \text{Eq. 2.13}$$

Where A, B, C, D, E, F, G, and H are constants and T is 1/1000 of the specified reaction temperature in K. With the specific enthalpy and entropy values, the thermomechanical exergy for each chemical species can be calculated. To finalize the calculation of the specific exergy of a compound, the standard exergy value for the compound must be looked up in literature. Values for the enthalpy change and standard entropy for liquid sulfuric acid were taken from the work of Giauque, et al, where the sulfuric acid was assumed to be the 6.5 hydrarte.[107] A summary of the enthalpy, entropy, and standard chemical exergy of the compounds in Eq. 2.3-2.6 is shown in Table 2.2.

Compound	$\bar{h}_f^0$ (kJ/kmol)	$\bar{s}_0^f$ (kJ/kmol K)	$\overline{ex}^{ch}$ (kJ/kmol)
$H_2O\ (g)$	-241,818	188.84	9,500
$H_2O\ (l)$	-285,830	69.65	900
$SO_2\ (g)$	-296,840	248.22	313,400
$H_2SO_4\ (l)$	-814,000	157	163,730
$H_2SO_4\ (g)$	-735,130	298.78	163,730
$H_2S\ (g)$	-20,630	206	812,000
$SO_3\ (g)$	-395,770	256.77	244,255
$O_2\ (g)$	0	205.07	3,970
$H_2\ (g)$	0	130.68	236,090

Table 2.2: Summary of enthalpy of formation, standard entropy, and standard chemical exergy for the major compounds in the S-S Cycle

With all of the pertinent thermodynamic data, Eq. 2.7, 2.10, 2.12, and 2.13 can be solved for each individual chemical species, the four major reactions, and for the total process. The total exergetic efficiency can be calculated through comparing the exergy entering and leaving the system, while taking the heat flow into account

$$\eta_{ex} = \frac{\overline{ex}_{out}}{\overline{ex}_{in}} \qquad \text{Eq. 2.14}$$

2.2 Results and Discussion

The summary of the reaction temperatures, heat flow, inlet exergy, outlet exergy, exergetic efficiency for each process and total exergetic efficiency is show in Table 2.3, utilizing a reference temperature of 298 K.

Reaction	Temp (K)	Q (kJ/kmol)	$\overline{ex}_{in}$ (kJ/kmol)	$\overline{ex}_{out}$ (kJ/kmol)	η_{ex}
$4SO_{2_{(IL)}} + 4H_2O \rightarrow H_2S_{(IL)} + 3H_2SO_{4_{(IL)}}$	373	94,474	420,217	407,274	.791
$3H_2SO_{4_{(IL)}} \rightarrow 3SO_{3_{(g)}} + 3H_2O_{(g)}$	433	97,020	165,993	255,910	.973
$3SO_{3_{(g)}} \rightarrow 3SO_{2_{(g)}} + 1.5O_{2_{(g)}}$	1173	96,782	274,831	344,436	.927
$H_2S_{(g)} + 2H_2O_{(g)} \rightarrow SO_{2_{((g))}} + 3H_{2_{(g)}}$	1100	75,163	293,419	359,888	.976
Total					.697

Table 2.3: Reaction temperature, heat flow, inlet/outlet exergy, and exergetic efficiency for the major reactions in the S-S Cycle

For the "standard" temperatures used for this analysis, an exergetic efficiency of 69.73% was found, which compares favorably to published literature of other thermochemical cycles.[30,89]

To continue the analysis of the four major reactions and their efficiencies, a parametric study was performed by altering the reaction and reference temperature of each reaction and determining the effect of the change on the exergetic efficiency. The results are shown below in Figure 2.1A-2.1D.

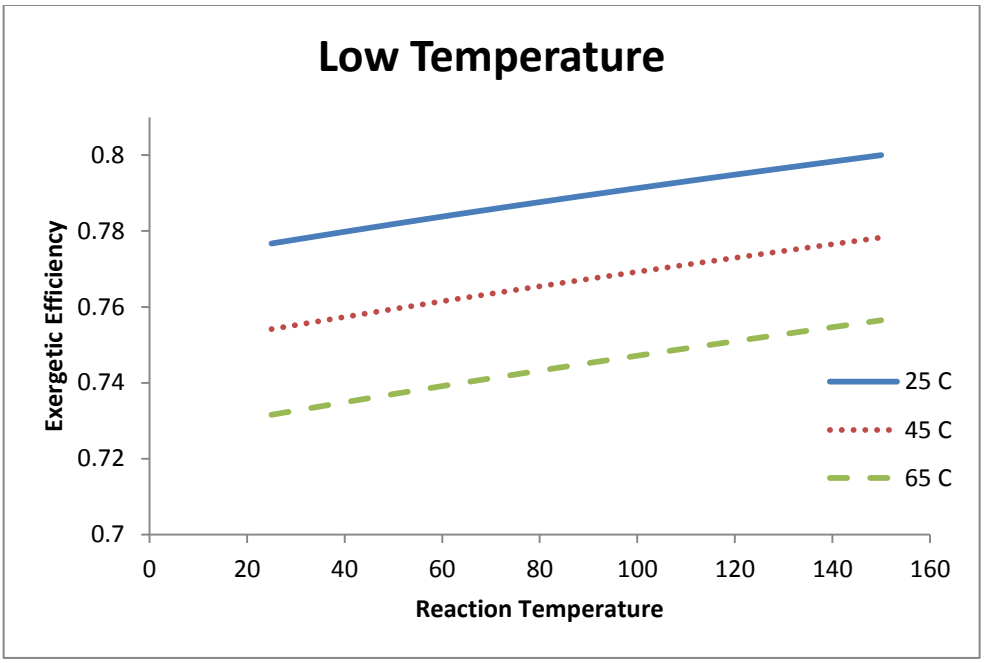
Low Temperature
Exergetic Efficiency
0.8
0.78
0.76
0.74
0.72
0.7
0
20
40
60
80
100
120
140
160
Reaction Temperature
25 C
45 C
65 C

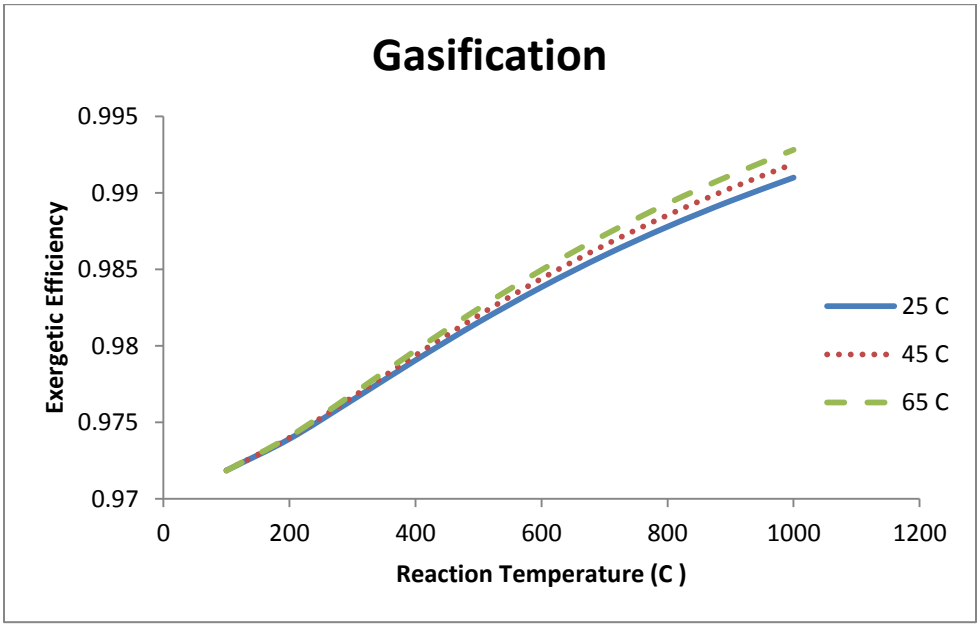
Gasification
Exergetic Efficiency
0.995
0.99
0.985
0.98
0.975
0.97
0
200
400
600
800
1000
1200
Reaction Temperature (C)
25 C
45 C
65 C

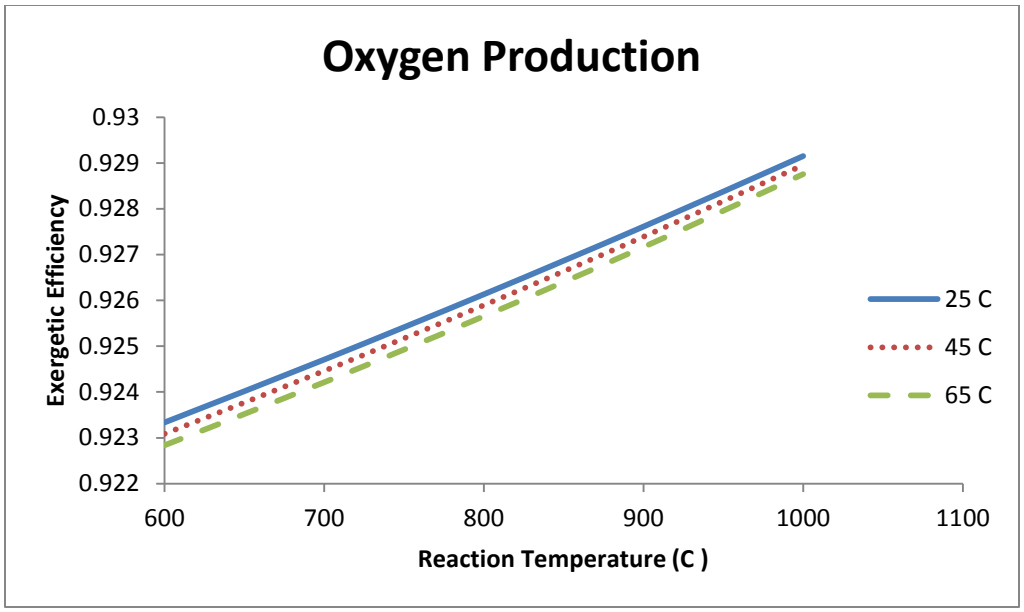

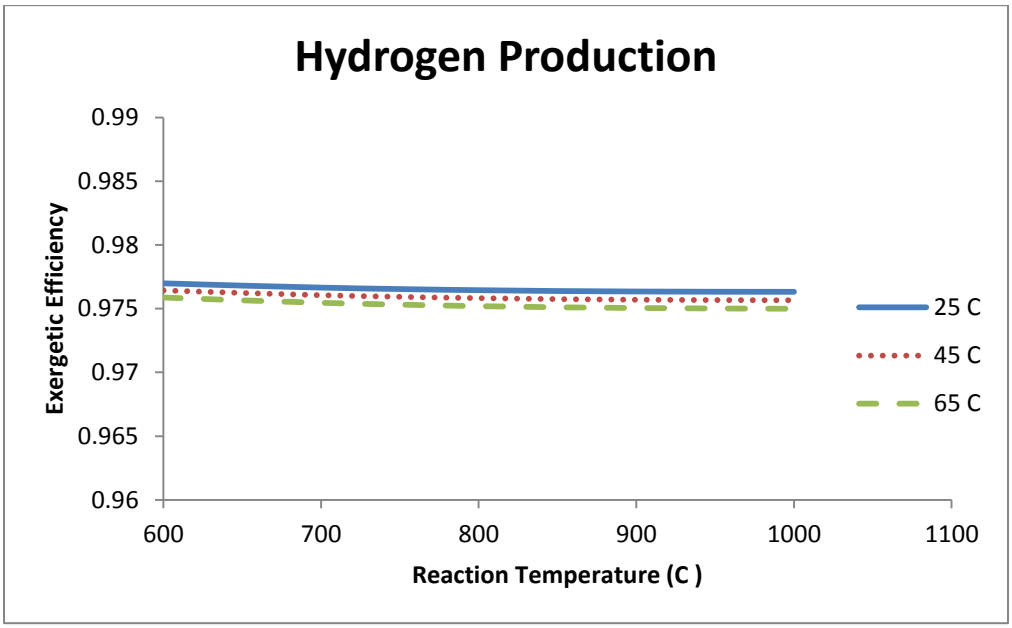

Figure 2.1A-2.1D: Effect of individual reaction temperature and reference temperature on the individual reaction exergetic efficiency

Figure 2.1A-2.1D shows the change in total exegetic efficiency over the temperature ranges of 25-150°C, 100-1000°C, 600-1000°C, and 600-1000°C for the Low

Temperature Reaction, Gasification of Sulfuric Acid, Oxygen Producing, and Hydrogen Producing Reactions, respectively.

As can be seen in the above Figures, the reaction that is most responsive to a change in either the reaction or reference temperature is the Low Temperature Reaction, increasing by nearly 2.5% with an increase in the reaction temperature of 125 K. The exergetic efficiency of the Gasification of Sulfuric acid reaction increases by approximately 2%, but does so over a temperature change of 900 K. The change reaction temperature appears to have minimal effect on the Oxygen Producing and Hydrogen Producing reactions, changing by less than .1% over a 500 K increase.

The reference temperature appears to have little effect on the Gasification of Sulfuric Acid, the Oxygen Production, or the Hydrogen Production reactions, altering the exergetic efficiencies by minimal amounts. However, the reference temperature of the Low Temperature reaction changes the exergetic efficiency by over 2% for every 20 K increase in temperature. The changes in the exergetic efficiency of the Low Temperature reaction could possibly be attributed to the change in the exergy of destruction of the liquid water, shown in Table 2.4.

Reaction T (°C)	$ex_{dest.}$ H_2O (l)	$ex_{dest.}$ SO_2 (g)	$ex_{dest.}$ H_2S (g)	$ex_{dest.}$ H_2SO_4 (l)	N($ex_{dest.}$ H_2O (l))	N($ex_{dest.}$ SO_2 (g))	N($ex_{dest.}$ H_2S (g))	N($ex_{dest.}$ H_2SO_4 (l))
323	1180.82	417923.6	270702.3	136489.2	0.622369	0.999052	0.999695	1
348	1460.54	418076.9	270734.4	136489.2	0.769799	0.999419	0.999814	1
373	1897.3	418320.2	270784.8	136489.2	1	1	1	1

Table 2.4: Exergy of destruction of all species in Low Temperature reaction, with "normalized" exergy displaying relative change over increase in reaction temperature

Table 2.4 shows that the reaction temperature has what amounts to negligible effects on the exergy of destruction of the sulfur bearing compounds in the Low Temperature reaction, whereas the exergy of liquid water can change upwards of 38%

with a 50 K increase in temperature. The only other aspect of the Low Temperature reaction that changes with respect to the reaction temperature is the theoretical heat required to make the spontaneous, shown below in Figure 2.2.

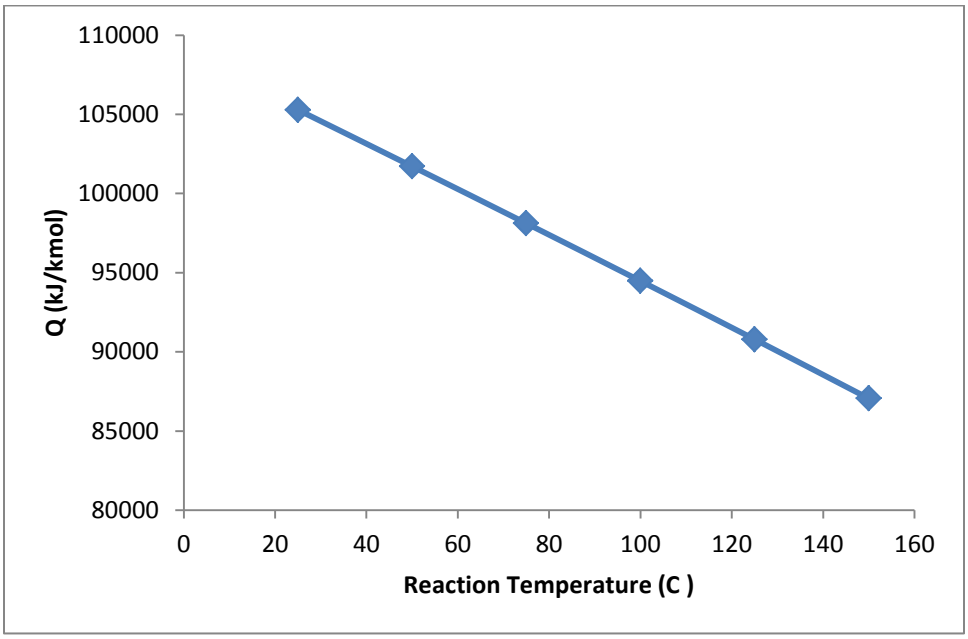

Figure 2.2: Effect of reaction temperature on theoretical heat required for Low Temperature reaction

As the reaction temperature increases, the reaction heat for the Low Temperature reaction step decreases with a nearly linear relation. The decrease in the heat load and the high variation in the exergy of destruction associated with liquid water implies that these two operating parameters play the most significant role in the Low Temperature reaction and warrant experimental observation.

2.3 Conclusions

A thorough thermodynamic analysis of the four major reactions of the theoretical sulfur-sulfur thermochemical water splitting cycle for hydrogen production has been performed. The study included energetic and exergetic balances on the major

reactions, and considered the operational conditions of the individual steps. The results of the analysis allow several conclusions to be drawn about this new theoretical cycle. The information garnered from this work strongly suggests that this newly developed cycle could be a potentially effective method of large scale, clean hydrogen production with efficiencies that are very comparable to other published work. For the "standard temperatures" of each reaction, an overall exergetic efficiency of 69.68% was found. Similar work done by Orhan found an overall exergetic efficiency of 48% for the Copper-Chlorine Thermochemical Water Splitting Cycle.[89]

More specifically, the overall efficiency was determined by parametrically altering the reference and reaction temperature of the four major reactions. This ultimately lead to the conclusion that the exergetic efficiency of the Low Temperature Reaction, involving the combination of two reactions in series, changes by over 2.5% over a temperature change from reference (25°C) to the upper limit for this reaction in this study (150°C). This increase dwarfs the other efficiency increase with respect to reaction temperature of the other three reactions, even when the other reactions had substantially larger temperature increases. An increase in the reference temperature had minimal effect on all reactions with the exception of the Low Temperature reaction, where an increase in reference temperature of 20 K decreased the efficiency of the reaction by over 2%.

This work also has a great effect on the future of this theoretical cycle. With the favorable theoretical exergy balance, there is enough evidence to begin experimentally exploring this new thermochemical cycle, specifically the study of the Low Temperature reaction.

3. EXPERIMENTAL RESULTS AND DISCUSSION

Previous work has laid out the basic chemical model for the development of a new thermochemical cycle for hydrogen production. This approach seeks to minimize some of the difficulties associated with the well-known Sulfur-Iodine cycle, including material compatibility and seeks to eliminate the need to separate sulfuric and hydroiodic acids. The goal of this work is to further explore the capability and viability of the low temperature reaction pair described in Eq. 3.1 and 3.2.

$$4I_{2_{(IL)}} + 4SO_{2_{(IL)}} + 8H_2O_{(IL)} \rightarrow 4H_2SO_{4_{(IL)}} + 8HI_{(IL)} \qquad \text{Eq. 3.1}$$

$$8HI_{(IL)} + H_2SO_{4_{(IL)}} \rightarrow H_2S_{(IL)} + 4H_2O_{(IL)} + 4I_{2\,(IL)} \qquad \text{Eq. 3.2}$$

Initial experiments utilized the high extinction coefficient of iodine by using UV-visible spectroscopy to monitor the reaction progress. The disappearance of iodine in the reaction system would directly relate to the Bunsen Reaction (Eq. 3.1) and the reappearance would be attributed to the Hydrogen Sulfide Production Reaction (HSPR, Eq. 3.2). The monitoring of the iodine UV/Vis absorption would allow for the tracking of the reaction progression and allow for the determination of kinetic parameters.

3.1 "Standard" Reaction Conditions

To begin the experimental aspect of this project, a "standard" set of experiments were performed. The "standard" refers to a concentration ratio of water to iodine and sulfur dioxide to iodine in which the remainder of experiments would be built upon or compared to.

3.1.1 Materials and Methods

To determine experimental kinetics for the pair of low temperature reactions, two solutions were prepared in separate sealed containers. For each experimental run, .07 grams of solid iodine (99.5%, Fluka) was dissolved in 4 milliliters of the hydrophobic

ionic liquid 1-butyl-3-methylimidazolium bis(trifluorosulfonyl) imide, hereafter referred to as BMIM TF2N (Aldirch), in a 10 milliliter amber vial. The amber vial was sealed with a silicone septum after a stir bar had been placed inside. The vial was placed into a specially crafted aluminum heating mantle, whose temperature was monitored through a thermocouple and heating cartridge attached to a temperature controller. The entire unit was placed on top of a stir plate to ensure mixing.

To create the sulfur dioxide solution, 1 milliliter of BMIM TF2N was injected into a sealed 2 milliliter HPLC sampling vial. Anhydrous sulfur dioxide (Airgas) was bubbled through the vial for 10 minutes to saturate the ionic liquid, venting into the fume hood. The venting needle that was placed in the septa cap of the sampling vial was removed and the sulfur dioxide gas was allowed to equilibrate inside the vial for an additional 10 minutes. This solution was remade approximately every week, or as needed.

When the iodine had fully dissolved in the ionic liquid at the required temperature, .5 milliliters of HPLC grade water (Mallinckrodt Chemicals) was injected through the silicone septum and allowed to mix with the iodine/ionic liquid solution for approximately 20-30 minutes to get the entire solution to reaction temperature. The sulfur dioxide/ionic liquid solution was placed on top of the heating mantle and allowed to reach reaction temperature as well.

While the two solutions were allowed to reach the respective reaction temperature, an Avantes AvaSpec-3648 UV/Vis spectrophotometer was turned on and the Avantes Avalight DHc (halogen and deuterium) light bulb was allowed to warm up. A 4 milliliter quartz cuvette was filled with 2 milliliters of dichloromethane (Aldrich) and fitted with a stir bar, which served as a background and solvent for the spectrophotometer measurements. The initial concentration of iodine was found by removing a 5 microliter aliquot from the iodine, water and ionic liquid solution and injected into the quartz cuvette. The spectrum was allowed to equilibrate and mix for

approximately 30 seconds and was saved through the computer program that was linked to the Avantes spectrophotometer. Previous work had indicated that the iodine peak at 294 nanometers was the most consistent peak to monitor the UV concentration.

After sufficient mixing and heating time .2 milliliters of the sulfur dioxide/ionic liquid solution were injected into the sealed amber vial, marking the injection as time=0. The final concentration ratios of water to iodine and sulfur dioxide to iodine were approximately 120:1 and 2:1, respectively. Aliquots of 5 microliters were continually removed from the reaction vessel and injected into the dichloromethane filled cuvette, where their respective spectrum were measured and saved. This process was repeated with the same concentrations of the initial reactants, but at temperature ranging from 35-50°C for the Bunsen reaction and 75-105°C for the hydrogen sulfide production reaction. The differences in temperature relate to the speed of each reaction and were chosen to allow for the simple UV measurements to monitor the iodine concentrations. The Bunsen reaction is has been found to be substantially faster than the hydrogen sulfide production reaction, and therefore needed a lower reaction temperature in order to be measured through this method.

3.1.2 Results and Discussion

A sample representation of how a reaction proceeds is shown below in Figure 3.1.

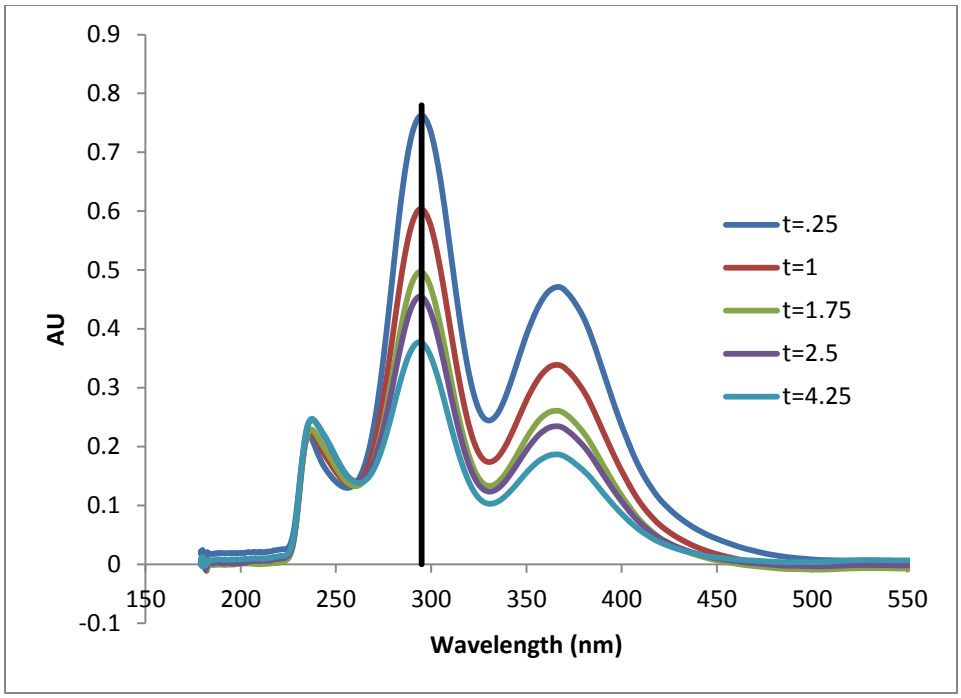

Figure 3.1: Sample graph showing the change in the absorbance of iodine over time (t is in minutes)

Figure 3.1 demonstrates that, after the introduction of sulfur dioxide into the reaction system, the iodine concentration, suggesting the progression of the Bunsen reaction. Progression such as this was used to track the iodine absorbance through all of the subsequent experiments.

Beer's Law was used to associate the spectrophotometer data with iodine concentration, as shown in Eq. 3.3, where A is equal to the peak absorbance in absorbance units (A.U.), e is the molar absorptivity (L mol-^{1} cm^{-1}), b is the path length in centimeters, and C is the concentration (mol L^{-1})

$$A = ebC \qquad \text{Eq. 3.3}$$

This equation can be used to develop calibration curves to relate absorption to concentration quickly. However, Eq. 3.3 can be simplified even further through

normalization, eliminating the need to know the path length or the molar absorptivity. This is shown in Eq. 3.4.

$$\frac{A_n}{A_0} = \frac{ebC_n}{ebC_0} = \frac{C_n}{C_0} \qquad \text{Eq. 3.4}$$

This manipulation removes the need to find the molar absorptivity and path length as long as an initial concentration is known. This relationship is used for all of the iodine based experiments as an initial concentration and absorbance of iodine, as well as the time=*n* absorbance of iodine during the reaction, are known.

The absorption measurements collected from the "Sample" experiments was fitted to a pseudo-first order, with respect to iodine, kinetic equation as it was consumed (for the Bunsen reaction) and regenerated (for the HSP reaction), shown in Eq. 3.5, where C_{I_2} is iodine concentration (M), k_m is the reaction rate constant of either the Bunsen or HSP reaction (min^{-1}) and t is time (min). This model assumes that the concentrations of water and sulfur dioxide remain approximately the same.

$$\frac{dC_{I_2}}{dt} = k_m C_{I_2} \qquad \text{Eq. 3.5}$$

Eq. 3.5 can be solved and manipulated to introduce absorption into the equation (through Eq. 3.4) and presented in such a way that it will be useful for comparing experimental data. The result is shown in Eq. 3.6, where $A_{I_{2_n}}$ is the iodine absorbance at time n and A_0 is the initial iodine absorbance.

$$\ln\left(\frac{A_{I_{2_n}}}{A_0}\right) = -k_m t \qquad \text{Eq. 3.6}$$

By plotting the natural log of the normalized iodine absorbance against time, the slope of the resulting linear relationship results in the reaction rate constant for that particular experiment. An example for the Bunsen reaction and HSP reaction are shown in Figure 3.2A and B, respectively.

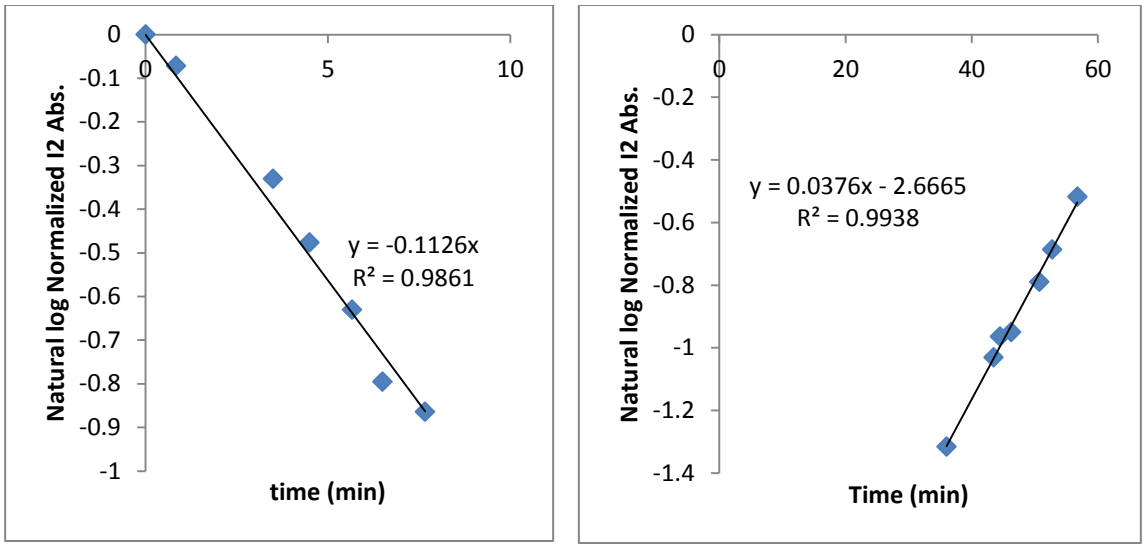

Figure 3.2A/B: Experimental data plotted to extract the reaction rate constant for the Bunsen reaction (left, T=35°C) and the HSP reaction (right, T=98°C)

The reactions rate constants that are extracted from the various triplicate temperature measurements can be further manipulated into determining the Arrhenius parameters for each reaction. The Arrhenius equation is shown in Eq. 3.7 below, where k is reaction rate constant (min^{-1}), E_a is the activation energy in Joules/mole, R is the universal gas constant (8.314 J mol^{-1} K^{-1}), T is temperature in Kelvin, and k_0 is the pre-exponential term (min^{-1}).

$$\ln(k) = -\frac{E_a}{R}\frac{1}{T} + \ln(k_0) \qquad \text{Eq. 3.7}$$

The activation energy and pre-exponential terms for the Bunsen reaction are readily attainable through linearly plotting the average reaction rate constant against its respective temperature. However, the Arrhenius parameters for the HSP reaction require further manipulation due to the nature of the experimental design. Within the reaction vessel, there is an excess of both sulfur dioxide and water, with iodine being both the limiting reagent and the species that is being tracked to monitor reaction progression. Within the reaction vessel, it follows that both the Bunsen and HSP

reaction are progressing at the same time. This can be seen in Figure 3.3, where there is a substantial "equilibration" period between the initial stages where the Bunsen reaction dominates and when it appears that the HSP reaction begins to dominate the equilibrium.

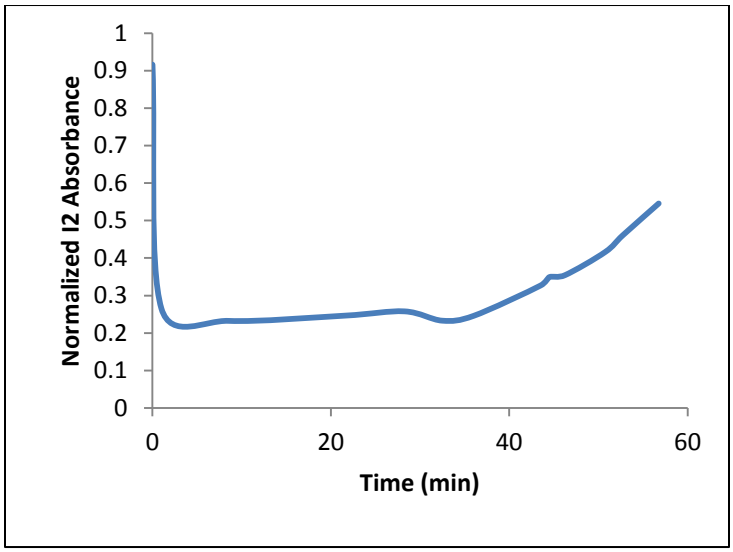

Figure 3.3: Reaction progression over time

The equilibration period shown in Figure 3.3 (from approximately 2 minutes to approximately 35 minutes) suggest that iodine is being both consumed and regenerated at an approximately equal rate. If both reactions are proceeding simultaneously, it suggests that the reaction rate constant of the HSP reaction extracted from the experimental data is the *effective* reaction rate constant, which take the continuation of the Bunsen reaction into account. The real reaction rate constant for the HSP reaction can be found as shown in Eq. 3.8, where k_{actual} is the real reaction rate constant for the HSP reaction, $k_{effective}$ is the reaction rate constant extracted from the experimental data and $k_{Bunsen}(T)$ is the reaction rate constant of the Bunsen reaction at the specified temperature, extrapolated from the activation energy and pre-exponential term found from the experimental data.

$$k_{2_{actual}} = k_{2_{effective}} * k_{Bunsen}(T) \quad \text{Eq. 3.8}$$

This same process is not done for the Bunsen reaction because the time frame in which the kinetic data for the Bunsen reaction is collected is so small that the HSP reaction is believed to not have any effect on the progression. Table 3.1 shows the relationship between the effective and actual reaction rate constants for the HSP reaction, as well as the substantial difference in the magnitude of the Bunsen and HSP reactions are higher temperatures.

Temperature (K)	$k_{2_{effective}}$ (min^{-1})	$k_{Bunsen}(T)$ (min^{-1})	$k_{2_{actual}}$(min^{-1})
348	.0263	8.91	.2346
363	.0333	33.55	1.118
371	.0369	65.12	2.401

Table 3.1: Relationship between effective and actual reaction rate constants for HSP reaction for "standard" conditions

With the actual reaction rate constants for the HSP reaction determined for the "standard" condition, the Arrhenius parameters can be found by plotting the natural log of the reaction rate constants against the inverse of temperature in Kelvin. Figure 3.4 shows these plots, with their respective error multiplied by 100 in order to be visible.

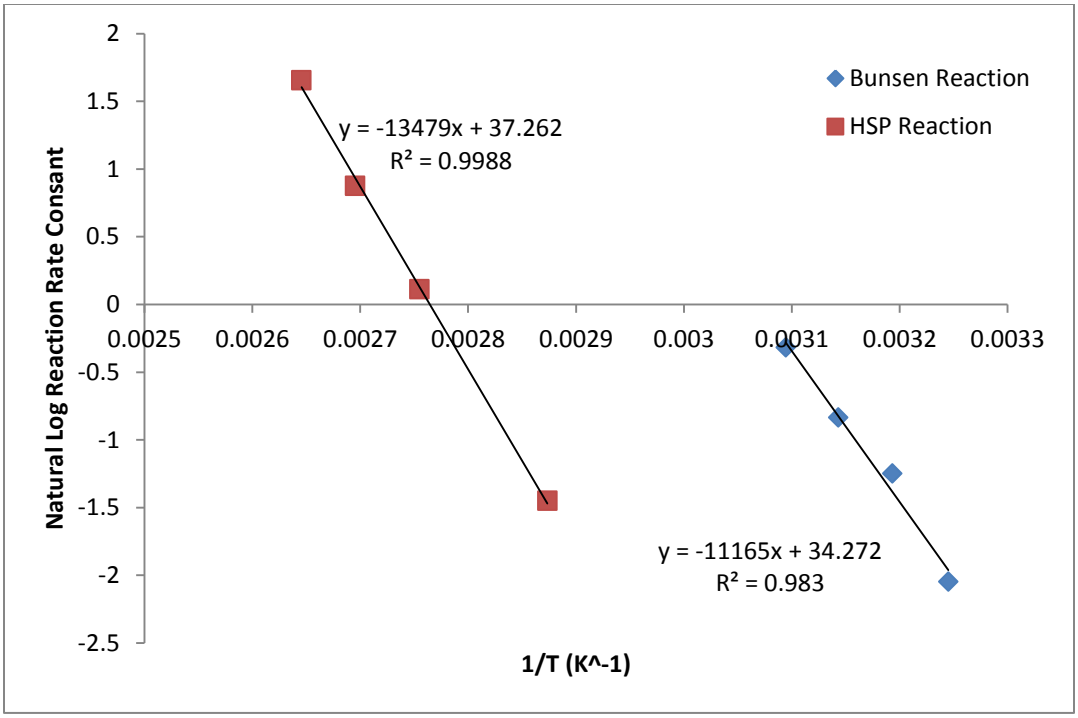

Figure 3.4: Arrhenius Plot for "standard" reaction conditions for Bunsen and HSP reactions. Error bars are present but too small to discern on the plot.

From Figure 3.4, the slope and y-intercept of the linear regression equations can be simply converted into the appropriate Arrhenius terms for both reactions. For the Bunsen reaction, the activation energy and pre-exponential term were found to be 92.83 kJ/mole and 7.65E+14 min^{-1}, while for the HSP reaction, they were determined to be 117.09 kJ/mole and 7.73E+16 min^{-1}.

3.2 Iodine Recovery

Through combining and balancing Eq. 3.1 and 3.2, the net chemical reaction can be determined.

$$4SO_{2_{(IL)}} + 4H_2O_{(l)} \rightarrow H_2S_{(IL)} + 3H_2SO_{4_{(IL)}} \qquad \text{Eq. 3.9}$$

As there are no species that contain iodine in the net reaction, it follows that, should the pair of reactions run to completion, 100% of the initial molecular iodine will be recovered. This is important, as it would not require any extra processing to recover the iodine, eliminating one of the major steps in the original Sulfur-Iodine process, and would allow the iodine to remain in the ionic liquid/water solution.

3.2.1 Materials and Methods

The materials and methods for the iodine recovery experiments are generally the same as described in Section 3.1.1. There are only slight differences in the methodology. Three temperatures were used for this study: 75, 90, and 105°C. Concentrations of iodine, water, and sulfur dioxide are as described above. UV absorption spectra were monitored through the previously described method until the absorption of iodine returned to its initial concentration or reached a stable maximum. The aliquots from each experimental run were taken at predetermined times such that an average representation of the iodine recovery at each temperature could be determined.

3.2.2 Results and Discussion

Through triplicate runs at each of the listed temperatures, it was found that the initial amount of molecular iodine in the reaction vessel was completely recovered. Figure 3.5 shows the average representations of the three temperatures.

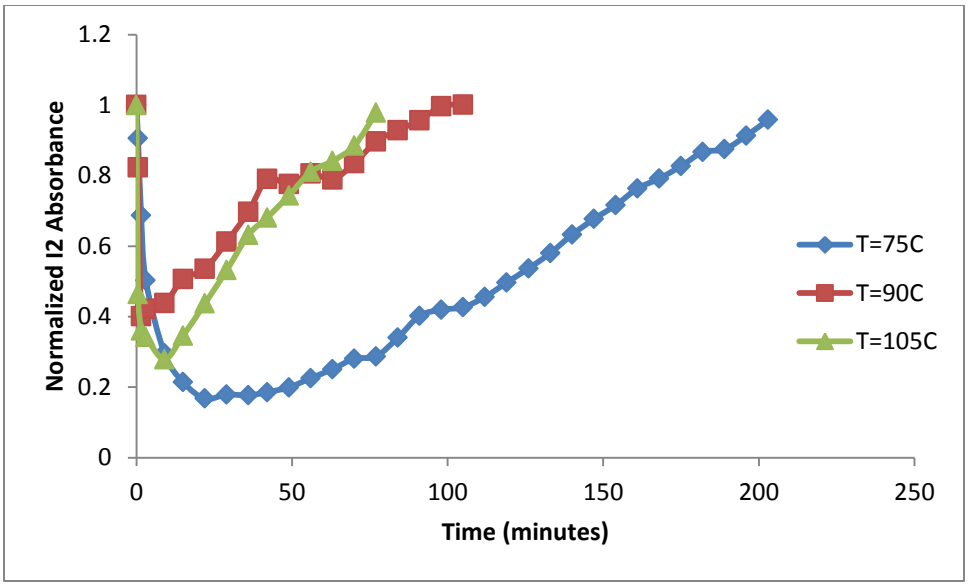

Figure 3.5A: Average representation of iodine recovery at various temperatures

The time needed to completely recover the initial iodine was found to be 77, 105, and 203 minutes for the temperatures of 105, 90, and 75°C, respectively, as shown in Figure 3.6.

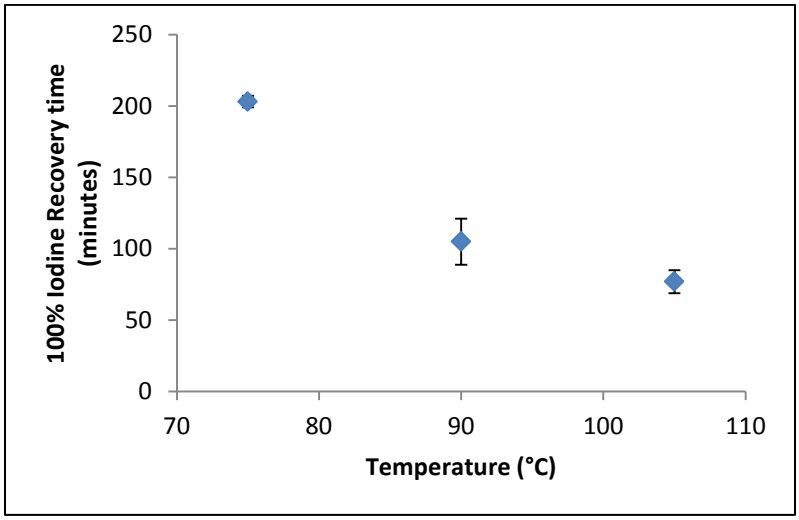

Figure 3.5B: Time necessary to regenerate initial iodine concentration at various temperatures

It appears that there is an exponential growth in the time needed to recover the iodine with a fairly small change in temperature. It would follow that continuing to raise the temperature would shorten the amount of time needed to recover the iodine to a point. This point would theoretically be at such a temperature that the water used to catalyze the Bunsen reaction would have a vapor pressure high enough that the progression of the overall reaction would slow. The results of this group of experimental runs led to the exploration of the effects of water on the reaction system.

3.3 Effects of Water on Kinetics

3.3.1 Materials and Methods

The materials and methods for the iodine recovery experiments are generally the same as described in Section 3.1.1. There are only slight differences in the methodology. The concentration of water was changed by altering the amount of water injected into the reaction vessel: using the already determined .5 mL and varying it by adding .4 mL and .3 mL of water. While the addition of varying amounts of water changes the overall volume, it will only do so by less than 2.5%. Operating under the assumption that most of the dissolved species (iodine and sulfur dioxide) exist in the ionic liquid phase, the experiments can progress as though there was no change in the overall volume.

3.3.2 Results and Discussion

With a “standard” to base future results upon, the effects of water on the kinetics of both the Bunsen and HSP reaction were explored. With the ratio of water to iodine in the “standard” being approximately 120:1, ratios of 105:1 and 93:1 were used in this next bout of experiments. Arrhenius parameters were found for both reactions, and the results are shown in Figure 3.6A and B.

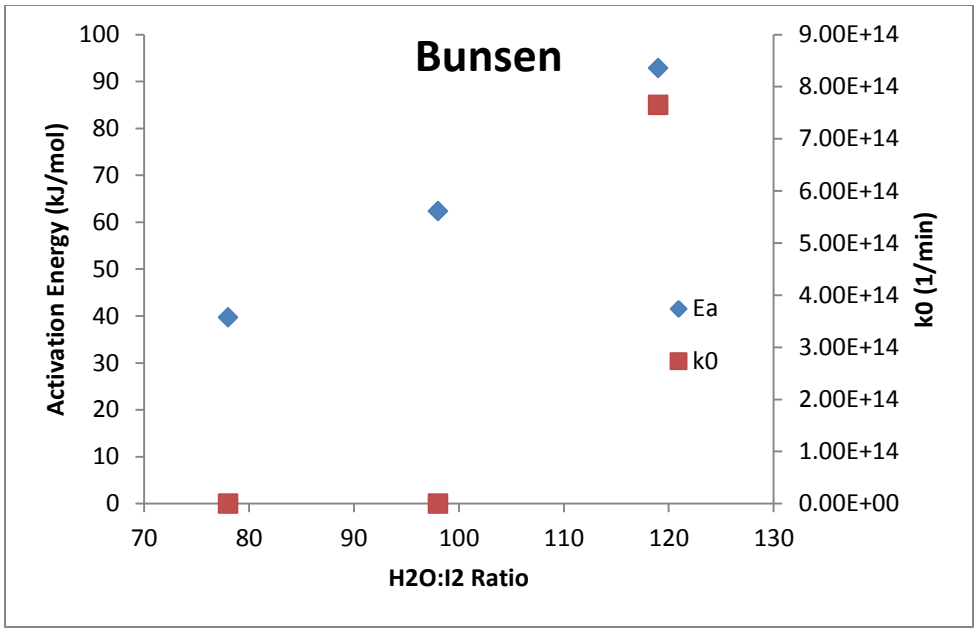

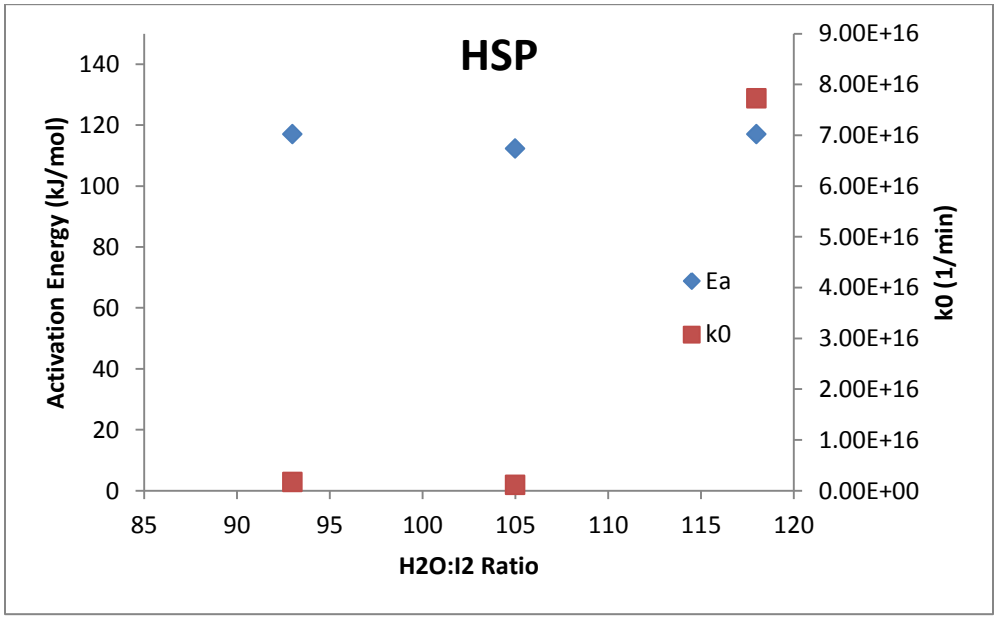

Figure 3.6A/B: Top – Change in activation energy and pre-exponential term for Bunsen reaction. Bottom - Change in activation energy and pre-exponential term for HSP reaction.

In both reactions the water drastically changes the pre-exponential term, changing it by an order of magnitude for each (10E+14 to +15 for the Bunsen reaction

and 10E+15 to +16 for the HSP reaction). The activation energy for the Bunsen reaction changes as well, increasing over the water to iodine ratio range while the HSP reaction activation energy remains approximately the same.

While this data may be useful for modeling or comparative purposes, it tells little of what is physically happening inside the reaction vessel. In order to better understand the kinetics of the two step reaction that is being viewed, the actual reaction rate constants for both reactions were compared with rising temperature and water to iodine ratios. The results are shown in Figure 3.7A and B

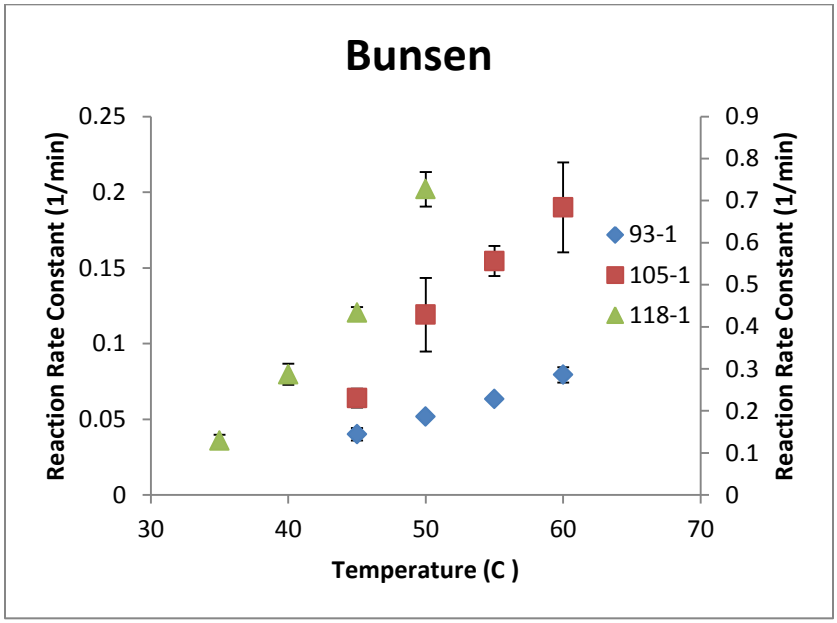

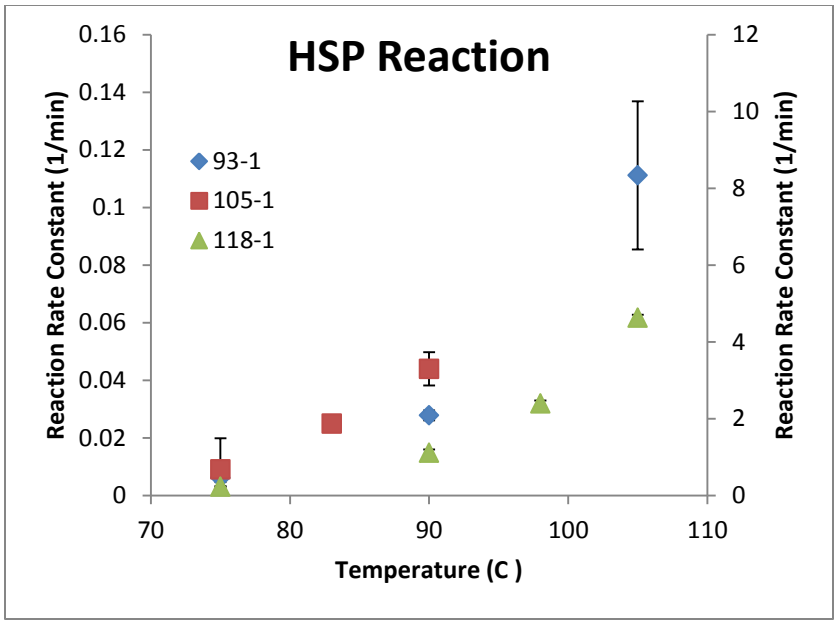

Figure 3.7A/B: Top – Reaction rate constants across various temperature and water to iodine ratio for the Bunsen reaction. Bottom – Same for HSP reaction. The reaction rate constants for the water to iodine ratio of 118:1 are on the secondary y-axis for both figures.

Figures 3.7A and B show that the reaction rate constants for both reactions increase with both temperature, as would be expected, and with an increase in the concentration of water. The increase in the reaction rate constant would be expected for the Bunsen reaction, purely do to mass action: an increase in the concentration of one of the initial reactants would drive the reaction forward. This can be seen in Figure 3.7A, especially in combination with an increase in temperature. There are apparent exponential rises in all three water to iodine ratios, but with the highest water to iodine ratio and the highest temperature, the reaction rate constant is nearly two orders of magnitude higher than the next highest constant.

While the results of the Bunsen reaction were expected, the results of the HSP reaction were initially surprising. Through the simple idea of mass action, it would be

expected that the addition of large quantities of water to the reaction vessel would inhibit the HSP reaction progression as water is a product. However, a secondary force appears to come into play and overwhelm the mass action. With the exponential increase in the reaction rate constant of the Bunsen reaction, it would follow that more of the Bunsen reaction products and the initial HSP reaction reactants (hydrogen iodide and sulfuric acid) were formed at a much higher rate. This increase in formation of the HSP reactants would drive the HSP reaction overall, even if it may be inhibited by the presence of the excess water, by mass action.

This can be seen in the actual reaction rate constants as well, as seen in Table 3.2A and the ratio of the Bunsen reaction rate constants against the HSP reaction rate constants in Table 3.2B

H2O:I2 Ratio	93		105		118	
Temp. (°C)	**Bunsen**	**HSP**	**Bunsen**	**HSP**	**Bunsen**	**HSP**
75	.3116	.0048	1.001	.0159	9.647	.2146
90	.6812	.0255	2.727	.0789	35.823	1.140
105	1.400	.1188	6.863	.3453	119.87	5.304

Table 3.2A: Reaction rate constants (all in min^{-1}) of the Bunsen and HSP reactions at various temperatures and water to iodine ratios.

	H2O:I2 Ratio			
Temp. (°C)	**93**	**105**	**118**	**Average**
75	64.92	62.96	44.95	57.61
90	26.71	34.56	31.42	30.90
105	11.78	19.87	22.60	18.09

Table 3.2B: Ratio of the reaction rate constant of the Bunsen reaction to the reaction rate constant of the HSP reaction across various temperatures and water to iodine ratios

Through the comparison of the ratio of the reaction rate constants of the Bunsen and HSP reactions across constant temperature and constant water to iodine ratio, several conclusions can be drawn. Across a constant temperature, the reaction rate constant ratio remains approximately the same as the water to iodine ratio increases. However, as temperature increases the reaction rate constant ratio decreases by over a third on average with a 30 degree rise in temperature. Since the reaction rate constants of the Bunsen reaction are increasing, this change in the ratio suggests that the reaction rate constants of the HSP reaction are increasing more with an increase in temperature. This is more than likely due to a combination of factors.

An increased temperature would increase the vapor pressure of water, leading to a decrease in the actual amount of water present in the liquid phase, perhaps lessening the inhibition of mass action on the second reaction. As can be seen in Table 3.2A, the reaction rate constants for the Bunsen reaction are much higher than those of the HSP reaction. Even at the highest temperature and water to iodine ratio, the reaction rate constant of the Bunsen reaction is still 20 times larger than that of the HSP reaction. The magnitude of the reaction rate constants of the Bunsen reaction continues to help drive the HSP reaction through an increase in the speed and

production of hydrogen iodine and sulfuric acid. This contributes to the shrinking of the reaction rate constant ratio with an increase in temperature.

3.4 Recycling the Ionic Liquid

While this novel thermochemical cycle is intended to be continuous, it is foreseeable that the ionic liquid medium will need to be purified and tested, due to the highly reactive nature of the cycle and the species therein. The process for recycling the ionic liquid is based around the work of Earle et al. and is based around chemistry that is strikingly similar to the Bunsen reaction.[108]

3.4.1 Materials and Methods

The protocol consisted of mixing a solution of DI water with approximately 50 grams of sodium thiosulfate and 10 grams of KOH. The volume of water should be approximately twice that of the ionic liquid, as the ionic liquid will be diluted with an equal volume amount of dichloromethane. The dichloromethane/ionic liquid and aqueous solutions are mixed and burped in a separatory funnel and allowed to separate. The aqueous phase, in which the iodine and sulfur bearing species migrate, is discarded. This process is repeated several times until any discoloration in the ionic liquid is gone. The dichloromethane was removed via rotovap, until only the cleaned ionic liquid remained.

Experiments were repeated with the recycled ionic liquid using concentrations of iodine, sulfur dioxide and water as described in Section 3.1.1. The recycled ionic liquid was used to make both the iodine solution (4 mL) and the sulfur dioxide solution (.2 mL). Triplicate experiments were performed for both the Bunsen reaction and HSP reaction at the temperatures used in Section 3.1, as a comparison.

3.4.2 Results and Discussion

Kinetic data was collected for both the Bunsen and HSP reactions similar to that described in Section 3.1. Figure 3.8 shows the Arrhenius plot for both reactions, while Table 3.3 compares the Arrhenius parameters extracted from this data compared to that using "fresh" ionic liquid."

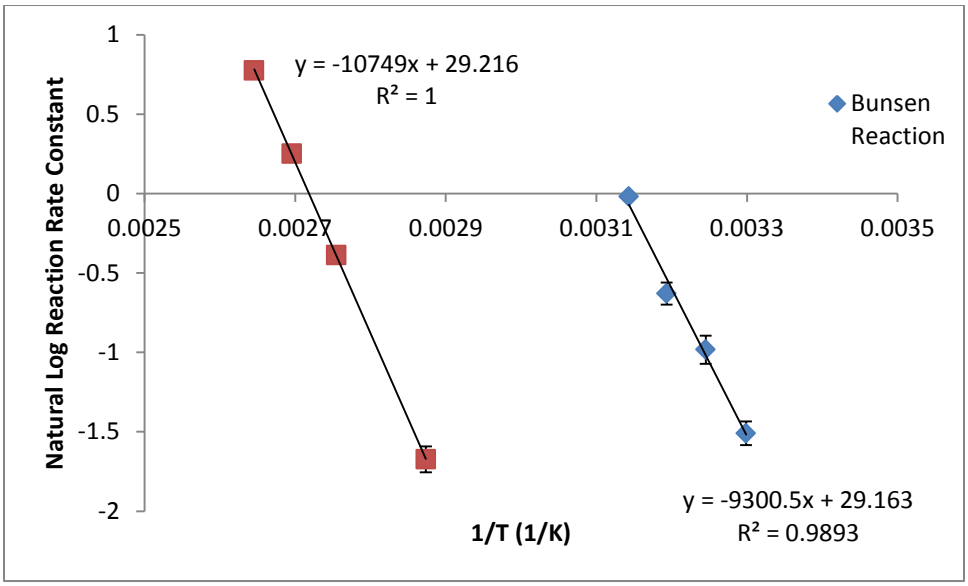

Figure 3.8: Arrhenius plot for Bunsen and HSP reactions using recycled ionic liquid. Error bars are present on all data points, but some may be too small to see

	Bunsen Reaction		HSP Reaction	
	E_a (kJ/mol)	k_0 (1/min)	E_a (kJ/mol)	k_0 (1/min)
Fresh	92.83	7.66E+14	117.10	7.73E+16
Recycled	77.33	4.63E+12	89.43	5.74E+12

Table 3.3: Comparison of the Arrhenius parameters for the Bunsen and HSP reactions between Fresh and Recycled ionic liquids

Table 3.3 shows that there are dramatic differences between the Arrhenius parameters of both reactions when comparing the fresh and recycled ionic liquids. As in Section 3.2, it is helpful to view the reaction rate constants for both reactions to visibly see the differences.

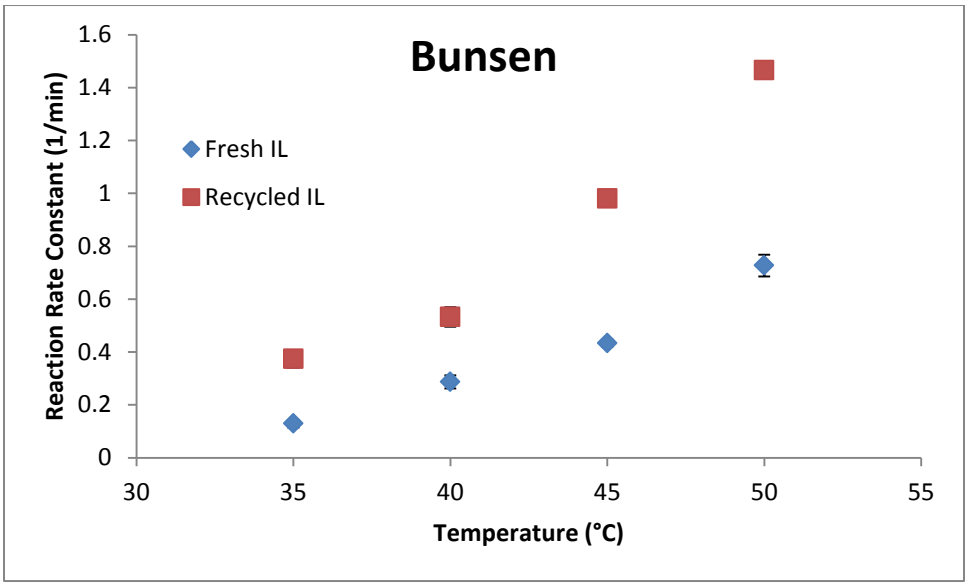

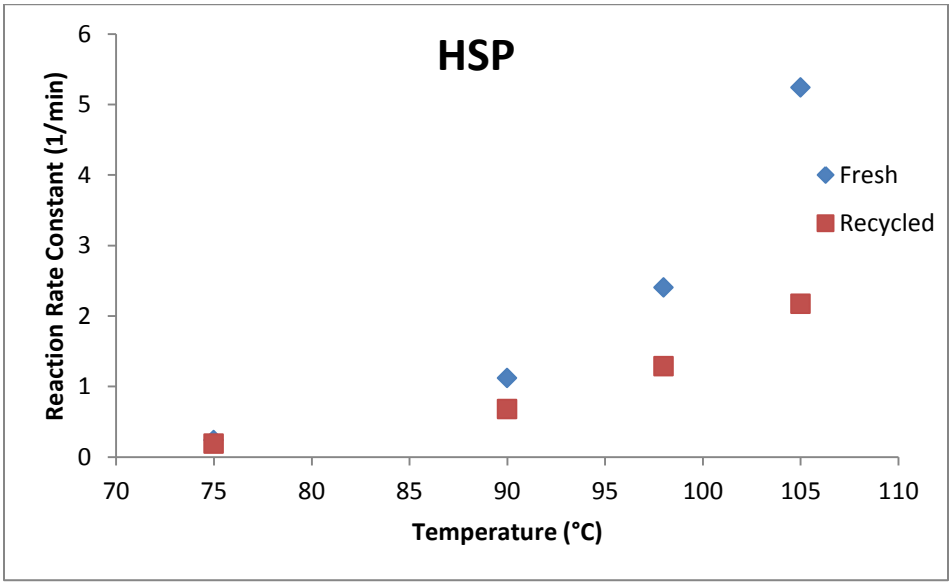

Figures 3.9A/B: Comparison of the reaction rate constants using fresh and recycled ionic liquid in the Bunsen (above, A) and HSP (below, B) reactions. Error bars are present, but possibly too small to see

Figures 3.9A and B show that, to go along with seemingly large changes in the Arrhenius parameters from the fresh to the recycled, there is are fairly substantial differences in the actual reaction rate constants. A consistency across these trends is the relative size of the reaction rate constants.

The substantial differences suggest that something is remaining is the "cleaned" ionic liquid. In order to check the cleanliness of the ionic liquid, UV absorption spectra were taken of both the fresh and recycled ionic liquid, shown below in Figure 3.10.

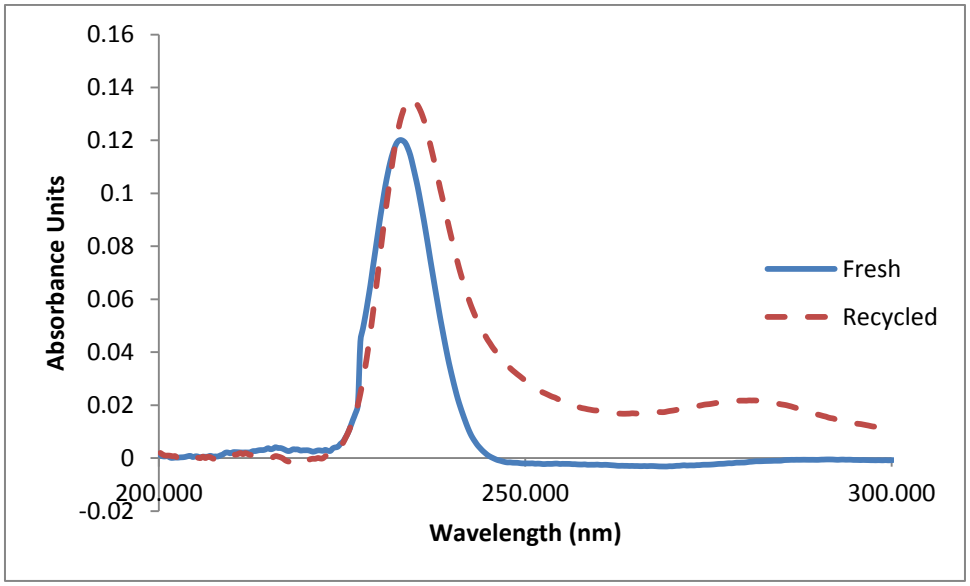

Figure 3.10: UV Absorption Spectra of Fresh and Recycled Ionic Liquid

Figure 3.10 shows the continued presence of a contaminant at approximately 280-290 nm. It would follow that this may have contributed to the differences in the reaction rate constants discussed previously.

In order to completely remove the contaminant from the ionic liquid, an additional wash was added to the ionic liquid recycling protocol. A solution of .1 M hydrochloric acid (Malinckrodt) was created and an equi-volume amount was added to the ionic liquid solution, following the above listed water washes described in the protocol. Figure 3.11 shows the results of the acid washing.

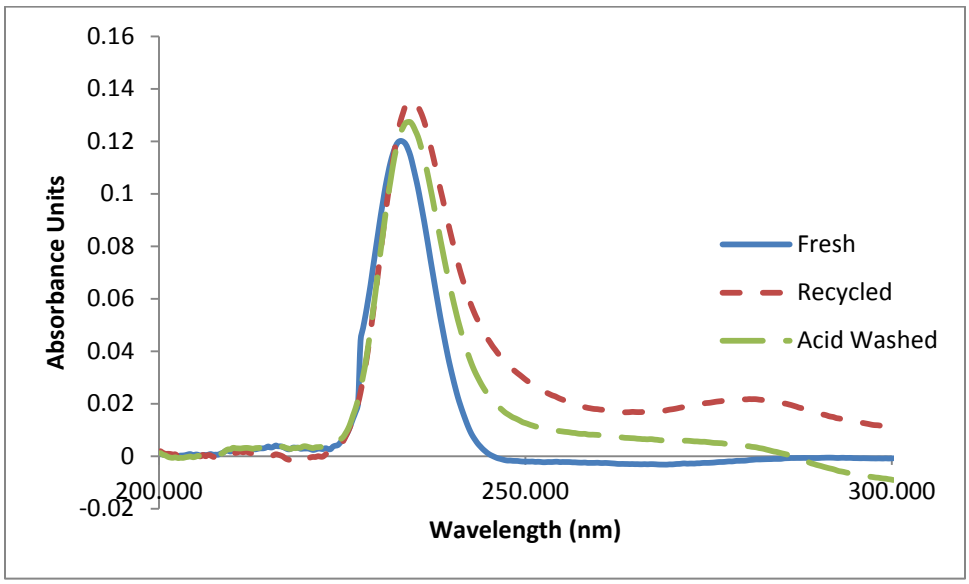

Figure 3.11: UV Spectra of fresh, recycled, and acid washed ionic liquid

As can be seen in the above Figure, the addition of the acid wash appears to mostly eliminate the presence of the contaminant. This was further confirmed through comparing the reaction rate constant at a single temperature for both the Bunsen and HSP reactions, shown in Figure 3.12A/B.

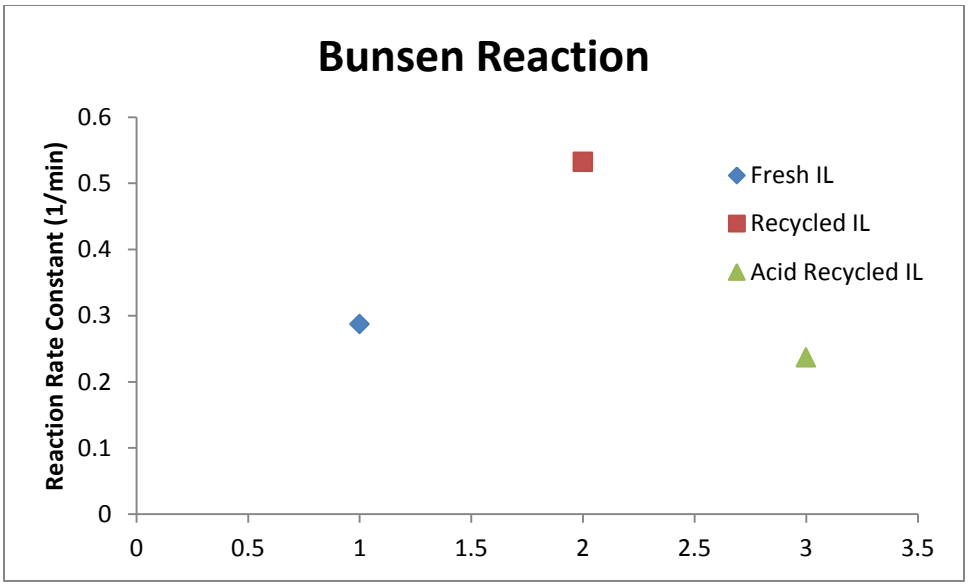

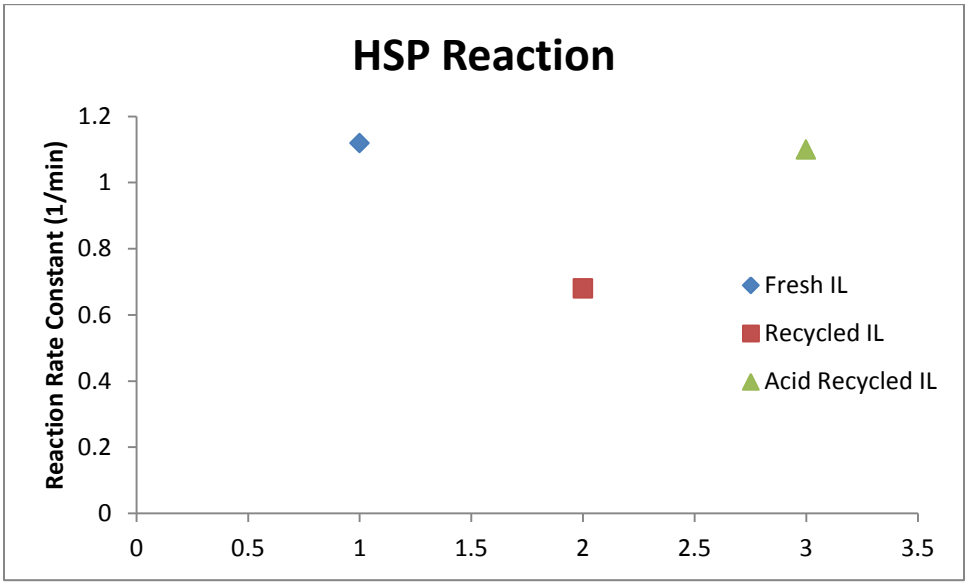

Figure 3.12A/B: Reaction rate comparison for the Bunsen (A, above) and HSP (B, below) reactions using fresh, recycled and acid washed ionic liquid. Error bars are present but may be too small to see.

Figure 3.12A/B show that the reaction rate constants utilizing the acid recycled ionic liquid are very similar to those using the fresh ionic liquid, suggesting that the

addition of the acid wash step allows for nearly complete regeneration of the fresh ionic liquid.

3.5 Lewis Base Catalysis

With the accomplishment of recycling and regenerating the ionic liquid for regular experimental reuse, the initial results of those experiments opened a new pathway for accelerating the reaction. The use of catalysts in thermochemical hydrogen production is a common practice, thoroughly discussed in the Introduction. However, a majority of this catalysis, at least in recent research, is focused on gas-solid interaction and is therefore subject to the limitations of mass transfer, minimal conversion, and catalyst degeneration. For this work, focused on an all fluid, continuous process, it would be ideal to insert homogenous catalysts, as it helps mitigate some of the limitations of heterogeneous catalysis.

3.5.1 Materials and Methods

The methodology for choosing the catalysts were based upon the pK_b of various Lewis bases, where K_b is the equilibrium constant between the base, water, and its conjugate acid/base pair.

$$B_{(aq)} + H_2O_{(l)} \leftrightarrow BH^+_{(aq)} + OH^-_{(aq)} \quad \text{Eq. 3.10}$$

$$K_b = \frac{\left[BH^+_{(aq)}\right]\left[OH^-_{(aq)}\right]}{\left[B_{(aq)}\right]} \quad \text{Eq. 3.11}$$

$$pK_b = -\log(K_b) \quad \text{Eq. 3.12}$$

The five Lewis bases chosen were triphenylamine (Aldrich), triphenylphosphine (TCI), tris(hydroxylmethyl)aminomethane (Mackron), phenol (JT Baker) and urea (Mallinckrodt) with reported pKb's in water of 19, 11.27, 4.05, 5.93, and 0.18, respectively.

For the experimental runs, equimolar amounts of the Lewis base was measured and added to a dissolved solution of 0.07 grams of molecular iodine and 4 milliliters of ionic liquid. After allowing for the Lewis base, iodine, and ionic liquid solution to reach reaction temperature, water, then sulfur dioxide were added in the same method as described above. A single temperature was studied for the reaction kinetics: 35°C for the Bunsen reaction and 90°C for the HSP reaction.

To accurately determine the effect of each base on the HSP reaction, the reaction rate constant at 90°C for each base must be determined. This value was extrapolated from the results of the 118-1 water to iodine ratio experimental kinetic data and the Lewis base Bunsen experimental kinetic data, operating under the assumption that the presence of the Lewis base caused a constant shift in the pre-exponential term in the Arrhenius parameters.

3.5.2 Results and Discussion

The reaction rate constant of both the Bunsen reaction and HSP reaction were determined in triplicate utilizing each Lewis base. The results are shown below in Figure 3.13A/B.

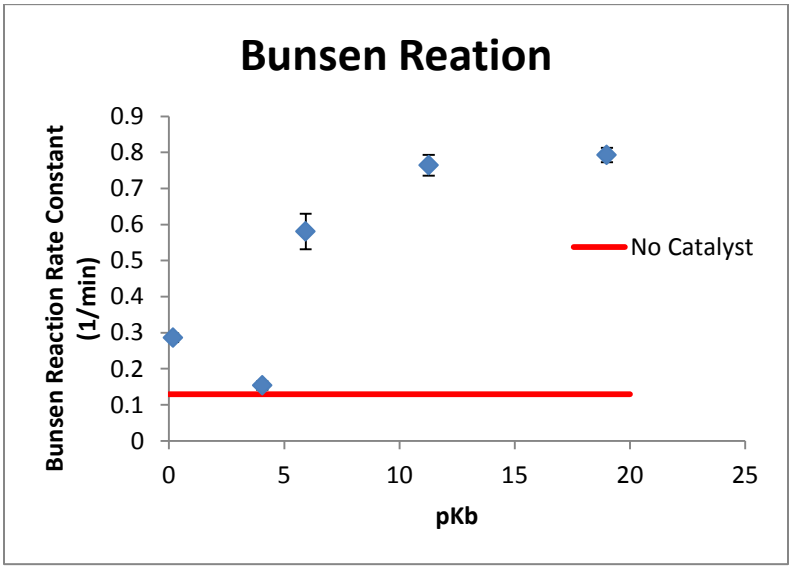

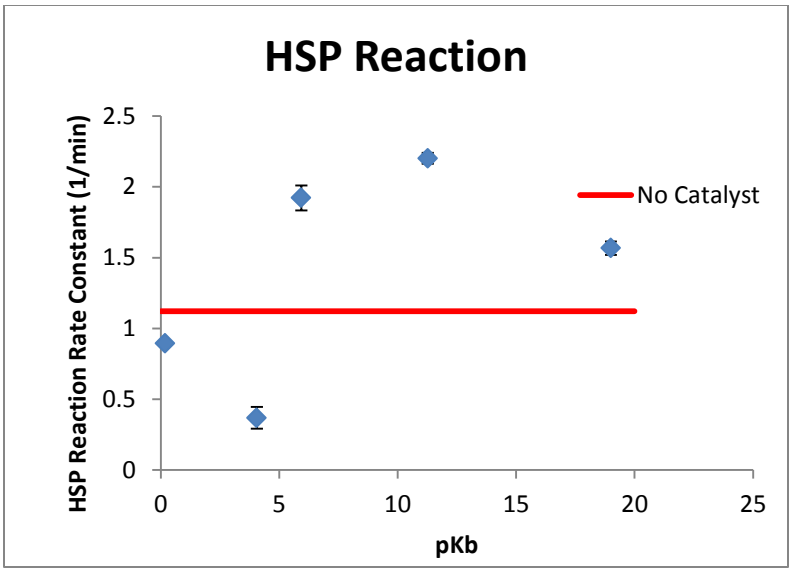

Figure 3.13A/B: Results of utilizing Lewis bases with various pKb as homogenous catalyst for the Bunsen (A, above), and HSP (B, below) reactions

From Figure 3.13A, it appears that increasing the pKb (i.e. decreasing the strength of the base) generally tends to increase the reaction rate constant for both reactions. The increase in the reaction rate constant with decreasing pKb can be explained through straightforward acid-base chemistry.

With the decrease in the base strength (increasing pKb), both the Bunsen and HSP reaction rate constants generally increase. A decrease in the base strength, when viewed through a steady equilibrium, can be viewed as a decrease in the interaction between the base and water, implying that the electron pair that defines the Lewis base is not removed. The results would suggest that the increased presence of the base with its electron pair intact would preferentially interact with the two strong acids that are produced via the Bunsen reaction. This interaction, presumed to be some kind of neutralization, would remove the two acids from the Bunsen reaction equilibrium, driving it forward with the decrease in concentration on the products side.

While the reasoning behind the increase in the reaction rate constants of the Bunsen reaction with an increase in pKb is fairly straightforward to explain, the results of the HSP reaction are, again, more complicated. For an explanation of why the reaction rate constants of the HSP reaction increase with decreasing base strength, Section 3.3.2 gives a possible explanation for the behavior. With a general increase in the reaction rate of the Bunsen reaction due to the presence of the Lewis base, the rate of the Bunsen reaction would increase. This increase is balanced through the subsequent removal of the two products of the Bunsen reaction from the reaction through neutralization with the Lewis base. Despite this phenomenon, however, the overall increase in the production would give rise to more interaction between the two Bunsen reaction products, increasing the rate of the HSP reaction.

This can be especially true for the bases triphenylamine and triphenylphospine, where the Bunsen reaction rate constant is upwards of six times higher than that with no catalyst present. This six fold increase in the rate of the Bunsen reaction only leads to an approximate two fold increase in the rate of the HSP reaction, giving credence to the suggestion that some of the acids produced are neutralized by the base or go through some other reaction pathway to otherwise inhibit the progression of the HSP reaction. Further exploration utilizing these homogenous catalysts is warranted, mainly focused on the actual generation of hydrogen sulfide in a catalyst free reaction mixture against the generation with the variety of catalysts.

3.6 Equilibration Period

One of the more curious aspects of studying this reaction pair is the presence of what has been referred to as an “equilibration period” between them. This can be seen in Figure 3.14 below, approximately between the times of 1 minute to approximately 30 minutes where the concentration of iodine remains relatively constant. This phenomenon warranted further investigation and three separate parametric studies

were undertaken: altering the initial water and sulfur dioxide concentration and the reaction temperature.

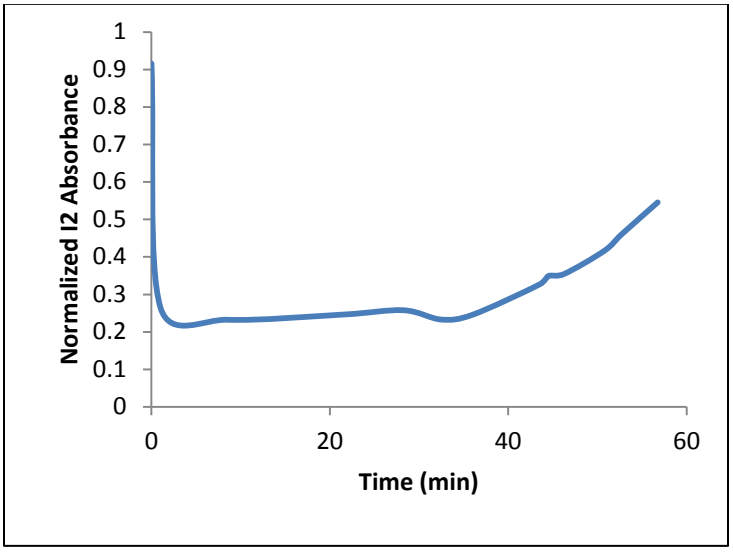

Figure 3.14: Presence of an "equilibration period" within the reaction pair

3.6.1 Materials and Methods

The methodology described in Section 3.1.1 applies to this set of experiments. The water to iodine ratios explored are 118-, 105-, and 93-1, the sulfur to iodine ratios are 2.01-, 1.34-, and 0.67-1, and the temperatures used are 75°C, 90°C, and 105°C. The equilibration period displayed in Figure 3.14 was studied for all 9 of these experimental sets with a hope to determine the effects on the equilibration time and the normalized iodine concentration at which the equilibration takes place.

3.6.2 Results

The results of this analysis are seen below in Figure 3.15A, B, and C, for the effect of water, sulfur dioxide and temperature, respectively, with the general trends summarized in Table 3.4.

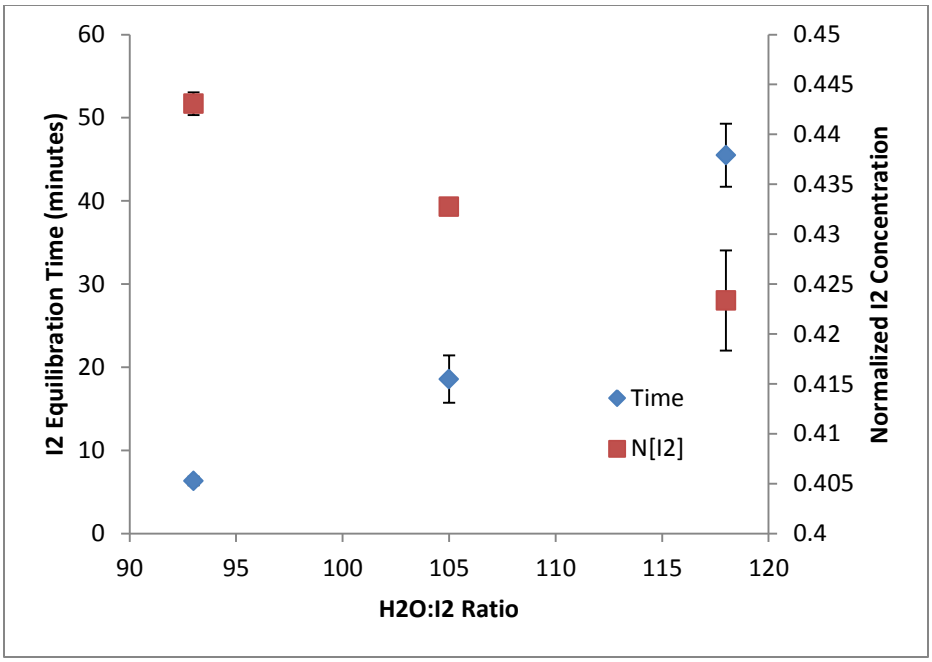
I2 Equilibration Time (minutes)
Normalized I2 Concentration
H2O:I2 Ratio
Time
N[I2]
0
10
20
30
40
50
60
0.4
0.405
0.41
0.415
0.42
0.425
0.43
0.435
0.44
0.445
0.45
90
95
100
105
110
115
120

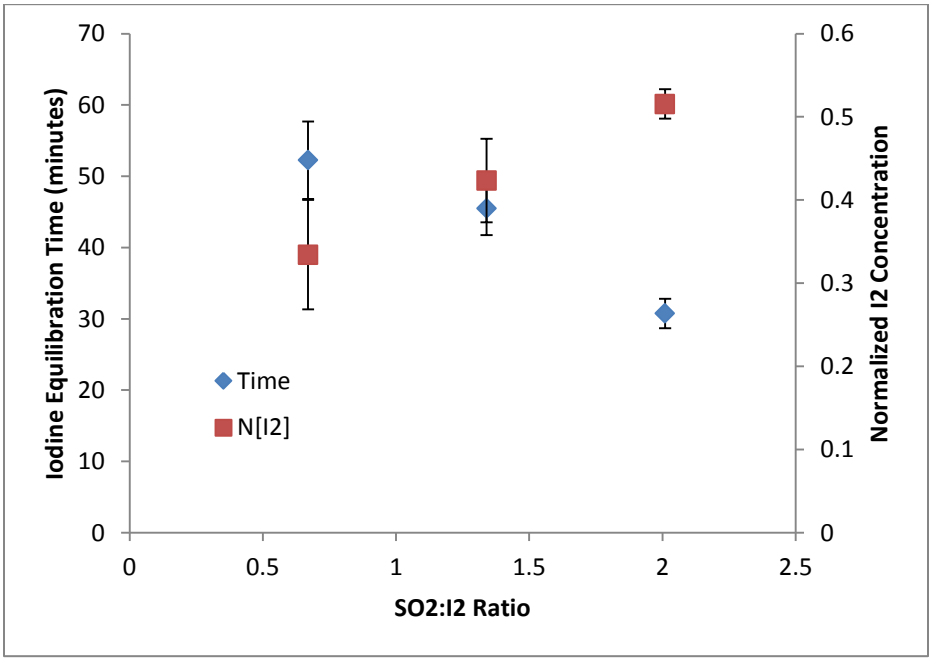
Iodine Equilibration Time (minutes)
Normalized I2 Concentration
SO2:I2 Ratio
Time
N[I2]
0
10
20
30
40
50
60
70
0
0.1
0.2
0.3
0.4
0.5
0.6
0
0.5
1
1.5
2
2.5

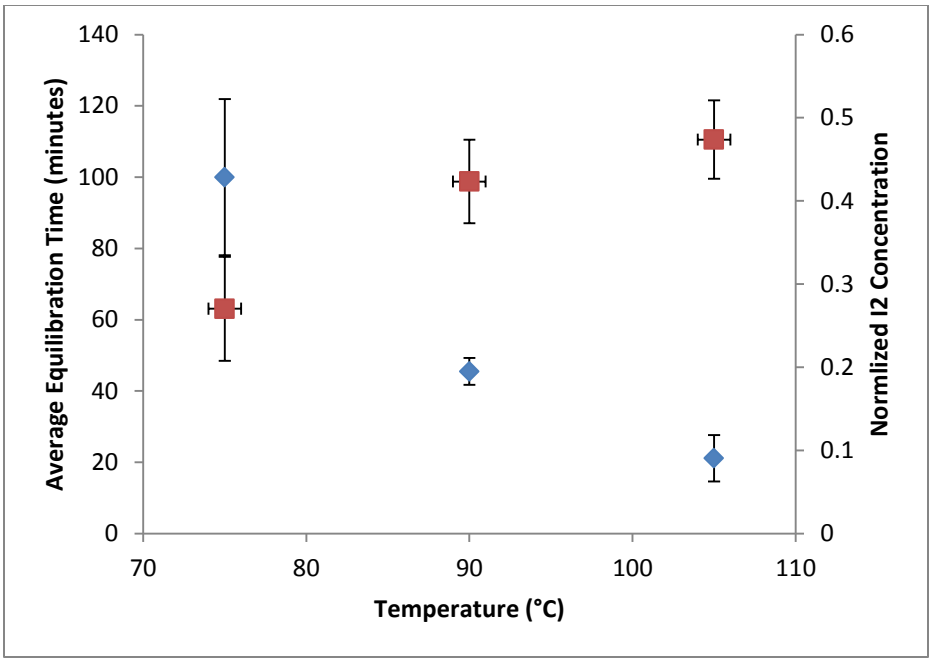

Figure 3.15 A/B/C: Effect of the initial concentration of water (A, top) and sulfur dioxide (B, middle) and temperature (C, bottom) on the average equilibration time and normalized iodine concentration between the Bunsen and HSP reaction

	Equilibration Time	Equilibration Concentration
Increasing H_2O: I_2	Increase	Decrease
Increasing SO_2: I_2	Decrease	Increase
Increasing Temperature	Decrease	Increase

Table 3.4: Summary of the trends of the equilibration period based on changing initial water concentration, sulfur dioxide concentration, and reaction temperature

There are several important characteristics about this reaction pairing that can be gleaned from these experiments. It appears that minimizing the amount of water and maximizing the sulfur dioxide and reaction temperature should create a reaction system which reaches the phase of the reaction in which the HSP reaction dominates the fastest. Increasing the reaction temperature, clearly, increases the overall rate of

the reaction, as discussed above. Decreasing the amount of water present in the system would suggest that, while shown in Section 3.3.2 to increase the overall rate of the system, the addition of water is actively hindered the dominance of the HSP reaction within the system and, more than likely, the overall rate of hydrogen sulfide production. Increasing the amount of sulfur dioxide in the system decrease the amount of time until the HSP reaction dominates the system. This can be explained through simple mass action as the increase in the initial reactant of the Bunsen reaction would drive it forward at a much higher rate and produce the products of the Bunsen reaction/reactants of the HSP reaction much faster. For future work, it would appear to be judicious to minimize the amount of water needed and maximize the sulfur dioxide introduced to the system.

The average equilibration concentration with increasing water, sulfur dioxide, and temperature decreases, increases, and increases, respectively. The increase in the equilibration concentration with an increase in temperature can be explained through the overall increase in the reaction rate of both reactions, as an increase in the Bunsen products brought about by the high temperatures would initiate the HSP reaction much faster. The effect is similarly felt with an increase in the initial amount of sulfur dioxide. The increase of the initial concentration of water in the system decreases the average equilibration concentration through increasing the rate of the Bunsen reaction while suppressing the rate of the HSP reaction, both due to mass action.

3.7 Initial Monitoring of Sulfur Species

The use of iodine to monitor the progress of the Bunsen and HSP reaction was done due to the relative simplicity of determining the iodine concentration and its presence in both reactions. However, as has been previously discussed, the target molecule of this reaction pair is hydrogen sulfide and, in a continuous process utilizing this new cycle, the sulfur bearing species in this reaction pair (sulfur dioxide, hydrogen

sulfide, and sulfuric acid) all play very significant roles. The processing of sulfuric acid was discussed heavily in the Literature Review and will not be approached in this work. Initial exploration on the behavior of sulfur dioxide and the generated hydrogen sulfide were undertaken.

3.7.1 Sulfur Dioxide Behavior

Based off of the theoretical stoichiometry, it was assumed that the sulfur dioxide would decrease linearly as it is consumed in the Bunsen reaction. Experiments were undertaken to monitor the liquid phase behavior of sulfur dioxide under various conditions.

The concentrations used for these initial analyses are based off of the "standard" reaction set discussed in Section 3.1.1. The difference lies in the analytical methodology once again. Rather than utilizing the Avantes UV/Vis spectrophotometer, an SRI 8610C Gas Chromatograph with an inline Flame Photometric Detector (FPD) was used to determine sulfur dioxide concentrations. The reaction flask, containing .07 grams of iodine, .2 mL of sulfur dioxide, .5 mL of water, and 4 mL of ionic liquid, was heated to 90°C. Sampling was performed through a step-wise dilution, due to the detection limits imposed by the GC. A volume of the reaction mixture was removed through the vial (5 μL), then diluted in dichloromethane (100-700 μL). The volume of dichloromethane decreases as time goes on because of a decrease in the concentration of sulfur dioxide in the liquid phase.

$$GC\ Count \rightarrow Calibration\ Curve \rightarrow Mole\ SO_2\ in\ GC$$

$$mol\ SO_2 = \frac{mol\ SO_2\ in\ GC}{V\ injected\ to\ GC} * \frac{V_{dichloromethane}}{V_{sample}} * 4700\ \mu L$$

A 2.5 μL aliquot was taken from the dichloromethane dilution and injected into the GC. This protocol allowed for a detection of higher levels of sulfur dioxide, with the

detrimental side effect of introducing a massive dichloromethane peak, increasing the time between samples. Three experimental runs were performed following this protocol, with the results displayed below in Figure 3.16.

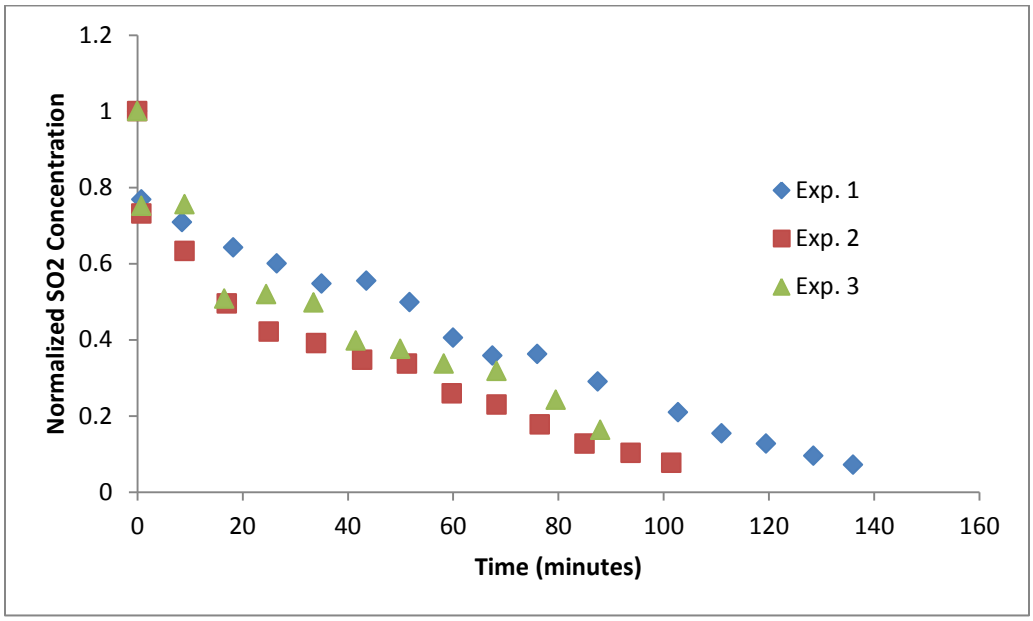

Figure 3.16: Normalized sulfur dioxide concentration in experimental runs

Figure 3.16 displays a curious trend. There is an initial drop in the sulfur dioxide concentration of approximately 25% in the first 45 seconds after the initiation of the Bunsen reaction. However, after this first 45 seconds, all three experimental runs display a constant, linear decline in the concentration of sulfur dioxide in the liquid phase. The previous work and the initial steep drop in the sulfur dioxide concentration suggest that the Bunsen reaction is progressing as expected. However, the behavior after the initial drop in concentration gives rise to the theory that something else is happening in the liquid phase. To further explore this phenomenon, two Blanks were performed where the sulfur dioxide concentration in the liquid phase was monitored: one without the presence of iodine and one without the presence of iodine and water. The results of these experiments are shown in Figure 3.17, as well as an average of the three experimental runs for comparative purposes.

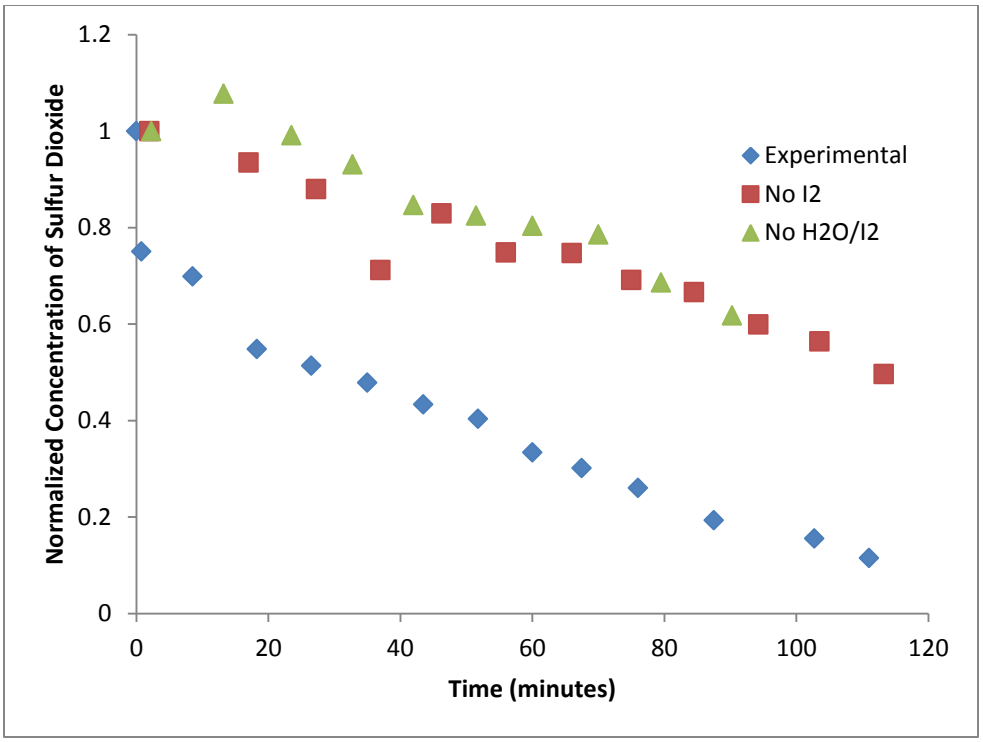

Figure 3.17: Monitoring of liquid phase sulfur dioxide concentration two blanks and experimental runs

The results of the two blank experiments come as a bit of a surprise. Whereas the experimental runs displayed a drop of approximately 25% of the initial sulfur dioxide concentration, neither Blank behaved in this manner. While this isn't completely unexpected, the similarity in the behavior after the first sample is nearly identical. Further examination of the rate of change of sulfur dioxide in the iodine-free blank, iodine- and water-free blank and the experimental runs found values of -.0044, -.0048, and -.005, respectively. These rates of change are within approximately 6% of each other, suggesting that a similar phenomenon occurring in all three runs. A distinct possibility is the movement of the sulfur dioxide from the liquid phase into the gas phase, explored in Figure 3.18.

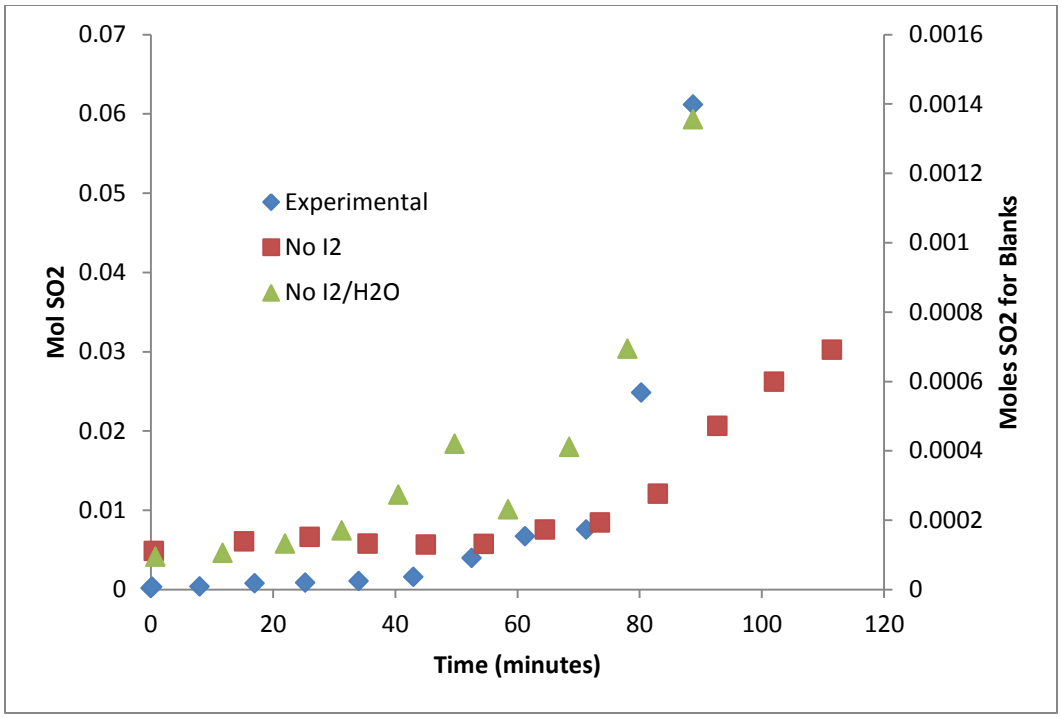

Figure 3.18: Gas phase moles of sulfur dioxide for experimental runs and two Blanks (Blanks are on the secondary y-axis)

Figure 3.18 shows that there is an increase in the moles of sulfur dioxide in the gas phase over time for both blanks and the experimental runs. The moles of sulfur dioxide in the gas phase for the Blanks (shown on the secondary y-axis) are nearly an order of magnitude lower than that of the experimental runs. The apparent exponential behavior of the amount of sulfur dioxide in the gas phase may be attributed to possible absorption of sulfur dioxide by the septa used to seal the reaction vessel. However, attempts made at a quantifying this hypothesis proved unsuccessful, with a change in the mass of the septa on the range of .01%. The same tests to measure the change in the mass of the septa found that the mass of the reaction vessel, reaction mixture, stir bar, and septa remained constant at various temperatures as the reaction progressed, suggesting that the sulfur dioxide gas, or any gas for that matter, is escaping the vessel.

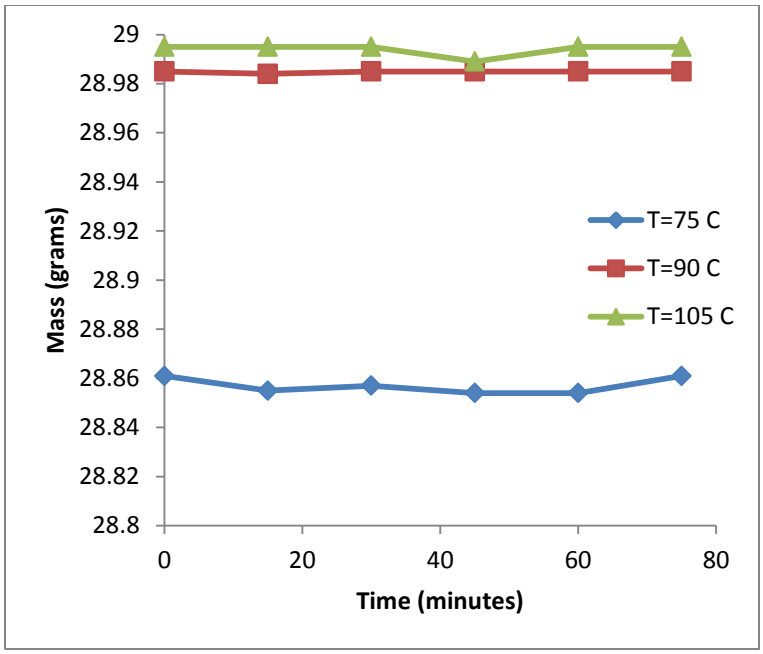

Figure 3.19: Mass of the reaction vessel, reaction mixture, septa, and stir bar at various temperatures over time

Despite the relatively large difference in the amount of sulfur dioxide in the gas phase between the experimental runs and the two Blanks, the overall increase of sulfur dioxide in the gas phase suggests that the behavior of sulfur dioxide in the liquid phase can at least partly be attributed to mass transfer.

3.7.2 Hydrogen Sulfide Behavior

Hydrogen sulfide is the target molecule of the Bunsen/HSP reaction pair and is therefore important to understand how it is generated within these reaction conditions. Experiments were performed as described in Section 3.7.2. The difference in protocol for the monitoring of hydrogen sulfide in the liquid would be the dichloromethane dilution. Rather than the volume of dichloromethane decreasing over time (to account for a decrease in the amount of sulfur dioxide), the volume of dichloromethane used for the dilution increases. This presents a greater difficulty in monitoring hydrogen sulfide

in the liquid phase as the dilution of dichloromethane required is not known as the rate of generation of hydrogen sulfide is unknown.

However, after some initial tests, it was determined that the concentrations generated would generate a response in the GC without the need for the dichloromethane dilution. Unfortunately, the high boiling point ionic liquid [BMIM][TF2N] would remain in the GC column, potentially inhibiting the operation of the column for future use. To get around this issue, a pre-column "filter" was installed, consisting of a small piece of steel tubing packed with glass wool. The filter would allow for the reaction mixture to be injected directly into the GC by keeping the ionic liquid in the filter through surface tension and allowing the volatile species to pass through unimpeded. The design of the filter, using cheap tubing and glass wool, allows for simple discarding after substantial use with little-to-no adverse effects on the column. Utilizing the pre-column filter, an experiment was performed to determine the liquid phase concentration of hydrogen sulfide over time, with the results shown in Figure 3.20

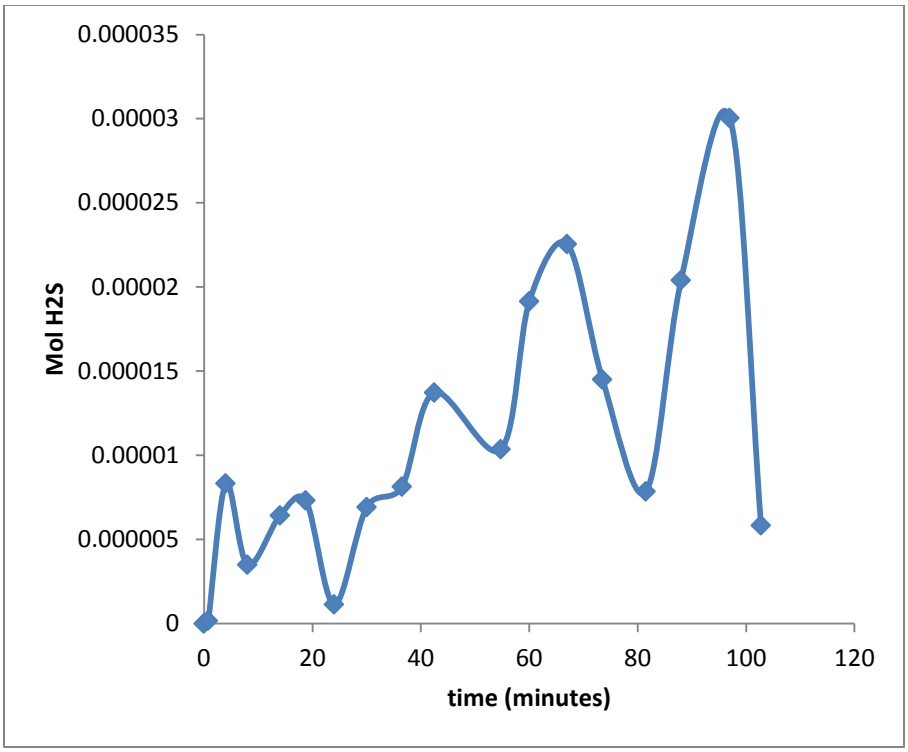

Figure 3.20: Moles of hydrogen sulfide in the liquid phase over time

Figure 3.20 displays unexpected behavior in the oscillating of the hydrogen sulfide concentration. While this appears to contradict the hypothesis that hydrogen sulfide will be generated at a fairly linear rate over time, the amount does increase fairly linearly over time, especially when examining the individual peak maximums. However, this oscillating behavior brings several questions to light, the most important of which is determining what is actually causing the oscillations. While there are several theoretical reactions that may be taking place (due to the high number of oxidation states and species of both iodine and sulfur), one of the more well-known oscillating reactions may give potential clues to this mechanism: the iodate variation of the iodine-clock reaction, shown below.

$$IO_{3\,(aq)}^{-} + 3HSO_{3\,(aq)}^{-} \rightarrow I_{(aq)}^{-} + 3HSO_{4\,(aq)}^{-} \qquad \text{Eq. 3.13}$$

$$IO_{3\,(aq)}^{-} + 5I_{(aq)}^{-} + 6H_{(aq)}^{+} \rightarrow 3I_{2(aq)} + 3H_2O \qquad \text{Eq. 3.14}$$

$$I_{2(aq)} + HSO_{3\ (aq)}^{-} + H_2O \rightarrow 2I_{(aq)}^{-} + HSO_{4\ (aq)}^{-} + 2H_{(aq)}^{+}$$ Eq. 3.15

There was little to no evidence of oscillation in any of the experimental work performed measuring iodine, so it is difficult to say with a degree of certainty that this reaction is indeed taking place. However, the oscillation of hydrogen sulfide in the reaction mixture is cause for concern and is a problem that will need to be addressed in the near future.

4. Modelling

A predictive model was developed with the purpose of successfully monitoring the progression of iodine through the reaction system. A straightforward approach utilized first principles mass balance of the four major species involved: iodine, sulfur dioxide, sulfuric acid, and hydrogen sulfide. The model was compared to the kinetic experimental data for both the Bunsen and HSP reactions across a change in the initial concentration of water. Because water was in a several fold excess of in comparison to both iodine and sulfur dioxide, it is not considered to diminish from its initial concentration.

$$\frac{d[I_2]}{dt} = -k_1[I_2][SO_2] + k_2[H_2SO_4] \quad \text{Eq. 4.1}$$

$$\frac{d[SO_2]}{dt} = -k_1[I_2][SO_2] \quad \text{Eq. 4.2}$$

$$\frac{d[H_2SO_4]}{dt} = k_1[I_2][SO_2] - k_2[H_2SO_4] \quad \text{Eq. 4.3}$$

$$\frac{d[H_2S]}{dt} = k_2[H_2SO_4] \quad \text{Eq. 4.4}$$

$$\frac{d[H_2O]}{dt} = 0 \quad \text{Eq. 4.5}$$

$$\mathrm{X}^2 = \frac{1}{v}\Sigma\left(\frac{([\mathrm{I}_2]_e - [I_2]_m)^2}{\sigma^2}\right) \quad \text{Eq. 4.6}$$

A MATLAB sequence was created to allow for the input of experimental data (in time and concentration of iodine) and initial concentrations of the relevant species ($[I_2]_0 = .064\ M$, $[SO_2]_0 = .113\ M$, and $[H_2SO]_0 = [H_2S]_0 = 0$ at $t = 0$). The sequence would then allow for the input of an initial "guess" of the reaction rate constants k_1 and k_2. Utilizing the Matlab solver function "ode45" to simultaneously solve the listed mass balances (Eq. 4.1 to 4.4) and "fminsearch" to determine the values of k_1 and k_2 that minimize the reduced chi squared value (Eq. 4.6) between the experimental

concentration data and the concentrations generated by the model, the program was able to generate model reaction rate constants (k_{1_m} and k_{2_m}). The reduced chi squared test is an analysis of the variance between the predicted and observed concentrations of iodine generated from the model and experimental work. The resulting reaction rate constants generated from the program were used in conjunction with the experimental data to visually inspect the overlay of the model and experimental data. A visual representation of this pathway is seen below. The goal of this MATLAB pathway is for the generation of reaction rate constants for the Bunsen and HSP reactions to compare to those extracted from the experimental data.

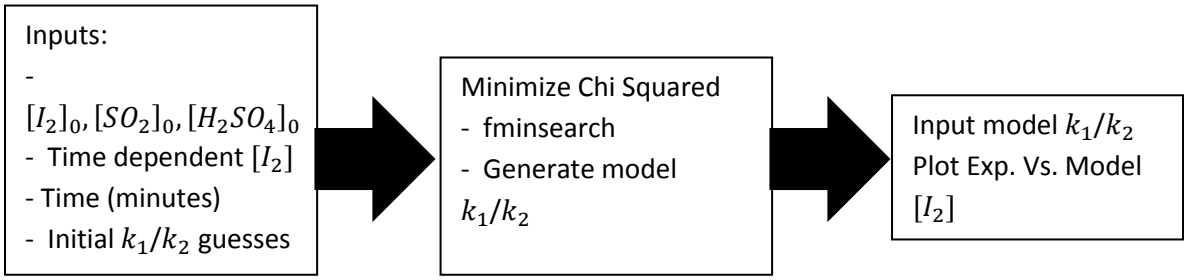

Figure 4.1: Matlab pathway to solve for model reaction rate constants

4.1 Bunsen Reaction

Despite the fairly straight forward MATLAB pathway, there are two separate methods for the input of the raw iodine concentration data: either solve each individual run one at a time and average the results or combine all three runs together. Both methods were examined using the Bunsen reaction at a water to iodine ratio of 118:1 and temperature of 35°C, with the graphical and numerical results shown below. The reaction rate constant for the HSP reaction in the analysis of the Bunsen was assumed to be negligibly small based on the previous experimental work.

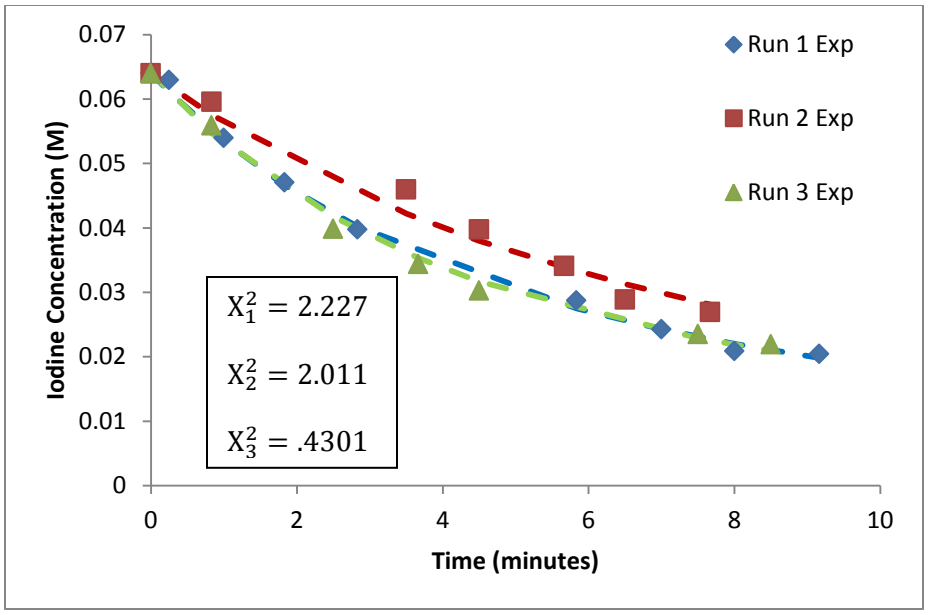
Run 1 Exp
Run 2 Exp
Run 3 Exp
$X_1^2 = 2.227$
$X_2^2 = 2.011$
$X_3^2 = .4301$
Iodine Concentration (M)
Time (minutes)
0.07
0.06
0.05
0.04
0.03
0.02
0.01
0
0
2
4
6
8
10

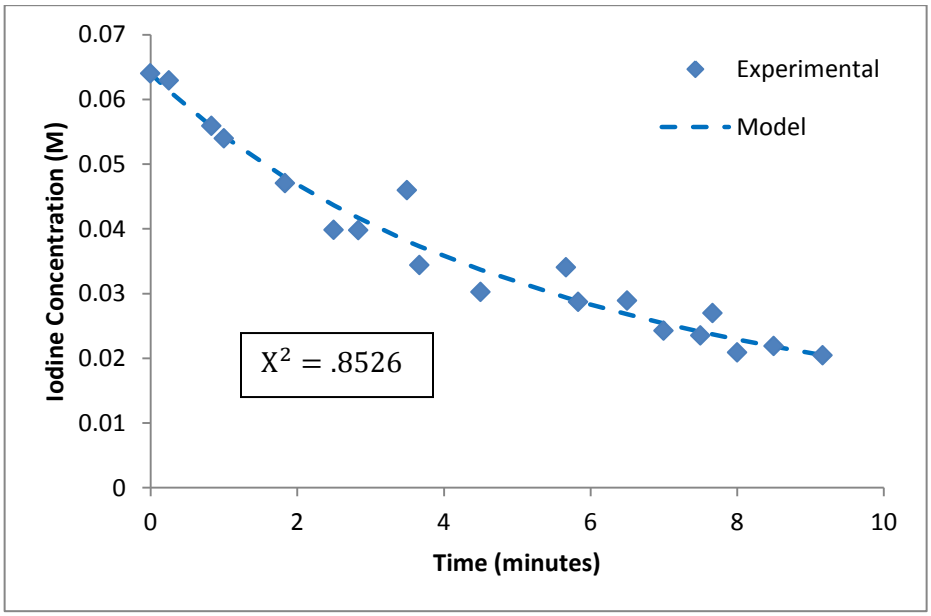
Experimental
Model
$X^2 = .8526$
Iodine Concentration (M)
Time (minutes)
0.07
0.06
0.05
0.04
0.03
0.02
0.01
0
0
2
4
6
8
10

All k_1 in min^{-1}	Separate Runs		Single Run	
	k_{1_e}	k_{1_m}	k_{1_e}	k_{1_m}
Run 1	.1354±.0057	1.6861±.0057		
Run 2	.1126±.0038	1.1756±.0019		
Run 3	.1393±.0082	1.7434±.0057		
Average	**.1291±.0059**	**1.5350±.0044**	**.1309±.0143**	**1.5195±.0072**

Figure 4.2: Difference in the methods for inputting raw iodine data into MATLAB pathway

Performing this initial analysis of the validity of the MATLAB program and the best method to input the raw iodine concentration data has led to several important discoveries. At first glance it appears that the method for inputting the iodine concentration data does not alter the reaction rate constants generated by the model, which is supported by the relatively similar values for the Chi squared function shown in Figure 4.2 for the "Single Entry" and "Triple Entry" methods. However, the reaction rate constants generated by the model appear to be an approximate order of magnitude larger than those determined from the Arrhenius analysis of the experimental data. Utilizing the "Single Run" method for the input of the raw iodine concentration data, the remaining temperatures for the water to iodine ratio of 118 to 1 were analyzed to determine the model reaction rate constants, with the results displayed below in Table 4.1.

Temperature (°C)	k_{1_e} (min^{-1})	k_{1_m}(min^{-1})	k_{1_e}/k_{1_m}
35	0.1309±.0143	1.5195±.0072	0.086147
40	0.2869±.0129	3.3278±.0168	0.086213
45	0.4315±.0069	5.0076±.0073	0.086169
50	0.7321±.0064	8.4029±.0056	0.087125

Table 4.1: Comparison between the experimentally determined and model generated reaction rate constants for the Bunsen reaction at a water to iodine ratio of 118-1

Applying the model to the remaining experimental data for the Bunsen reaction yields a similar ratio between the experimental and model generated reaction rate constants (k_{1_e}/k_{1_m}).

$H_2O: I_2$	Temperature (°C)	k_{1_e}(min^{-1})	k_{1_m}(min^{-1})	k_{1_e}/k_{1_m}
105-1	45	0.0639±.0052	0.715±.0034	0.08946387
	50	0.1191±.0049	1.2757±.0072	0.09338298
	55	0.1545±.0105	2.0208±.0044	0.07647136
	60	0.1899±.0105	2.3993±.0076	0.07917587
93-1	45	0.0401±.0076	0.5935±.0033	0.06756529
	50	0.0518±.0043	0.5952±.0017	0.08707582
	55	0.0634±.0068	0.7782±.0022	0.08150591
	60	0.0794±.0079	1.167±.0021	0.0680377

Table 4.2: Comparison between experimentally determined and model generated reaction rate constants for the Bunsen reaction at water to iodine ratios of 105-1 and 93-1

The complete analysis of the Bunsen reaction kinetics with varying initial concentrations of water finds that there is a constant value between the generated and experimentally determined reaction rate constants of $\overline{K}$ =.0823 ± .0081. The significance of this difference can be seen graphically in the comparison between the Arrhenius parameters of the two sets of data, demonstrating what appears to be a shift in the pre-exponential term (intercept) with approximately constant activation energy (slope).

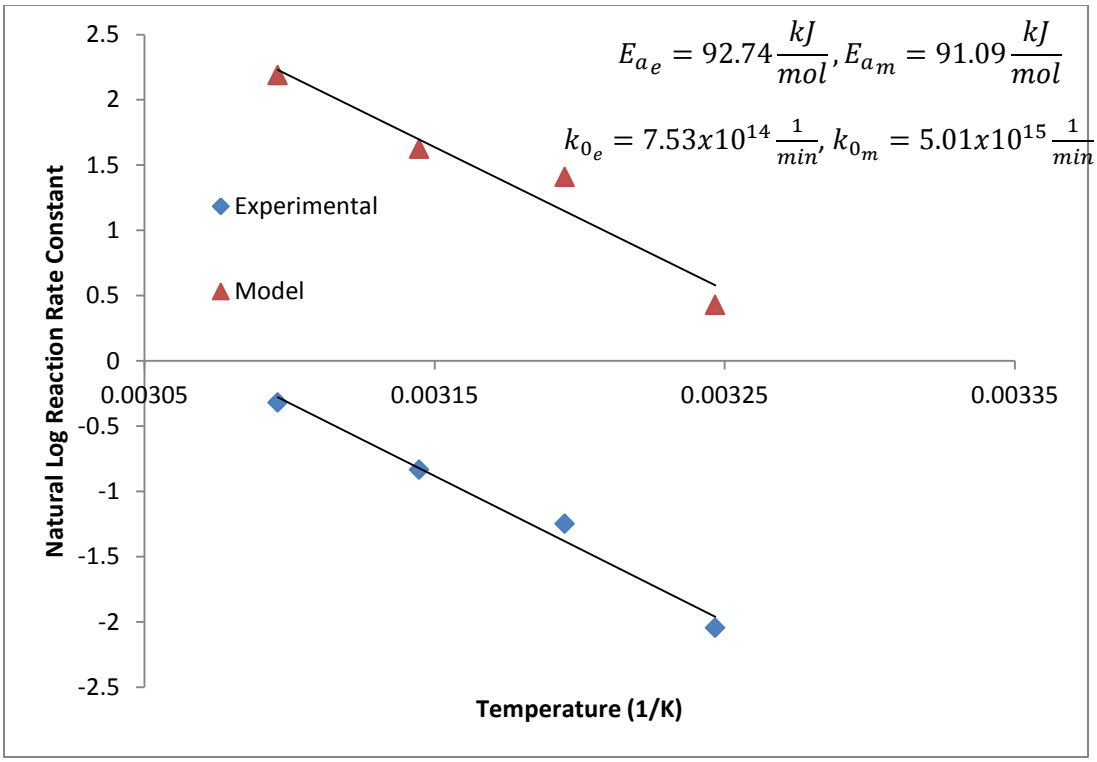

Figure 4.3: Comparison between the Arrhenius parameters of the Bunsen reaction at a water to iodine ratio of 118-1

The presence of this constant value across the breadth of the Bunsen reaction data suggests that there is a fundamental flaw in the model design. To determine the physical property that is responsible for $\overline{K}$, a simple algebraic path based upon the mass balance for iodine is laid out below

$$\frac{d[I_2]}{dt} = -k_{1_e}[I_2], model\ used\ for\ experimental\ reaction\ rate\ constant$$

Eq. 4.6

$$\frac{d[I_2]}{dt} = -k_{1_m}[I_2][SO_2], model\ used\ for\ model\ reaction\ rate\ constant$$ Eq. 4.7

$$\overline{K} = \frac{\Sigma\left(\frac{k_{1e}}{k_{1m}}\right)}{n}, where\ n\ is\ the\ number\ of\ temperatures$$ Eq. 4.8

$$k_{1_e}[I_2] = k_{1_m}[I_2][SO_2] \quad \text{Eq. 4.9}$$

$$[SO_2] = \frac{k_{1_e}}{k_{1_m}} = \overline{K} \quad \text{Eq. 4.10}$$

Eq. 4.6 to 4.10 lay out a simple algebraic path to suggest that the constant value that differentiates the experimental and model generated reaction rate constants is the initial concentration of sulfur dioxide. This finding in the model can further support the findings in Section 4.6.1, which studied the experimental behavior of sulfur dioxide in the liquid phase and found that the sulfur dioxide was, after an initial decrease in concentration within the first minute after the reaction had begun, did not appear to participate in the actual reaction, but was rather consumed or absorbed through some other process. In taking the value of $\overline{K}$ and utilizing it to adjust the reaction rate constants generated by the predictive model, the comparison between experimental and theoretical becomes much clearer, as seen below in a direct comparison between the reaction rate constants and a comparison in the Arrhenius parameters in both graphical and tabulated format.

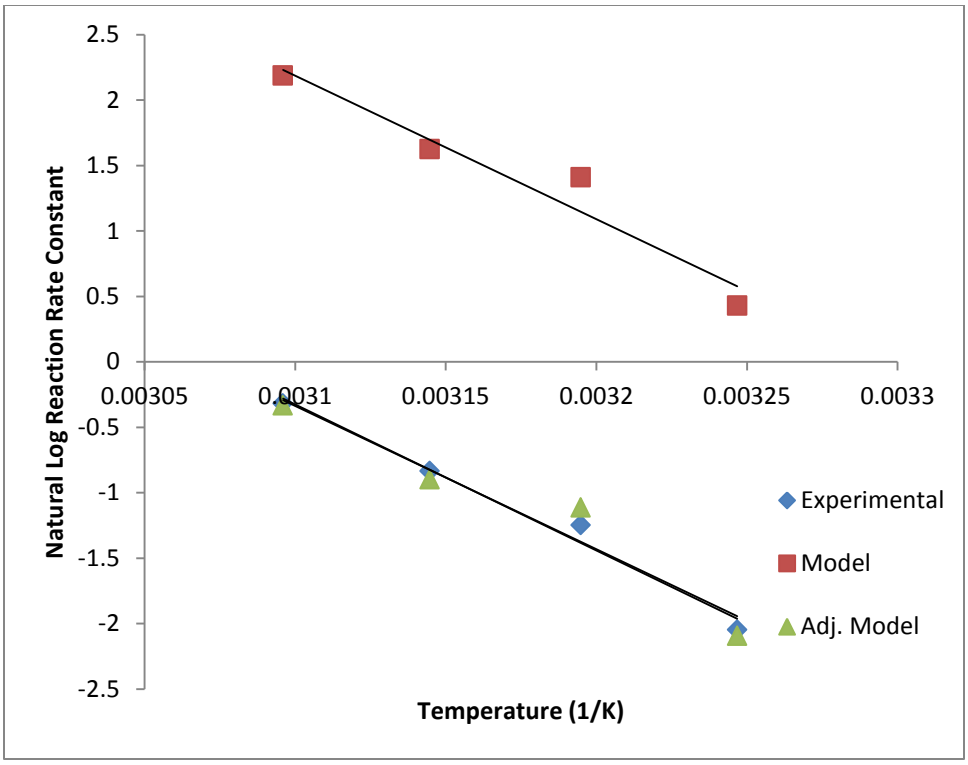

Figure 4.4: Comparison between Arrhenius plot of experimental, original model, and adjusted model for the Bunsen reaction at a water to iodine ratio of 118:1. The error bars are present, but too small to be seen.

	93-1		105-1		118-1	
	Ea	k0	Ea	k0	Ea	k0
Experimental	42.34	3.62E+05	62.29	1.22E+09	92.74	7.52E+14
Model	40.21	1.65E+05	72.26	4.88E+10	91.08	4.02E+14

Table 4.3: Comparison between the Arrhenius parameters of the Bunsen reaction at various water to iodine ratios

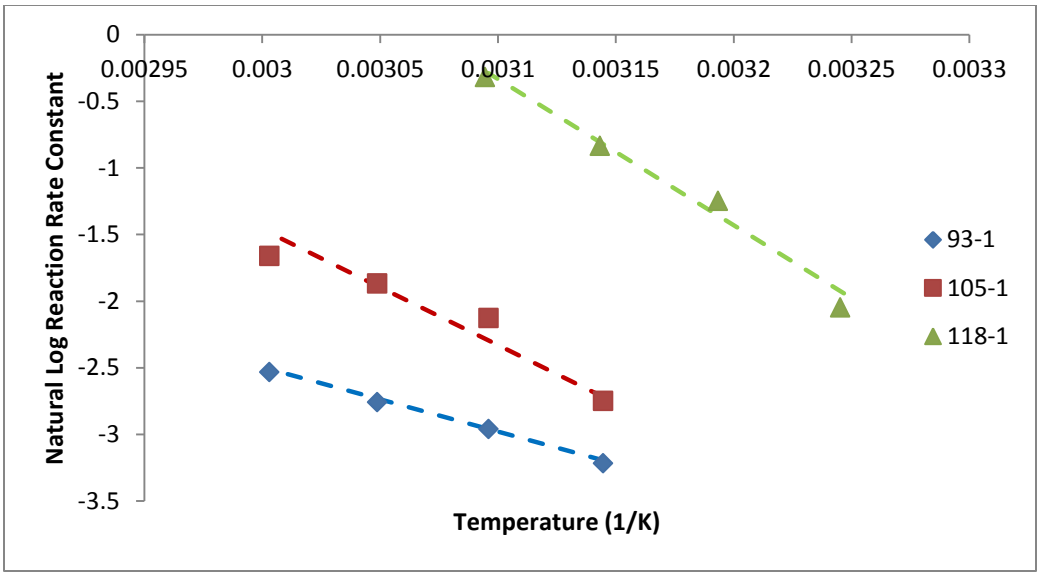

Figure 4.5: Comparison between the Arrhenius plots of the experimental and the adjusted model reaction rate constants for the Bunsen reaction at various water to iodine ratios. Note that the dashed lines represent the model generated Arrhenius data

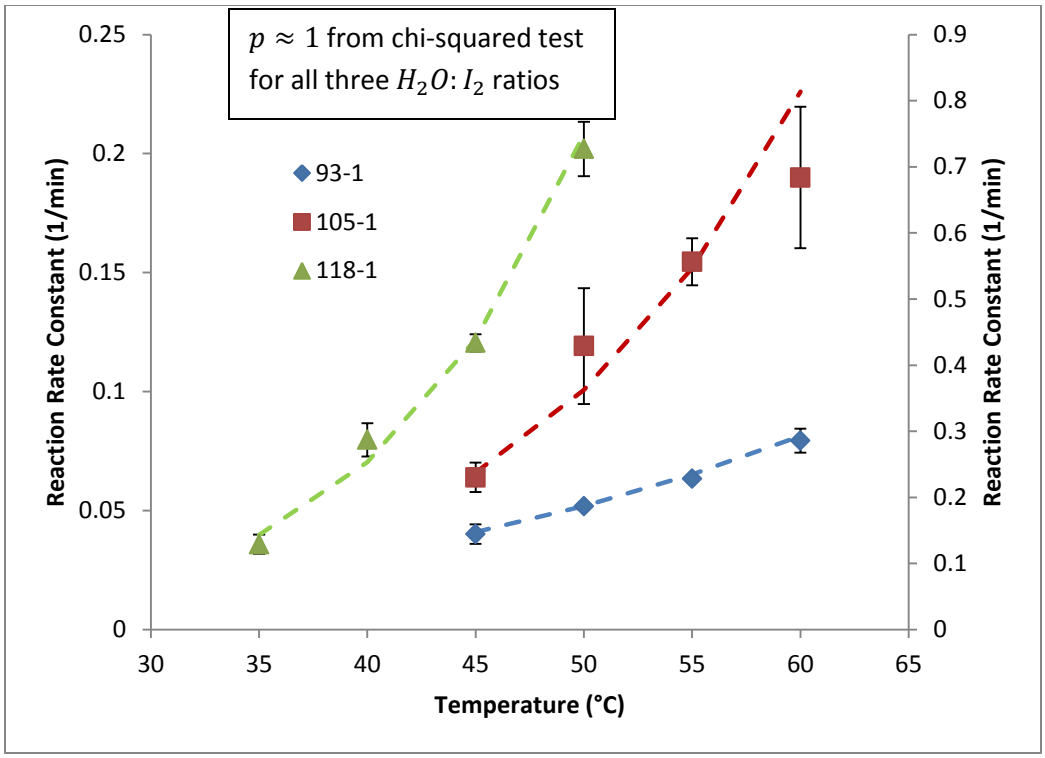

Figure 4.6: Comparison between the experimentally determined and adjusted model generated reaction rate constants for the Bunsen reaction. Note that the data for the water to iodine ratio of 118-1 is on the secondary y-axis and that the dashed lines represent the model generated data

4.2 HSP Reaction

The successful modification and application of the predictive MATLAB model to the raw experimental data for the Bunsen reaction allows for application to the HSP reaction. As a reminder, there is a dependence on the effective reaction rate constant for the HSP reaction on the reaction rate constant of the Bunsen reaction at that temperature.

$$k_{2_{actual}} = k_{2_{effective}} * k_{Bunsen}(T) \qquad \text{Eq. 4.11}$$

The same MATLAB pathway described in Figure 4.1 was applied to the HSP reaction. However, unlike modelling the Bunsen reaction, where the reaction rate constant for the HSP reaction was effectively negligible, the reaction rate constant for the Bunsen reaction plays a significant role in determining the kinetics. In order to determine the model generated HSP reaction rate constant that best fits the experimental data, the Bunsen Arrhenius data that was generated by the model was used to extrapolate to the temperatures needed for the HSP reaction. Given the good fit between the Arrhenius constants of the model generated and experimental iodine data, it is assumed that extrapolation to higher temperatures is in agreement with experimental data.

The variance between the experimental data and the model was adjusted by first setting the reaction rate constant of the Bunsen reaction (k_{1_m}) and adjusting the reaction rate constant of the HSP reaction (k_{2_m}) until the variance was minimized. Applying this method to the HSP reaction experimental data at a water to iodine ratio of 118-1 yields results very similar to the initial Bunsen reaction experiments.

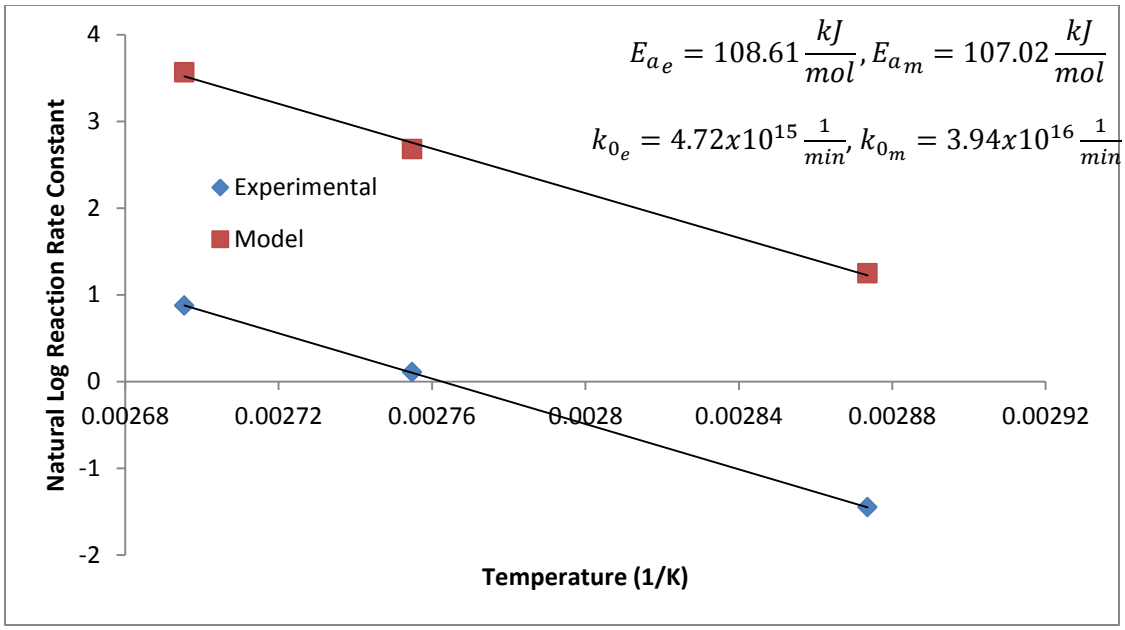

Figure 4.7: Comparison between the Arrhenius parameters of the experimental and model generated Arrhenius parameters for the HSP reaction at a water to iodine ratio of 118-1

Having seen a similar trend in the application of the predictive model to the Bunsen reaction, it is readily apparent that the results of the Bunsen reaction analysis need to be applied to the HSP reaction through the adjustment of the model. This can be achieved through the combination of Eq. 4.10 and 4.11.

$$[SO_2] = \frac{k_{1_e}}{k_{1_m}} = \bar{K} \quad \rightarrow \quad k_{1_m} = \frac{k_{1_e}}{\bar{K}} \qquad \text{Eq. 4.10}$$

$$k_{2_{m_{actual}}} = k_{2_{m_{effective}}} * k_{1_m}(T) \qquad \text{Eq. 4.11}$$

$$k_{2_{m_{actual}}} = k_{2_{m_{effective}}} * \frac{k_{1_e}}{\bar{K}} \qquad \text{Eq. 4.12}$$

What Eq. 4.12 essentially displays is that the different methods for determining the reaction rate constants for the Bunsen reaction, the experimental excluding the initial concentration of sulfur dioxide and the model not), effects the HSP reaction rate

constants as well. This is clearly evident through the analysis of the reaction rate constants for all three water to iodine ratios and the temperatures used therein.

$H_2O:I_2$	Temperature (°C)	k_{2_e}(min^{-1})	k_{2_m}(min^{-1})	$\overline{K} = k_{2_e}/k_{2_m}$
118-1	75	0.2346±.0351	3.485±.0398	0.0673
	90	1.1137±.2008	14.557±.1981	0.0765
	98	2.4007±.2360	35.385±.2491	0.0678
105-1	75	0.0091±.00036	0.1079±.00053	0.0757
	83	0.0250±.00058	0.2768±.00068	0.0530
	90	0.0439±.0018	0.4053±.0028	0.0982
93-1	75	0.0061±.00056	0.0666±.00059	0.0927
	90	0.0278±.0011	0.2750±.00084	0.1011
	105	0.1110±.0064	1.050±.0071	0.1057

Table 4.4: Comparison between experimental and model reaction rate constants for the HSP reaction, as well as the ratio between them

The algebraic explanation for the discrepancies seen in the comparison between the model and experimental data for the HSP reaction match up with what is seen in Table 4.4. A value of .0792±.018 was found for the ratio of the experimental to model reaction rate constants, a value slightly smaller than what was seen in the Bunsen reaction. The difference in values may be small enough to not be statistically significant, but a highly probable cause for the difference is merely due to a general increase in reaction temperature forcing more of the sulfur dioxide into the gas phase due to the liquid-vapor equilibrium.

Utilizing the value for $\overline{K}$ found from analyzing the HSP reaction data, the model was subsequently adjusted for this common factor and the data was re-analyzed, with the results of the numerical (Table 4.5) and graphical Arrhenius parameters (Figure 4.8), as well as a direct comparison between the reaction rate constants (Figure 4.9/4.10), shown below.

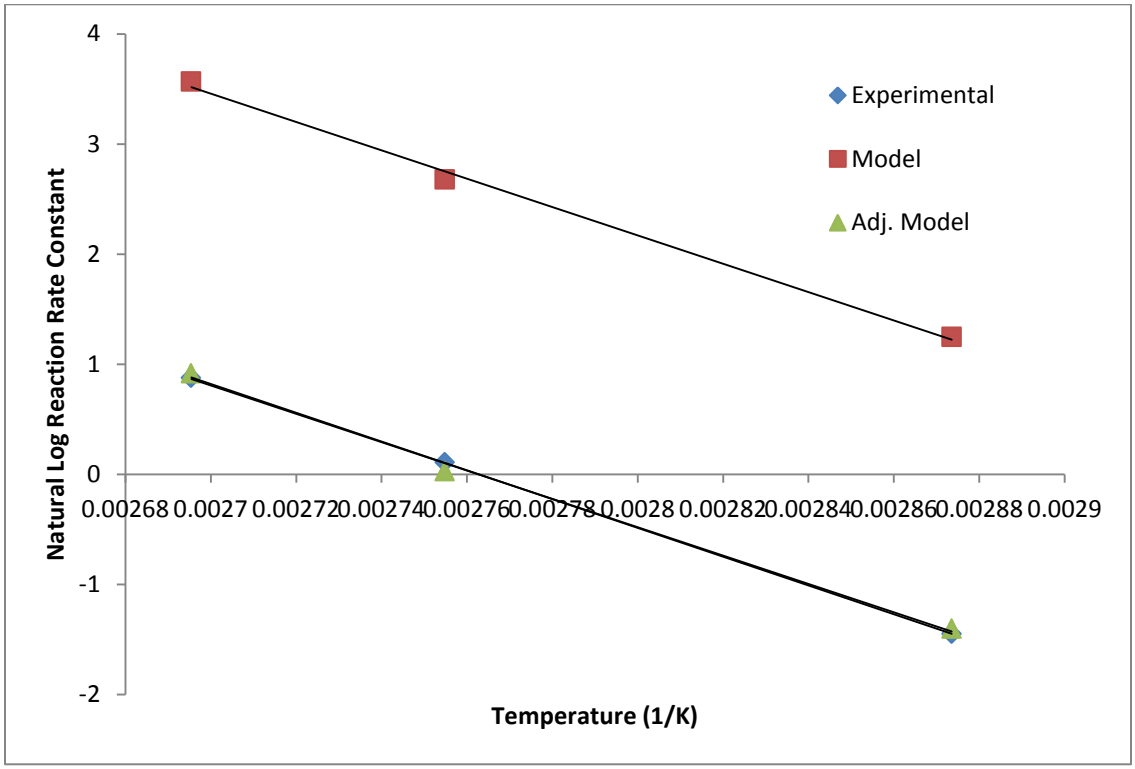

Figure 4.8: Comparison between the Arrhenius parameters of the experimental, model, and adjusted model generated Arrhenius parameters for the HSP reaction at a water to iodine ratio of 118-1. Error bars are present but may be too small to see.

	93-1		105-1		118-1	
	Ea	k0	Ea	k0	Ea	k0
Experimental	105.56	4.31E+13	117.84	4.36E+15	108.60	4.72E+15
Model	100.48	8.02E+12	111.91	6.13E+14	107.01	2.78E+15

Table 4.5: Comparison between the Arrhenius parameters of the HSP reaction at various water to iodine ratios

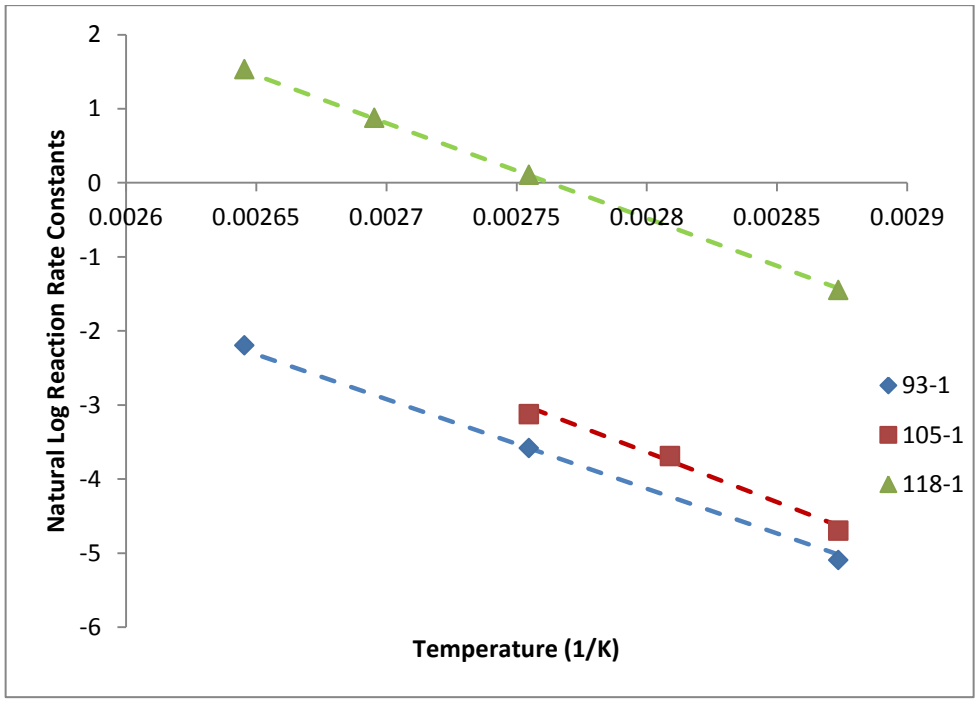

Figure 4.9: Comparison between the Arrhenius plots of the experimental and the adjusted model reaction rate constants for the HSP reaction at various water to iodine ratios. Note that the dashed lines represent the model generated Arrhenius data

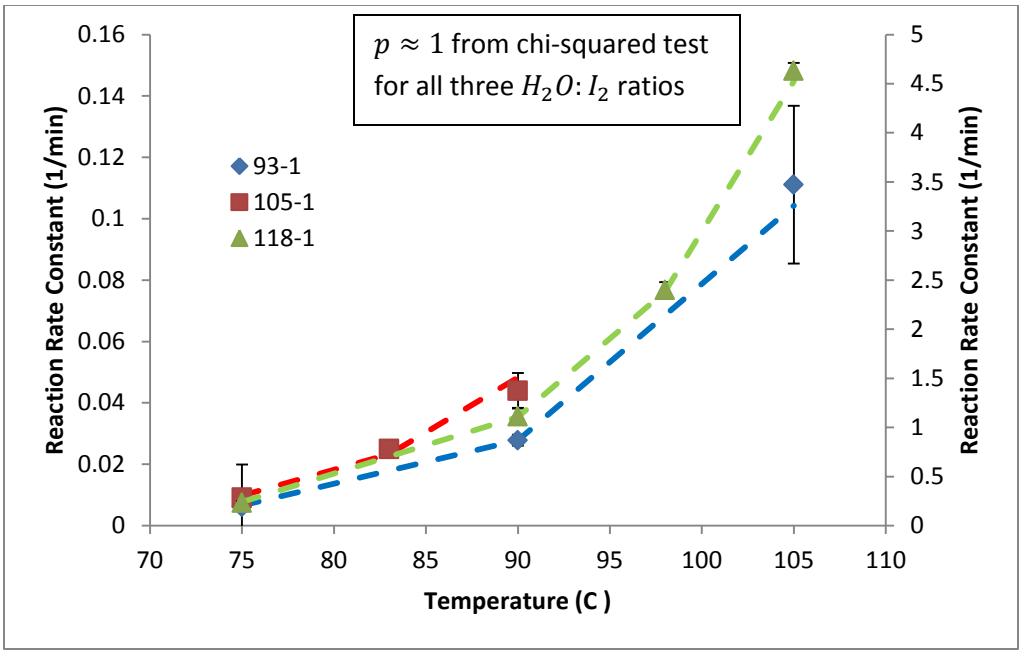

Figure 4.10: Comparison between the experimentally determined and adjusted model generated reaction rate constants for the HSP reaction. Note that the data for the water to iodine ratio of 118-1 is on the secondary y-axis and that the dashed lines represent the model generated data

4.3 Modelling Conclusions

The successful development of a predictive kinetic model surrounding the Bunsen and HSP reactions of the novel sulfur-sulfur thermochemical cycle has laid the groundwork for future advancement and exploration of the cycle. By combining the results of Sections 4.1 and 4.2 and applying it to the raw kinetic data, the progress of the Bunsen/HSP reaction pair can be predicted based on the reaction temperature and the initial concentration of water, two of the more significant processing variables. An example of this can be seen in Figure 4.11, demonstrating the effectiveness of the predictive model.

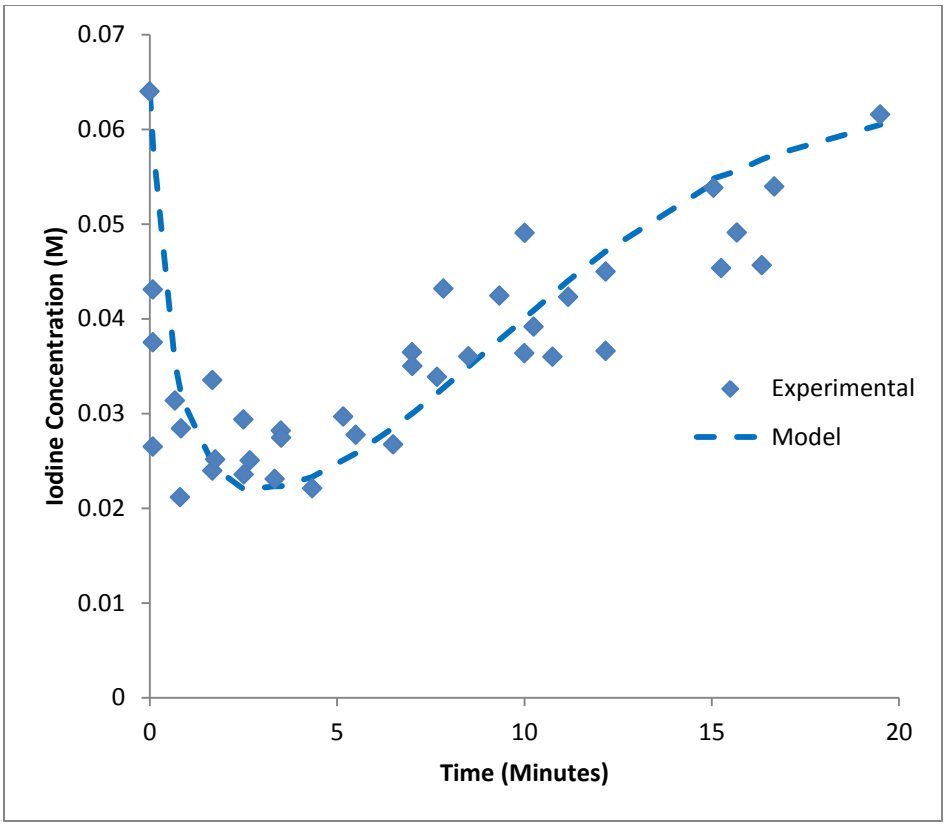

Figure 4.11: Application of predictive model to raw kinetic data for experimental run at 105°C and a water to iodine ratio of 118-1. The raw experimental data is the combination of 3 separate experimental runs using the same parameters

While the experimental data perhaps shows a greater amount of variance than would be preferred, the application of the reaction rate constants determined by the model analysis accurately predicts the progression of the two step reaction effectively.

5. Conclusions and Future Work

5.1 Conclusions

Sustainable and efficient production of hydrogen has been an elusive goal over the last half century, limited by a wide array of issues included difficult separations, storage, infrastructure and methods of production. Through the application of production methods such as thermochemical cycles, the goal of producing a hydrogen based economy, or at least for hydrogen based systems to increase their market share, could potential come to fruition.

This work sought to expand and alter one of the more well-known thermochemical water splitting cycles, the Sulfur-Iodine cycle, into something that could potentially mitigate some of the major issues associated with it. This work expanded the work performed by Auyeung, with a particular focus on the low temperature reaction pair the produces hydrogen sulfide.[9]

A detailed exergetic analysis was performed on the theoretical energy balance of the entire reaction system. The results of this analysis found that the exergetic efficiency of the entire cycle was approximately 70%, not including any pump or electrical generation processes. This value is very comparable to previously published work by Orhan et al.[89] Further analyses of the individual reactions steps and their effect on the total exergetic efficiency found that the hydrogen sulfide production step (the sum of the two reactions studied in this work) changed the most with a significantly smaller change in temperature in comparison to the other three steps.

The effects of water on the reaction kinetics of both the Bunsen and HSP reactions was explored and it was found that an increase in the amount of water present in the batch reactor system increases the reaction rate of both reactions, with the overpowering increase in the Bunsen reaction rate causing an increase in the HSP

rate through the increase in the formation of the products of the former. This kinetic data was utilized for the development of a predictive kinetic model to effectively monitor the concentration of iodine based off of the reaction temperature and the initial concentration of water, with a good deal of success. While the Arrhenius terms generated by the predictive model and those extracted from the experimental data have a small degree of variance, it has been shown that the model can give an accurate prediction of the iodine concentration and works well over a range of temperatures and water concentrations.

Several processing parameters were explored as well. The used ionic liquid from the previous experiments underwent a simple treatment laid out by Earle et al. in which the sulfur and iodine species were removed from the ionic liquid. It was found that the addition of an acid washing step to neutralize any remaining base was useful in the purification of the ionic liquid for reuse. This is of vital importance as the ionic liquid used ([BMIM][TF2N]) is expensive and could potentially be a limiting factor for the implementation of this system at a larger scale. Regeneration of the ionic liquid, therefore, is of vital importance.

Through the results of the regeneration of the ionic liquid, it was seen that the presence of what was hypothesized as a Lewis base affect the kinetics of both reactions. This discovery led to several Lewis bases being purposefully applied to the reaction system in equimolar with iodine amounts. It was found that an increase in the pKb, the measure of the basicity of the species, increased the reaction rate of both reactions, though the Bunsen increased more. While this is initially promising, more work must be done to fully understand the effect and the mechanism of this reaction pathway.

It is important to fully utilize the chemicals that are being used for this reaction system. Since this entire novel thermochemical cycle is predicated on the idea that the iodine in the reaction system is completely regenerated, a set of experiments was

undertaken to determine the amount of iodine that was able to be reformed at various temperatures. It was found that, even at a relatively low temperature of 75°C, that the iodine was able to completely regenerate back to its initial concentration based on the UV/Vis measurements. This is extremely important as far as advancing the development of this process as it potentially eliminates the need for the difficult HIx processing step discussed in the Literature Review.

The equilibration period between the Bunsen and HSP reactions was investigated by changing the initial concentrations of water and sulfur dioxide, as well as the reaction temperature. It was found that the ideal processing parameters would be to minimize the amount of water, maximize the amount of sulfur dioxide and maximize the reaction temperature to shorten the equilibration period time as much as possible.

Initial exploration on the behavior of the sulfur bearing species in the reaction system was undertaken, with several important findings. It appeared as though the effect of sulfur dioxide is only felt within approximately the first minute upon injection, suggesting that a majority of the iodine in the reaction system is consumed in the Bunsen reaction within that first minute. The steady decline of sulfur dioxide found in the two Blanks suggests that the sulfur dioxide is migrating out of the liquid phase and into the gas phase, where the concentration appears to grow exponentially. The behavior of hydrogen sulfide is perhaps even more curious than that of sulfur dioxide. The presence of an oscillating reaction within the liquid phase makes for extremely difficult analysis of what is actually occurring. This is complicated by the sheer volume of possible species present in the system due to the high number of oxidation states of iodine and sulfur.

Ultimately, exploring the low temperature reaction paring of the Bunsen and HSP reactions was successful in helping to determine the relative rates of both reactions and how both reaction respond to other stimuli, such as initial reactant concentration

and homogenous catalysts. Fundamental processing questions were answered in that the ionic liquid can be successfully regenerated, although under batch conditions) and that the initial iodine can be completely recovered for reuse. The kinetic model developed will allow for theoretical observations on how the reaction system will behave under various circumstances and allow for a better design of experiments in the future.

5.2 Future Work

This work has laid the basis for a great deal of work on the Sulfur-Sulfur thermochemical water splitting cycle. The next batch of experimental work will move away from this reactor construct and a new reactor will be developed, allowing for the continuous introduction of sulfur dioxide into a mixture of the ionic liquid, iodine, and water. Figure 5.1 displays the theoretical P&ID of the future reactor.

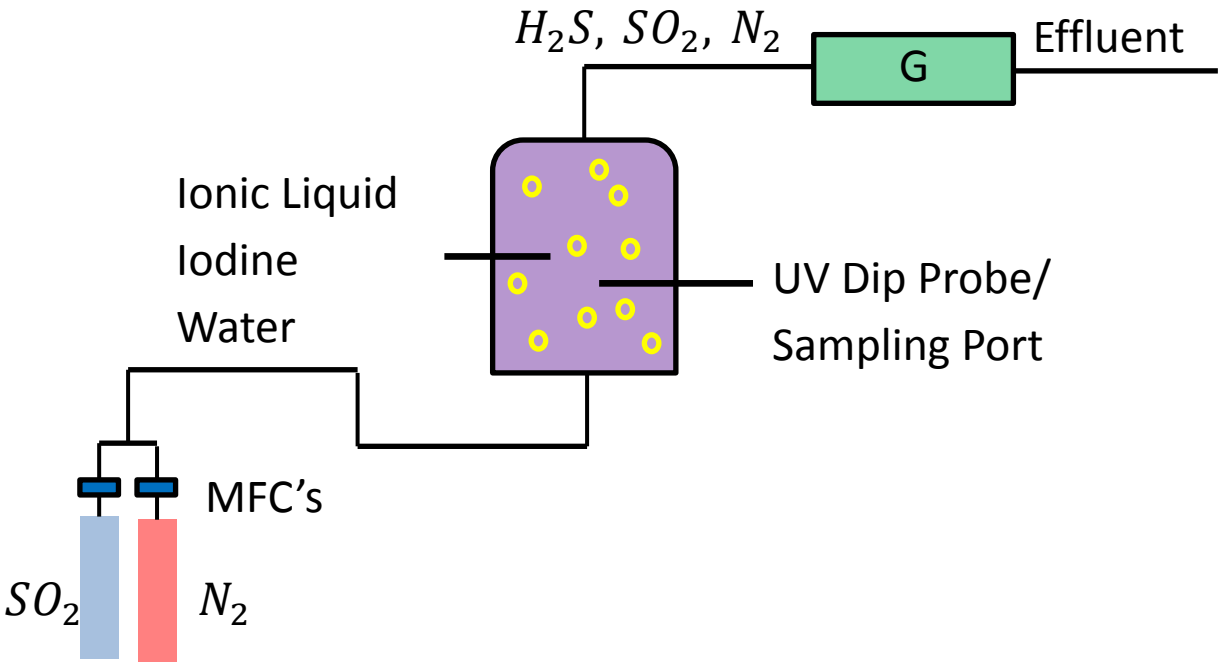

Figure 5.1: Theoretical P&ID for next generation Sulfur-Sulfur cycle reactor

This next generation reactor would be designed such that a dilute stream of sulfur dioxide could be continuously bubbled through the liquid phase reaction mixture and then vented directly into an in-line gas chromatograph for continuous measurement of the amount of sulfur dioxide that leaves the reactor and the amount of hydrogen sulfide generated by the reaction pair. This reactor set up has numerous advantages over the currently constructed batch design. The continuous introduction of sulfur dioxide allows for two beneficial processes: maximizing the amount of sulfur dioxide present in the reaction system (described in Section 3.6.2) and stripping the hydrogen sulfide that is produced from the liquid phase, potentially eliminating the oscillating reaction (described in Section 3.7.2).

It would also be extremely useful to determine is the regenerated iodine (i.e., iodine that has been consumed and produced through the cycle once before) will continue to be viable with no additional treatment, allowing the low temperature reaction to essentially reach a saturation of sulfuric acid in the liquid phase.

$$4SO_{2_{(IL)}} + 4H_2O_{(l)} \rightarrow H_2S_{(IL)} + 3H_2SO_{4_{(IL)}} \qquad \text{Eq. 5.1}$$

The effects of various initial concentrations of the 3 major initial reactants could be explored as far as their effects on processing time until sulfuric acid concentration, production of hydrogen sulfide, and potentially delving into the economic analysis of this cycle being implemented on a larger scale. Homogenous catalysts, such as those described in Section 3.5, could be implemented into this system easily and the ultimate results of their presence could be studied in-line with those experiments listed above.

There is a secondary exploration that would need to be performed in conjunction with the development of this new reactor: the production of an ionic liquid with dissolve iodine that is saturated with sulfuric acid. While the use of the previously described protocol for recycling and regenerating the ionic liquid is effectively for lab scale or bench top experiments, the implementation of such a process on a pilot plant

or full scale process would be extremely cost inefficient and time consuming. Therefore, the sulfur acid- and iodine-laden ionic liquid from the experiments above would be used for a separate batch of experiments, exploring the kinetics of the decomposition of sulfuric acid to sulfur trioxide within the ionic liquid and its subsequent removal via gas-liquid stripping.

This exploration is needed for the ultimate goal of turning the Sulfur-Sulfur cycle into a continuous process. The continuous, scaled-up design would call for a fraction of the ionic liquid to be removed from the main reactor, the sulfuric acid converted to sulfur trioxide, the sulfur trioxide removed from the ionic liquid, and the ionic liquid being returned to the main reactor with only iodine and, potentially, water remaining. The sulfur trioxide would then be sent downstream for the reformation of sulfur dioxide and oxygen. A continuous cycle such as this would dramatically decrease the cost of the ionic liquid regeneration through the elimination of the materials needed in the regeneration step and would eliminate all iodine treatments.

The results of these experiments can be used to further expand the kinetic model, allowing for the continuous nature of the sulfur dioxide and the new reactor conditions. A process flow sheet can be developed, with a focus on the low temperature reactor and its sensitivity to various parameters such as initial concentrations, temperature, pressure, and flow rates.

6. Works Cited

1. Campen, A; Mondal, K; Wiltowski, T; Separation of hydrogen from syngas using a regenerative system, *Int. J. Hydrogen Energy*, **2008**, 33, 332

2. Lutz, A. E.; Larson, R. S.; Keller, J. O., Thermodynamic comparison of fuel cells to the Carnot cycle. *International Journal of Hydrogen Energy* **2002,** *27* (10), 1103-1111.

3. Forsberg, C.W.; Hydrogen markets: implications for hydrogen production technologies. Proceedings of American Institute of Chemical Engineers Spring Meeting, Atlanta, Georgia; April 10-14, 2005

4. Kraus, T. Hydrogen fuel: An economically viable future for the transportation industry? Duke J. Economics Spring 2007, XIX

5. Lipman, T.E.; What will power the hydrogen economy? Analysis and report prepared for the Natural Resources Defense Council, publication no. UCD-ITS-RR-04-10. University of California, July 12, 2004

6. Giaconia, A.; Caputo, G.; Ceroli, A.; Diamanti, M.; Barbarossa, V.; Tarquini, P.; Sau, S., Experimental study of two phase separation in the Bunsen section of the sulfur–iodine thermochemical cycle. *International Journal of Hydrogen Energy* **2007,** *32* (5), 531-536

7. Perkins, C.; Weimer, A. W., Solar-Thermal Production of Renewable Hydrogen. *AIChe Journal* **2009,** *55* (2), 286-293

8. Holbrey John, D.; Turner Megan, B.; Rogers Robin, D., Selection of Ionic Liquids for Green Chemical Applications. In *Ionic Liquids as Green Solvents*, American Chemical Society: Washington, DC, 2003; pp 2-12.

9. AuYeung, N.; Hydrogen Production via a Sulfur-Sulfur Thermochemical Water Splitting Cycle. Doctoral Thesis. Oregon State University. Corvallis: OSU Library, 2011

10. AuYeung, N.; Yokochi, A.F.T.; Steam reformation of hydrogen sulfide. *Int. J. Hydrogen Energy.* **2013,** 38, 6304-6313

11. Funk, J.E.; Thermochemical hydrogen production: past and present, *Int. J. Hydrogen Energy*, **2001**, 26, 185-190

12. Lewis, M.; Serban, M.; Basco, J.; Figueroa, J.; Low Temperature Thermochemical Cycle Development. Chicago, IL 2003

13. Beghi, G.E.; A decade of research on thermochemical hydrogen at the joint research center, Ispra. *Int. J. Hydrogen Energy*. **1986** 11, 761

14. BROWN, L. C.; FUNK, J. F.; SHOWALTER, S. K. *INITIAL SCREENING OF THERMOCHEMICAL WATER-SPLITTING CYCLES FOR HIGH EFFICIENCY GENERATION OF HYDROGEN FUELS USING NUCLEAR POWER*; University of Kentucky Sandia National Laboratory General Atomics: April 2000, 2000.

15. Steinfeld, A.; Solar thermochemical production of hydrogen – a review, *Solar Energy*, **2005**, 78, 603-615

16. Nakamura, T.; Hydrogen production from water utilizing solar heat at high temperatures. *Solar Energy*. **1977**, 19, 467

17. Kodama, T.; High-temperature solar chemistry for converting solar heat to chemical fuels, *Pro. Energy and Combustion Science*, **2003**, 29, 567-597

18. Tofighi, A.; Sibieude, F.; Ducarrorr, M.; Benezech, G.; Decomposition thermique a lair de la magnetite au foyer dun four solaire. *Rev. Int. Htes. Temp Refract*, **1978**, 15, 7-13

19. Sibieude, F.; Ducarroir, M.; Tofighi, A.; Ambriz, J.; High temperature experiments with a solar furnace: the decomposition of Fe3O4, Mn3O4, CdO. *Int. J. Hydrogen Energy,* **1982**, 7(1), 79-88

20. Palumbo, R.; Lede, J.; Boutin, O.; Ricart, E.; Steinfeld, A.; Moller, S.; Weidenkaff, A.; Fletcher, E.; Bielicki, J.; The production of Zn from ZnO in a high temperature solar decomposition quenc process. I. The scientific framework for the process. *Chem Engr. Sci.* **1998**, 53(14), 2503-2517

21. Palumbo, R.; Solar thermal chemical processing: challenges and changes, *J. Phys. IV Fr.* **1999**, Pr3-35-40n

22. Weidenkaff, A.; Brack, M.; Moller, S.; Palumbo, R.; Steinfeld, A.; Solar thermal production of zinc: program strategy and status of research. *J. Phys. IV Fr*, **1999** 9, Pr-313-8

23. Weidenkaff, A.; Steinfeld, A.; Wokaun, A.; Auer, P.; Eichler, B.;' Reller, A.; Direct solar thermal dissociation of zinc oxide: condensation and crystallization of zinc in the presence of oxygen, *Solar Energy*, **1999**, 65(1), 59-69

24. Weidenkaff, A.; Reller, A.; Wokaun, A.; Steinfleld, A.; Thermogravimetric analysis of the ZnO/Zn water splitting cycle, *Thermochem Acta.*, **2000**, 359, 69-75

25. Lungberg, M.; Model calculations on some feasible two-step water splitting processes. *Int. J. Hydrogen Energy*, **1993**, 18(5), 369-376

26. Ehrensberger, K.; Frei, A.; Kuhn, P.; Oswald, H.; Hug, P.; Comparative experimental investigations of the water splitting reaction with iron oxide $Fe_{1-y}O$ and iron manganese oxides $(Fe_{1-x}Mn_x)_{1-y}O$. *Solid State Ionics*, **1995**, 75, 151-160

27. Ehrensberger, K.; Kuhn, P.; Shklover, V.; Oswald, H.; Temporary phase segregation processes during the oxidation of $(Fe_{0.7}Mn_{0.3})_{.99}O$ in N2-H2O atmosphere. *Solid State Ionics*. **1996**, 90, 75-81

28. Kameyama, H.; Yoshida, K.; Br-Ca-Fe water decomposition cycles for hydrogen production, *Proceedings of the 2nd World Hydrogen Energy Conference*, **1978**, p 829

29. Rosen, M.A.; Naterer, G.F.; Sadhankar, R.; Suppiah, S.; Nuclear-based hydrogen production with a thermochemical copper-chlorine cycle and supercritical water reactor, *Canadian Hydrogen Association Workshop*, **2006**

30. Sakurai, M.; Bilgen, A.; Tustsumi, A.; Yoshida, K.; Solar UT-3 Thermochemical cycle for Hydrogen production, *Solar Energy*, **1996**, 57(1), 51-58

31. Rosen, M.A.; Advances in hydrogen production by thermochemical water decomposition: a review, *Energy*, **2010**, 35, 1068-1076

32. Aihara, M.; Umida, H.; Tsutsumi, A.; Yoshida, K.; Kinetic study of UT-3 thermochemical hydrogen production process, *Int. J. Hydrogen Energy*, **1990**, 15(1), 7-11

33. Sakurai, M.; Aihara, M.; Miyake, N.; Tsutsumi, A.; Yoshida, K.; Test of one-loop flow scheme for the UT-3 thermochemical hydrogen production process, *Int. J. Hydrogen Energy*, **1992**, 17(8), 587-592

34. Nakayama, T.; Yoshioda, H.; Furutani, H.; Kameyama, H.; Yoshida, K.; Mascot – A bench scale plant for producing hydrogen by the UT-3 thermochemical decomposition cycle, *Int. J. Hydrogen Energy*, **1984**, 9(3), 187-190

35. Kameyama, H.; Tomino, Y.; Sat, T.; Amir, R.; Orihara, A.; Aihara, M.; Yoshida, K.; Process simulation of Mascot plant using the UT-3 thermochemical cycle for hydrogen production, *Int. J. Hydrogen Energy*, **1989**, 14(5), 323-330

36. Amir, R.; Sat, T.; Tamamoto, K,; Kabe, T.; Kameyama, H.; Design of solid reactants and reaction kinetics concerning the iron compounds in the UT-3 thermochemical cycle, *Int. J. Hydrogen Energy*, **1992**, 17(10), 783-788

37. Amir, R.; Shizaki, S.; Tamamoto, K.; Kabe, T.; Kameyama, H.; Design development of iron solid reactants in the UT-3 water decomposition cycle based on ceramic support materials, *Int. J. Hydrogen Energy*, **1993**, 18(4), 283-286

38. Aochi, A.; Tadokoro, Y.; Yoshida, K.; Kameyama, H.; Nobue, M.; Yamaguchi, T.; Economic and technical evaluation of UT-3 thermochemical hydrogen production process for an industrial scale plant, *Int. J. Hydrogen Energy*, **1989**, 14(7), 421-429

39. Tadokoro, Y.; Kajiyama, T.; Yamaguchi, T.; Sakai, N.; Kameyama, H.; Yoshida, K.; Technical evaluation of UT-3 thermochemical hydrogen production process for an industrial scale plant. *Proc. 10th World Hydrogen Energy Conf.*, **1994,** Cocoa Beach, FL

40. Chukwu, C.; Naterer, G.F.; Rosen, M.A.; Process simulation of Nuclear-Produced Hydrogen with a Cu-Cl Cycle, *29th Conference on of the Canadien Nuclear Society*, **2008**, Toronto, Canada

41. Sivasubrmanian, P.; Ramasamy, R.P.; Freire, F.J.; Holland, C.E.; Weidner, J.W.; Electrochemical hydrogen production from thermochemical cycles using a proton exchange membrane electrolyzer, *Int. J. Hydrogen Energy*, **2007**, 32, 463-468

42. Gorensek, M. B.; Summers, W. A., Hybrid sulfur flowsheets using PEM electrolysis and a bayonet decomposition reactor. *International Journal of Hydrogen Energy* **2009,** *34* (9), 4097-4114.

43. Hinkley, J. T.; O'Brien, J. A.; Fell, C. J.; Lindquist, S.-E., Prospects for solar only operation of the hybrid sulphur cycle for hydrogen production. *International Journal of Hydrogen Energy In Press, Corrected Proof*.

44. Vitart, X.; Le Duigou, A.; Carles, P., Hydrogen production using the sulfur–iodine cycle coupled to a VHTR: An overview. *Energy Conversion and Management* **2006** *47*, 2740-2747.

45. Goldstein, S.; et al.; Upper bound and best estimate of the efficiency of the iodine sulphur cycle. *Int J. Hydrogen Energy*, **2005**, 30, 619-626

46. Besenbruch, G.E.; et al. **1982**, GA-A18257 report

47. Roth, M.; Knoche, K.F.; Thermochemical water splitting through direct HI-decomposition from H2O/HI/I2 solutions. *Int. J. Hydrogen Energy*, **1989**, 14, 545-549

48. Stewart, F. F.; Orme, C. J.; Jones, M. G., Membrane processes for the sulfur–iodine thermochemical cycle. *International Journal of Hydrogen Energy* **2007,** *32*, 457 – 462.

49. Onuki, K.; Hwang, G.J; Shimizu, S.; Electrodialysis of hydroiodic acid in the presence of iodine. *J. Membr. Sci.* **2000**, 175, 171-179

50. Hong, S-D.; Kim, J-K; Bae, KK; Lee, S-H; Choi, H-S; Hwang, G-J.; Evaluation of the membrane properties with changing iodine molar ratio in HIx (HI-I2-H2O mixture) solution to concentrate HI by electro-electrodialysis. *J Membr. Sci.*, **2007**, 291, 106-110

51. Onuki, K.; Hwang, G-J; Arifal, Shimizu, S.; Electro-electrodialysis of hydroiodic acid in the presence of iodine at elevated temperature, *J. Membr. Sci.,* **2001**, 192, 193-199

52. Tanaka, N.; Yamaki, T.; Asano, M.; Maekawa, Y.; Onuki, K.; Electro-electrodialysis of HI-I2-H2O mixture using radiation grafted polymer electrolyte membranes, *J. Membr. Sci*, **2010**, 346, 136-142

53. Hong, S-D.; Kim, J-K.; Kim, B-K.; Choi, S-I.; Bae, K-K.; Hwang, G-J.; Evaluation on the elctro-electrodialysis to concentrate HI from HIx solution by using two types of the electrode. *Int. J. Hydrogen Energy*, **2007**, 32, 2005-2009

54. Hwang, G-J.; Onuki, K.; Nomura, M.; Kasahara, S.; Kim, J-W.; Improvement of the thermochemical water splitting IS process by electro-electrodialysis, *J. Membr. Sci.,* **2003**, 220, 129-136

55. Kondamudi, K.; Upadhyayula, S.; Kinetic studies of sulfuric acid decomposition over Al-Fe2O3 catalyst in the sulfur iodine cycle for hydrogen production. *Int. J. Hydrogen Energy*, **2012**, 37, 3586-3594

56. Dokiya, M.; Kameyama, T.; Fukuda, K.; Kotera, Y.; The study of thermochemical hydrogen preparation. Iii. An oxygen evolving step through the thermal splitting of sulfuric acid. *Bulletin of the Chemical Society of Japan*, **1977**, 50(10), 2657-2660

57. Norman, J.: Myselse, K.; Sharp, R.; Williamson, D.; Studies of the sulfur-iodine thermochemical water splitting cycle. *Int. J. Hydrogen Energy*, **1982**, 7(7), 545-556

58. Ishikawa, H.; Ishii, E.; Uehara, I.; Nakane, M.; Catalyzed thermal decomposition of H2SO4 and production of hbr reaction of so2 with br2 and h2o, *Int. J. Hydrogen Energy*, **1982**, 7(3), 237-246

59. Tagawa, H.; Catalytic decomposition of sulfuric acid using metal oxides as the oxygen generating reaction in thermochemical water splitting process, *Int. J Hydrogen Energy.* **1989**, 14(1), 11-17

60. Barbarossa, V.; Brutti, S.; Diamanti, M.; Sau, S.; De Maria, G.; Catalytic thermal decomposition of sulphuric acid in sulfur iodine cycle for hydrogen production. *Ing. J. Hydrogen Energy*, **2006**, 31(7), 883-890

61. T-Ho Kim, T-taek Gong, Gwon, B.; Lee, K-young; Jeon, H-young, Shin C-ho, et al. Catalytic decomposition of sulfur trioxide on the binary metal oxide catalysts of fe/al and fe/ti. *Applied Catalysis*, **2006**, 305, 39-46

62. Ginosar, D.M.; Petkovic, L.M.; Glenn, A.W.; Burch, K.C.; Stability of supported platinum sulfuric acid decomposition catalysts for use in thermochemical water splitting cycles. *Int. J Hydrogen Energy*, **2007**, 32(4), 482-488

63. Petkovic, L.; Ginosar, D.; Rollins, H.; Burch, K.; Pinhero, P.; Farrell, H.; Pt/tio2 (rutile) catalysts for sulfurc acid decomposition in sulfur-based thermochemical water splitting cycles. *Applied Catalysis A: General*, **2008**, 338(1-2), 27-36

64. Banerjee, A.; Pai, M.; Bhattacharya, K.; Tripathi, A.; Kamble, V.; Bharadwaj, S.; et al. Catalytic decomposition of sulfuric acid on mixed cr/fe oxide samples and its application in sulfur-iodine cycle for hydrogen production. *Int. J. Hydrogen Energy*, **2008**, 33(1), 319-26

65. Nagaraja, B.M.; Jung, K.D. Yoo, K.S.; Synthesis of cu/fe/ti/al2o3 composite granules for so3 decomposition in si cycle, *Catalysis Letters*, **2008**, 128(1-2), 248-52

66. Ginosar, D.M.; Rollins, H.W., Petkovic, L.M.; Burch K.C.; Rush, M.J. High temperature sulfuric acid decomposition over complex metal oxide catalysts. *Int. J. Hydrogen Energy*, **2009** 34(9), 4065-4073

67. Karagiannakis, G.; Agrafiotis, CC.; Zygogianni, A.; Pagkoura, C.; Konstandopoulos, A.G.; Hydrogen production via sulfur-based thermochemical cycles,: part 1: synthesis and evaluation of metal oxide based candidate catalyst powders for sulfuric acid decomposition step. *Int. J. Hydrogen Energy*, **2010**, 36(4), 2831-2844

68. Guo, H.F.; Zhang, P.; Bai, Y.; Wang, L.J.; Chen, S.Z.; Xu, J.M.; Continuous purification of H2SO4 and HI phases by packed column in IS process, *Int. J. Hydrogen Energy,* **2010**, 35, 2836-2839

69. Ying, B.; Zhang, P.; Guo, H.; Chen, S>; Wang, L.; Xu, J.; Purification of sulfuric and hydrioidc acids phases in the iodine-sulfur process, *Chin. J. Chem. Eng*, **2009**, 17(1), 2000-2010

70. Byung, J.L.; Hee Cheon, N.O., Ho Joon Yoon, Seung Jun Kim, Eung Soo Kim, An optimal operating window for the Bunsen process in the I-S thermochemical cycle, In: Proceedings of ICAPP'09; **2009**

71. Sakurai, M.; Nakajimaa, H.; Amirb, R.; Onukia, K.; Shimizua, S., Experimental study on side-reaction occurrence condition in the iodine±sulfur thermochemical hydrogen production process. *International Journal of Hydrogen Energy* **2000,** *25*, 613-619.

72. Kubo, S.; Nakajima, H.; Kasahara, S.; Higashi, S.; Masaki, T.; Abe, H.; Onuki, K., A demonstration study on a closed-cycle hydrogen production by the thermochemical water-splitting iodine–sulfur process. *Nuclear Engineering and Design* **2004,** *233*, 347-354

73. Mason, C. F. V.; Bowman, M. G. In *Reactions for Improving Efficiencies in Thermochemical Cycles Related to the Sulfur Dioxide-Iodine Process*, 4th World Hydrogen Energy Conference, Pasadena, Switzerland, June 13-17, 1982; Vezirolglu, N.; Van Vorst, W. D.; Kelley, J. H., Eds. Pergamon Press Inc.: Pasadena, Switzerland, 1982; pp 665-674.

74. Giaconia, A.; Caputo, G.; Sau, S.; Prosini, P. P.; Pozio, A.; De Francesco, M.; Tarquini, P.; Nardi, L., Survey of Bunsen reaction routes to improve the sulfur-iodine thermochemical water-splitting cycle. *International Journal of Hydrogen Energy* **2009,** *34* (9), 4041-4048

75. Monriri, A.; Mertins, P.; Wang, H.; Exergy analysis of hydrogen production from different sulfur-containing compounds based on H2S splitting cycle, *Int. J. Hydrogen Energy*, **2012**, 37, 15003-15010

76. Moran, M.J.; Shapiro, H.N.; Fundamentals of engineering thermodynamics, 6th ed. Publisher Wiley, ISBN: 0471787353, **2008**

77. Sankaranarayanan, K.; de Swaan Arons J.; van der Kooi, H.J.; Efficiency and Sustainability in the energy and chemical industries: scientific principles and case studies. 1st ed. Publisher: CRC press, ISBN 0824708458, **2004**

78. Reddy, V.; Kaushik, S.; Tyagi, S.; Panwar, N.; An approach to analyse energy and exergy analysis of thermal power plants: a review, *Smart Grid and Renewable Energy*, **2010**, 1(3), 143-152

79. Rosen, M.A.; Scott, D.S.; Comparative efficiency assessments for a range of hydrogen production processes, *Int. J. Hydrogen Energy*, **1998**, 23(8), 653-659

80. Steinfeld, A.; Palumbo, R.; Solar thermochemical process technology. In: Mayara, RA, editor. Encyclopedia of physical science and technology. New York: Academic Press, ISBN, 0-12-227410-5, **2001**, 15, 237-256

81. Steinfeld, A.; Solar hydrogen production via a two-step water-splitting thermochemical cycle based on Zn/ZnO redox reactions, *Int. J. Hydrogen Energy*, **2002**, 27, 611-619

82. Abanades, S.; Charvin, P.; Flamant, G.; Neveu, P.; Screening of water-splitting thermochemical cycles potentially attractive for hydrogen production by concentrated solar energy, *Energy*¸**2006**, 31, 2805-2822

83. Hammache, A.; Bilgen, E.; Evaluation of thermal efficiency and cost of high temperature solar heat from central receiver systems to use in hydrogen producing thermochemical processes, *Int. J. Hydrogen Energy*, **1988**, 13(13), 539-546

84. Orhan, M.F.; Dincer, I.; Rosen, M.A.; The oxygen production step of a cooper-chlorine thermochemical water decomposition cycle for hydrogen production: energy and exergy analyses, *Chem. Eng. Sci.,* **2009**, 64, 860-869

85. Orhan, M.F.; Dincer, I., Rosen, M.A.; Energy and exergy analyses of the fluidized bed of a copper-chlorine cycle for nuclear based hydrogen production via thermochemical water decomposition, *Chem. Eng. Research and Design*, **2009**, 87, 684-694

86. Orhan, M.F.; Dincer, I.; Rosen, M.A.; Thermodynamic analysis of copper production step in a copper-chlorine cycle for hydrogen production*, Thermochimica Acta*, **2008**, 4 80, 22-29

87. Orhan, M.F.; Dincer, I.; Rosen, M.A.; Energy and exergy assessments of the hydrogen production step of a copper-chlorine thermochemical water splitting cycle driven by nuclear-based heat, *Int. J. Hydrogen Energy*, **2008**, 6456-6466

88. Orhan, M.F.; Dincer, I.; Rosen, M.A.; Energy and exergy analyses of the drying step of a copper-chlorine thermochemical cycle for hydrogen production, *Int. J. Hydrogen Energy*, **2009**, 6(6), 793-808

89. Orhan, M.F.; Energy, Exergy, and Cost Analysis of Nuclear-Based Hydrogen Production via Thermochemical Water Decomposition Using a Copper-Chlorine (Cu-Cl) Cycle, Master's Thesis, University of Ontario Institute of Technology, April , 2008

90. Huddleston, J.G.; Visser, A.E.; Reichert, W.N.; Willauer, H.D.; Broker, G.A.; Rogers, R.D.; characterization and comparison of hydrophilic and hydrophobic

ionic liquids incorporating the imidazolium cation. *Green Chem*, **2001**, 3(4), 156-164

91. Seddon, K.R.; Room-temperature ionic liquids: neoteric solvents for clean catalysis. *Kinetic Catal.*, **1996**, 37(5), 693-697

92. Rebelo, L. P. N.; Lopes, J. N. C.; Esperancüa, J. M. S. S.; Filipe, E., On the Critical Temperature, Normal Boiling Point, and Vapor Pressure of Ionic Liquids. *Journal of Physical Chemistry B* **2005,** *109*, 6040-6043

93. Lee, K. Y.; Taek Gonga, G.; Songb, K. H.; Kima, H.; Junga, K.-D.; Kima, C. S., Use of ionic liquids as absorbents to separate SO2 in SO2/O2 in thermochemical processes to produce hydrogen. *International Journal of Hydrogen Energy* **2008**

94. Brennecke, J. F.; Maginn, E. J., Ionic Liquids: Innovative Fluidsfor Chemical Processing. *AIChe Journal* **2001,** *47* (11), 2384-2389

95. Jork, C.; Kristen, C.; Pieraccini, D.; Stark, A.; Chiappe, C.; Beste, Y. A.; Arlt, W., Tailor-made ionic liquids. *J. Chem. Thermodyn.* **2005,** *37*, 537-558

96. Jiang, Y.-Y.; Zhou, Z.; Jiao, Z.; Li, L.; Wu, Y.-T.; Zhang, Z.-B., SO2 Gas Separation Using Supported Ionic Liquid Membranes. *The Journal of Physical Chemistry B* **2007,** *111* (19), 5058-5061

97. Huang, J.; Riisager, A.; Wasserscheid, P.; Fehrmann, R., Reversible physical absorption of SO2 by ionic liquids. *Chem. Commun.* **2006,** (38), 4027-4029

98. Shokouhi, M.; Adibi, M.; Jalili, A. H.; Hosseini-Jenab, M.; Mehdizadeh, A., Solubility and Diffusion of H2S and CO2 in the Ionic Liquid 1-(2-Hydroxyethyl)-3-methylimidazolium Tetrafluoroborate. *Journal of Chemical & Engineering Data* **2009**

99. Pomelli, C. S.; Chiappe, C.; Vidis, A.; Laurenczy, G. b.; Dyson, P. J., Influence of the Interaction between Hydrogen Sulfide and Ionic Liquids on Solubility: Experimental and Theoretical Investigation. *The Journal of Physical Chemistry B* **2007,** *111* (45), 13014-13019.

100. Anderson, J.L.; Dixon, J.K.; Maginn, E.J.; Brenneck, J.F.; Measurement of SO2 solubility in ionic liquids. *Phys. Chem. B: Letters*, **2006**, 110, 15059-15062

101. Rahmati-Rostami, M.; Ghotbi, C.; Hosseini-Jenab, M.; Ahmadi, A.N.; Jalili, A.H.; Solubility of H2S in ionic liquids [hmim][PF67], [hmim][BF4], and [hmim][TF2N], *J. Chem. Thermodynamics,* **2009**, 41, 1052-1055

102. De Beni, G.; Pierini, G.; Spelta, B.; The reaction of sulphur dioxide with water and a halogen. The Case of iodine: reaction in presence of organic solvents. *Int. J. Hydrogen Energy*, **1980**, 5(2), 141-149

103. Barbarossa, V.; Vanga, G.; Diamanti, M.: Cali, M.; Doddi, G.; Research notes: chemically enhanced separation of H2So4/Hi mixtures from the Bunsen reaction in the sulfur-iodine thermochemical cycle, *Ind. Eng. Chem. Res.*, **2009**, 48(19), 9040-9044

104. Zhu, Q.; Zhang, Y.; Zhou, C.; Wang, Z.; Zhou, J.; Cen, K.; Optimization of liquid-liquid phase separation characteristics in the Bunsen section of the sulfur-

iodine hydrogen production process, *Int. J. Hydrogen Energy*, **2012**, 37(8), 6407-6414

105. Taylor, M.L.; Elder, R.H.; Styring, P.; Allen, R.W.K.; Improved solvation routes for the Bunsen reaction in the sulphur iodine thermochemical cycle: Part I – Ionic liquids, *Int. J. Hydrogen Energy*, **2013**, 38, 1765-1774

106. Selcuk, B.; Calculation and Interpretation of the Standard Chemical Exegires of Elemetns Using the Chemical Reference Species. *Acta Phys. –Chim. Sin.,* **2009**, *25(8)*, 1645-1649

107. Giauque, W.F.; Hornung, E.W.; Kunzler, J.E.; Rubin, T.R.; The Thermodynamic Properites of Aqueous Sulfuric Acid Solutions and Hydrates from 15 to 300 K. *J.A.C.S* **1960**, *82*(1), 62-70

108. Earle, M. J.; Gordon, C. M.; Plechkova, N. V.; Seddon, K. R.; Welton, T., Decolorization of Ionic Liquids for Spectroscopy. *ANALYTICAL CHEMISTRY* **2007,** *79* (2), 758-764

7. Appendices

7.1 Appendix A: Exergetic Efficiency: Shomate Equations

Below are tabulated values for the various thermodynamic parameters used to calculate the properties needed for all of the species studied in the exergetic analysis.

Compound	A	B	C	D	E	F	G	H
$H_2O\ (l)$	-203.61	1,523.29	-3,196.4	2,474.46	3.86	-256.55	-488.72	-285.83
$SO_2\ (g)$	21.4304	74.3509	-57.752	16.3553	0.08673	-305.768	254.887	-296.84
$H_2S\ (g)$	26.8841	18.6780	3.43420	-3.37870	0.13588	-28.9121	233.374	-20.5020
H_2SO_4	47.29	190.33	-148.13	43.87	-0.74	-758.95	301.30	-735.13
$SO_3\ (g)$	24.03	119.46	-94.39	26.96	-0.12	-407.85	253.52	-395.77
$H_2O\ (g)$	30.092	6.83251	6.79343	-2.53448	0.08213	-250.881	223.396	-241.826
$O_2\ (g)$	31.3223	-20.2353	57.8664	-36.5062	-0.00737	-8.90347	246.794	0
$H_2\ (g)$	18.5630	12.2573	-2.8597	0.26823	1.97799	-1.1474	156.288	0

Table 7.1: Shomate equation parameters for various species in exergetic analysis.

7.2 Appendix B: Experimental vs. Model Data

7.2.1 Appendix B.1: Bunsen Reaction Data

118-1	T=35° C			T=40° C			T=45°C			T=50°C		
	t (min)	$[I_2]_e$	$[I_2]_m$	t (min)	$[I_2]_e$	$[I_2]_m$	t (min)	$[I_2]_e$	$[I_2]_m$	t (min)	$[I_2]_e$	$[I_2]_m$
	0	0.0640	0.0640	0	0.0640	0.0640	0	0.0640	0.0640	0	0.0640	0.0640
	0.25	0.0629	0.0613	0.1667	0.0592	0.0602	0.16667	0.0588	0.0584	0.25	0.0566	0.0549
	0.8333	0.0559	0.0558	0.25	0.0583	0.0584	0.16667	0.0580	0.0584	0.25	0.0519	0.0511
	1	0.0540	0.0543	0.25	0.0547	0.0584	0.25	0.0533	0.0558	0.25	0.0513	0.0511
	1.8333	0.0470	0.0479	0.8333	0.0455	0.0479	0.8333	0.0465	0.0417	0.75	0.0366	0.0341
	2.5	0.0398	0.0436	0.8333	0.0454	0.0477	0.8333	0.0420	0.0416	0.75	0.0326	0.0340
	2.8333	0.0398	0.0417	0.8333	0.0442	0.0475	1	0.0386	0.0385	0.83333	0.0367	0.0319
	3.5	0.0460	0.0381	1.66	0.0390	0.0369	1.5	0.0327	0.0307	1.5	0.0224	0.0192
	3.6667	0.0344	0.0373	1.66	0.0374	0.0368	1.66667	0.0308	0.0285			
	4.5	0.0303	0.0337	1.66	0.0370	0.0368	1.75	0.0276	0.0275			
	5.6667	0.0341	0.0294	2.5	0.0344	0.0289	2.25	0.0256	0.0221			
	5.8333	0.0287	0.0288	2.5	0.0301	0.0289	2.5	0.0224	0.0198			
	6.5	0.0289	0.0268	2.5	0.0282	0.0288	2.5	0.0223	0.0198			
	7	0.0243	0.0254	3.33	0.0286	0.0229	3	0.0178	0.0159			
	7.5	0.0235	0.0241	3.33	0.0254	0.0229						
	7.6667	0.0270	0.0237	3.33	0.0249	0.0229						
	8	0.0209	0.0229									
	8.5	0.0219	0.0218									
	9.1667	0.0204	0.0205									

105-1	T=45° C			T=50° C			T=55° C			T=60° C		
	t (min)	$[I_2]_e$	$[I_2]_m$	t (min)	$[I_2]_e$	$[I_2]_m$	t (min)	$[I_2]_e$	$[I_2]_m$	t (min)	$[I_2]_e$	$[I_2]_m$
	0	0.0640	0.0640	0	0.0640	0.0640	0	0.0640	0.0640	0	0.0640	0.0640
	0.25	0.0619	0.0629	0.2	0.0621	0.0619	0.25	0.0617	0.0611	0.25	0.0623	0.0605
	1	0.0589	0.0597	0.25	0.0612	0.0619	0.25	0.0561	0.0611	0.25	0.0573	0.0605
	1.25	0.0604	0.0588	1	0.0556	0.0562	0.8333	0.0528	0.0551	0.25	0.0559	0.0605
	1.75	0.0571	0.0569	1.5	0.0554	0.0545	0.8333	0.0526	0.0551	0.75	0.0515	0.0544
	2	0.0563	0.0560	1.75	0.0520	0.0513	1	0.0520	0.0536	1	0.0503	0.0517
	2.25	0.0549	0.0551	1.75	0.0517	0.0513	1.5	0.0490	0.0494	1	0.0502	0.0516
	2.5	0.0525	0.0542	2.25	0.0494	0.0485	1.75	0.0444	0.0474	1.5	0.0468	0.0469
	2.75	0.0517	0.0534	2.5	0.0478	0.0472	2.25	0.0461	0.0440	1.75	0.0454	0.0447
	3	0.0540	0.0526	3	0.0460	0.0447	2.25	0.0442	0.0440	1.75	0.0415	0.0447
	4.75	0.0474	0.0469	3	0.0436	0.0447	2.5	0.0414	0.0424	2.25	0.0441	0.0409
	5	0.0474	0.0469	3.75	0.0419	0.0414	2.8333	0.0399	0.0404	2.5	0.0414	0.0392
	6.25	0.0439	0.0439	5.25	0.0320	0.0359	4.25	0.0360	0.0336	2.5	0.0378	0.0392
	6.5	0.0419	0.0433	6	0.0343	0.0337	5	0.0322	0.0307	4.25	0.0307	0.0299
	8	0.0417	0.0402									

93-1	T=45° C			T=50°C			T=55°C			T=60°C		
	t (min)	$[I_2]_e$	$[I_2]_m$	t (min)	$[I_2]_e$	$[I_2]_m$	t (min)	$[I_2]_e$	$[I_2]_m$	t (min)	$[I_2]_e$	$[I_2]_m$
	0	0.0640	0.0640	0	0.0640	0.0640	0	0.0640	0.0640	0	0.0640	0.0640
	0.25	0.0629	0.0632	0.25	0.0629	0.0631	1	0.0591	0.0596	1	0.0565	0.0586
	1	0.0625	0.0609	0.25	0.0629	0.0631	1	0.0572	0.0596	1	0.0556	0.0586
	1.5	0.0621	0.0594	0.25	0.0625	0.0631	1	0.0561	0.0595	1.75	0.0541	0.0551
	2	0.0597	0.0587	1	0.0622	0.0604	1.75	0.0558	0.0566	1.75	0.0540	0.0551
	2.5	0.0550	0.0567	1	0.0618	0.0604	1.75	0.0552	0.0566	2	0.0513	0.0540
	3.75	0.0544	0.0536	1	0.0606	0.0604	1.75	0.0550	0.0566	2.5	0.0514	0.0519
	5.5	0.0516	0.0498	1.75	0.0578	0.0579	2.5	0.0554	0.0539	2.5	0.0504	0.0519
	6.75	0.0451	0.0475	1.75	0.0571	0.0579	2.5	0.0542	0.0539	2.75	0.0491	0.0509
	7.75	0.0476	0.0457	1.75	0.0563	0.0579	2.5	0.0524	0.0539	4	0.0479	0.0464
	8.25	0.0486	0.0449	2.5	0.0569	0.0556	4.75	0.0477	0.0470	4.5	0.0456	0.0448
	8.5	0.0421	0.0445	2.5	0.0551	0.0556	4.75	0.0464	0.0470	5	0.0443	0.0433
	9.5	0.0440	0.0430	2.5	0.0548	0.0556	6	0.0450	0.0439	6.5	0.0416	0.0393
	10.5	0.0392	0.0416	4.5	0.0495	0.0503	6	0.0443	0.0439			
	12	0.0395	0.0397	4.75	0.0512	0.0497	6.25	0.0440	0.0433			
	13	0.0380	0.0386	5	0.0501	0.0497	7.5	0.0405	0.0406			
	13.5	0.0358	0.0378	6	0.0476	0.0469						
				7	0.0450	0.0449						

Table 7.2: All Experimental and Model data for the Bunsen reaction at various temperatures and water to iodine ratios

7.2.2 Appendix B.2: HSP Reaction Data

118-1	T=75°C			T=90°C			T=98°C		
	t (min)	$[I_2]_e$	$[I_2]_m$	t (min)	$[I_2]_e$	$[I_2]_m$	t (min)	$[I_2]_e$	$[I_2]_m$
	0	0.064	0.064	0	0.064	0.064	0	0.064	0.064
	23.16667	0.020426	0.0176	33.75	0.02182	0.0194	36	0.017172	0.0151
	25.16667	0.024769	0.0216	34.5	0.017425	0.0188	42.5	0.020767	0.024
	25.75	0.023253	0.0231	36.16667	0.027607	0.0214	43.5	0.022824	0.0231
	26	0.025358	0.0232	37.5	0.019532	0.0231	44.5	0.024396	0.0272
	26.75	0.022524	0.0246	37.66667	0.030858	0.0231	46	0.024653	0.0294
	27.5	0.02764	0.0276	39	0.031769	0.0247	46.25	0.024759	0.0277
	30.83333	0.032972	0.0312	41.5	0.02306	0.0278	50.5	0.031443	0.032
	31.66667	0.025363	0.0336	43.16667	0.021628	0.03	50.75	0.029069	0.0319
	35.66667	0.030776	0.0392	43.33333	0.027538	0.0299	52.75	0.032227	0.0339
	38.75	0.040914	0.0417	44	0.033496	0.0311	54.75	0.030238	0.0356
	39.66667	0.039764	0.0425	46	0.029315	0.033	56.75	0.038116	0.0372
	39.75	0.030017	0.0432	46.16667	0.037044	0.033	57	0.036958	0.0373
	40.5	0.038882	0.0442	46.66667	0.027578	0.0334			
	45.5	0.044052	0.0481	48.33333	0.0317	0.035			
	47.25	0.046519	0.0516	50	0.037696	0.0371			
	48.75	0.041974	0.0502	51.16667	0.039049	0.0382			
	52.83333	0.04891	0.0528	52	0.03421	0.0388			
	55	0.048809	0.0541	54.25	0.032712	0.0403			
				55.25	0.042747	0.041			
				56.66667	0.037601	0.0417			
				64	0.047494	0.0466			
				64.25	0.050471	0.0465			
				65	0.047853	0.0476			
				69.5	0.056398	0.0493			
				73.25	0.055055	0.0512			

105-1	T=75°C			T=83°C			T=90°C		
	t (min)	$[I_2]_e$	$[I_2]_m$	t (min)	$[I_2]_e$	$[I_2]_m$	t (min)	$[I_2]_e$	$[I_2]_m$
	0	0.064	0.064	0	0.064	0.064	0	0.064	0.064
	24.75	0.036676	0.0246	19.5	0.038455	0.0306	15	0.024385	0.0177
	25	0.030462	0.025	21	0.039847	0.034	16.5	0.027606	0.0211
	26	0.037251	0.0263	22	0.036053	0.0362	18	0.026388	0.0248
	27.75	0.037288	0.0288	22.5	0.039667	0.0372	18.5	0.030819	0.0261
	30	0.035209	0.0321	23.5	0.042028	0.0393	19.5	0.027589	0.0286
	31.5	0.035948	0.0342	25.5	0.041034	0.043	19.75	0.031355	0.0292
	32.75	0.036285	0.036	27	0.041769	0.0455	20	0.03259	0.0299
	33.5	0.039406	0.0371	28.5	0.042564	0.0477	20.5	0.034685	0.0311
	34.5	0.04179	0.0384	29.75	0.04491	0.0494	22	0.029199	0.0346
	35.25	0.042211	0.0394				22.25	0.035862	0.0351
	36.5	0.041576	0.041				23.5	0.038127	0.0378
	37	0.042557	0.0416				23.75	0.034952	0.0383
	38.25	0.040572	0.0432				24	0.037069	0.0388
	43.75	0.043337	0.0488				24.75	0.039222	0.0402
							27.25	0.037711	0.0445
93-1	**T=75°C**			**T=90°C**			**T=105°C**		
	t (min)	$[I_2]_e$	$[I_2]_m$	**t (min)**	$[I_2]_e$	$[I_2]_m$	**t (min)**	$[I_2]_e$	$[I_2]_m$
	0	0.064	0.064	0	0.064	0.064	0	0.064	0.064
	6.25	0.032499	0.036	8.5	0.03879	0.0377	1.75	0.040783	0.0414
	7.75	0.034188	0.0348	8.75	0.032005	0.0379	3.25	0.0336	0.0413
	10	0.030742	0.0343	9	0.032227	0.0382	3.26	0.047636	0.0414
	10.005	0.035424	0.0343	9.5	0.041943	0.0388	4	0.050308	0.0426
	10.25	0.034756	0.0343	10	0.030816	0.0394	4.25	0.0377	0.0431
	11.5	0.035192	0.0344	10.25	0.04489	0.0396	5	0.0411	0.0447
	14.25	0.036169	0.0354	10.75	0.035279	0.0403	5.01	0.053331	0.0447
	15	0.032713	0.0357	11	0.042766	0.0406	5.75	0.054987	0.0464
	16	0.037145	0.0363	11.25	0.036031	0.0409	6.5	0.0478	0.0481
	17.25	0.034961	0.037	12.5	0.034879	0.0425	6.75	0.030436	0.0487
	17.75	0.040587	0.0373	12.75	0.049211	0.0428	7	0.032107	0.0492
	19	0.04037	0.0381	13.5	0.048402	0.0438	8	0.03653	0.0514
	19.75	0.034877	0.0386	14	0.039686	0.0444	8.01	0.0535	0.0514
	20.25	0.042201	0.0389	14.25	0.041226	0.0447	9.5	0.041631	0.0543
	22.25	0.035153	0.0403	15	0.050678	0.0457	10.75	0.045738	0.0564
	23.75	0.04719	0.0413	15.25	0.040259	0.046			
	25	0.036948	0.0422	15.5	0.042495	0.0464			

Table 7.3: All Experimental and Model data for the HSP reaction at various temperatures and water to iodine ratios

7.3 Appendix C: Sulfur Calibration Curves

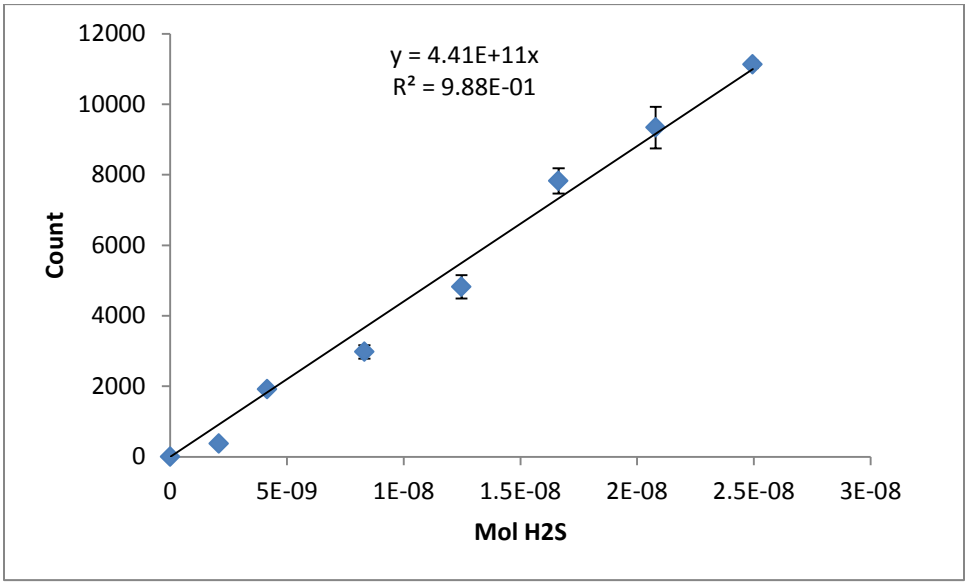

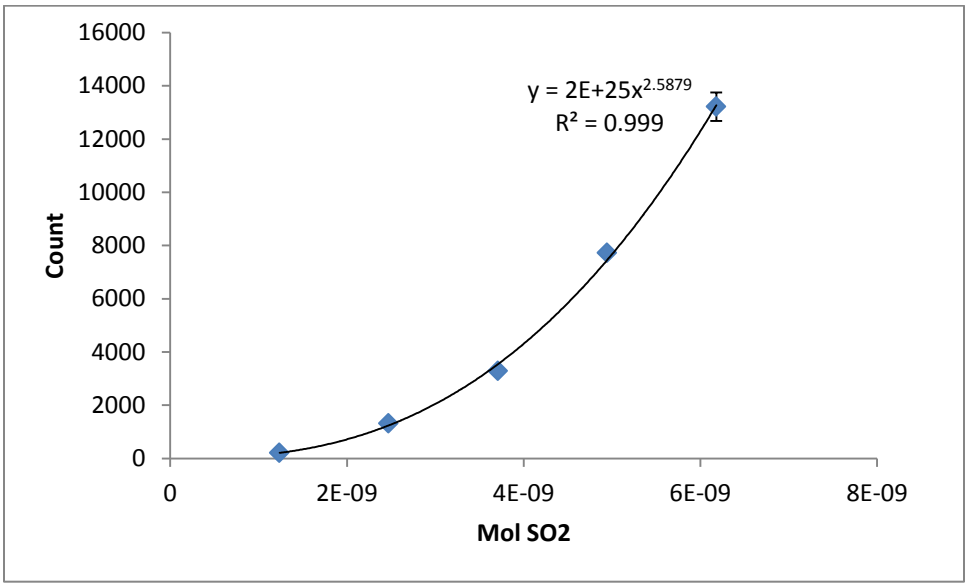

Figure 7.1: GC calibration curves for hydrogen sulfide and sulfur dioxide

7.4 Appendix D: Headspeace Volume Calculations

	1	2	3
Mass Vial/stir bar (g)	20.349	20.825	20.716
Mass +4.7 mL H2O (g)	25.092	25.564	25.487
Density 4.7 mL H2O (g/mL)	1.009	1.008	1.015
Mass full H2O (g)	34.968	34.811	34.748
Mass Headspace (g)	9.876	9.247	9.262
Volume Headspace (mL)	9.788	9.171	9.123
Inner Septa diameter (mm)	8.000	8.000	8.000
Outer septa diameter (mm)	14.000	14.000	14.000
Septa Height (mm)	10.500	10.500	10.500
Septa Volume (mm^3)	1088.562	1088.562	1088.562
Septa Volume (mL)	1.089	1.089	1.089
Headspace-Septa V (mL)	8.699	8.082	8.035
Actual headspace (mL)	**8.272**		

Table 7.4: Headspace volume calculation